Title

Muscarinic Modulation of Pyramidal Cell Excitability and Long Term Potentiation Across Dorsal-Ventral Axis of Mouse Hippocampus

Author

Jami, Shekib Ahmad

Publication Date

2018

Peer reviewed|Thesis/dissertation

UNIVERSITY OF CALIFORNIA

Los Angeles

Muscarinic Modulation of Pyramidal Cell Excitability and Long Term Potentiation Across Dorsal-Ventral Axis of Mouse Hippocampus

A dissertation submitted in partial satisfaction of the requirement for the degree of Doctors of Philosophy in Molecular, Cellular, and Integrative Physiology

by

Shekib Ahmad Jami

2018

ABSTRACT OF THE DISSERTATION

Muscarinic Modulation of Pyramidal Cell Excitability and

Long Term Potentiation

Across Dorsal-Ventral Axis of Mouse Hippocampus.

by

Shekib Ahmad Jami

Doctor of Philosophy in Molecular, Cellular, and Integrative Physiology

University of California, Los Angeles, 2018

Professor Thomas J. O'Dell, Chair

Behavioral, physiological, and anatomical evidence indicates that the dorsal and ventral zones of the hippocampus have distinct roles in cognition. How the unique functions of these zones might depend on differences in synaptic and neuronal function arising from the strikingly different gene expression profiles exhibited by dorsal and ventral CA1 pyramidal cells is unclear. To begin to address this question, I investigated the mechanisms underlying differences in synaptic transmission and plasticity at dorsal and ventral Schaffer collateral (SC) synapses.

Strikingly, although basal synaptic transmission is similar, SC synapses in the dorsal and ventral hippocampus exhibit markedly different responses to theta-frequency patterns of stimulation. In contrast to dorsal hippocampus, theta-frequency stimulation fails to elicit postsynaptic complex-spike bursting and does not induce LTP at ventral SC synapses. Moreover, EPSP-spike coupling, a process that strongly influences information transfer at synapses, is weaker in ventral pyramidal cells. All of these differences in postsynaptic function are due to an enhanced activation of SK-type K^+ channels that suppresses NMDA receptor (NMDAR)-dependent EPSP amplification at ventral SC synapses. Consistent with this, mRNA levels for the SK3 subunit of SK channels are significantly higher in ventral CA1 pyramidal cells. Together, my findings indicated that a dorsal-ventral difference in SK channel regulation of NMDAR activation has a profound effect on the transmission, processing and storage of information at SC synapses and thus likely contributes to the distinct roles of the dorsal and ventral hippocampus in different behaviors. SK channel activity at dendritic spines is strongly down-regulated by β-adrenergic (Carter et al. 2012) and muscarinic receptor activation (Buchanan et al. 2010; Giessel and Sabatini 2010). Thus, in addition to coincident pre- and postsynaptic activity, the induction of LTP at SC synapses in the ventral hippocampus may be highly state-dependent and require the release of modulatory neurotransmitters, such as norepinephrine or acetylcholine, to overcome the SK channel inhibition of NMDAR activation. Experiments in this dissertation focus on muscarinic neuromodulation of dorsal and ventral hippocampus and its effect on pyramidal cell excitability and LTP across dorsal-ventral axis of mouse hippocampus.

The dissertation of Shekib Jami is approved.

David L Glanzman

Christopher S Colwell

Felix Erich Shweizer

Thomas J. O'Dell, Committee Chair

University of California, Los Angeles,

2018

Dedication

To my mom.

Table of Contents

List of Figures

List of Tables

Acknowledgments

The work presented here would not be possible without the support of my advisor, Thomas O'Dell, whose guidance and advice has been invaluable. I would like to thank my thesis committee for the insightful advice and guidance not only during my time here at UCLA as a graduate student but also during my undergraduate years. I am also grateful for Walter Babiec for his guidance and friendship throughout my graduate studies. Finally, none of this would be possible without the sacrifices that my mom had to make to make sure I am alive. In addition, I would not be here today without the love and support of my wife, Jillian Jami, and my twin boys Jake Jami and Alex Jami. To my brothers Farid and Ahmad and his wonderful wife Daiwah and my niece and nephew Arzo and Jawade, I cannot thank you all enough for helping me reach this point. To Debbie Davis and Dennis Greenbaum, I am the luckiest man to have you two as my in-laws.

Chapter I is a version of Babiec, W. E., Guglietta, R., Jami, S. A., Morishita, W., Malenka, R. C., & O'Dell, T. J. "Ionotropic NMDA receptor signaling is required for the induction of long-term depression in the mouse hippocampal CA1 region." Journal of Neuroscience34.15 (2014): 5285-5290. Author contributions: W.E.B., R.G., S.A.J., W.M., R.C.M., and T.J.O. designed research; W.E.B., R.G., S.A.J., W.M., and T.J.O. performed research; W.E.B., R.G., S.A.J.,W.M., and T.J.O. analyzed data; W.E.B., R.M., and T.J.O. wrote the paper. This work was supported by grants from the National Institute of Mental Health (T.J.O. and R.C.M.). W.E.B. was supported by Grant T32NS007101 from the National Institute of Neurological Disorders and Stroke, and S.J. was supported by Grant T32GM065823-11 from the National Institute of General Medical Sciences.

Chapter II is a version of Loh, D. H., Jami, S. A., Flores, R. E., Truong, D., Ghiani, C. A., O'Dell, T. J., & Colwell, C. S. (2015). Misaligned feeding impairs memories. Elife, 4, e09460." DHL,

CAG, TJO'D, Conception and design, Acquisition of data, Analysis and interpretation of data, Drafting or revising the article ; SAJ, Acquisition of data, Analysis and interpretation of data, Drafting or revising the article; REF, DT, Acquisition of data, Analysis and interpretation of data; CSC, Conception and design, Drafting or revising the article.

Chapter III is a version of Babiec, W. E., Jami, S. A., Guglietta, R., Chen, P. B., & O'Dell, T. J. (2017). Differential Regulation of NMDA Receptor-Mediated Transmission by SK Channels Underlies Dorsal-Ventral Differences in Dynamics of Schaffer Collateral Synaptic Function. Journal of Neuroscience, 37(7), 1950-1964. Author contributions: W.E.B., S.A.J., R.G., P.B.C., and T.J.O. designed research; W.E.B., S.A.J., R.G., P.B.C., and T.J.O. performed research; W.E.B., S.A.J., R.G., P.B.C., and T.J.O. analyzed data; W.E.B., S.A.J., R.G., P.B.C., and T.J.O. wrote the paper. This work was supported by National Institute of Mental Health Grant R01MH060919-15 to T.J.O. W.E.B. was supported by National Institute of Neurological Disorders and Stroke Grant T32NS007101-34. S.A.J. was supported by National Institute of General Medical Sciences Grant T32GM065823-11. R.G. was supported by an ARCS Foundation Scholar Award.

Chapter IV describes the results from experiments in a manuscript currently being prepared: Jami S. A., O'Dell T. J. Muscarinic modulation of pyramidal cell excitability and Long Term Potentiation across Dorsal-Ventral axis of mouse hippocampus. In preparation for publication. Author contributions: S.A.J. and T.J.O. designed research; S.A.J. performed research; S.A.J. analyzed data; S.A.J. and T.J.O. wrote the paper. This work was supported by National Institute of Mental Health Grant R01MH060919-15 to T.J.O. S.A.J. was supported by National Institute of General Medical Sciences Grant T32GM065823-11.

Curriculum Vitae

Education
2003 **B.S.**, Department of Physiological Sciences and Department of Neuroscience, UCLA
Thesis: *Differential Classical conditioning of the gill-withdrawal reflex in Aplysia*
2018 **Ph.D. Candidate**, Molecular, Cellular and Integrative Physiology, David Geffen School of Medicine at UCLA: Dissertation: Muscarinic Modulation of Pyramidal Cell Excitability and Long-Term Potentiation Across the Dorsal-Ventral Axis of Mouse Hippocampus.

Professional Experience:
2012-Present Graduate Student Researcher, Dept. of Physiology, David Geffen School of Medicine, University of California, Los Angeles, CA
2008-12 Research Associate II, Dept. of Internal Med, UC Davis School of Medicine, UC Davis, Sacramento, CA
2007 Biomedical Technologist III, Jackson Laboratory, West Sacramento, CA
2003-06 Laboratory Assistant III, Department of Psychiatry and Biobehavioral Sciences, University of California, Los Angeles, CA
2001-03 Laboratory Assistant III, Department of Physiological Sciences, University of California, Los Angeles, CA

Professional Activities

Teaching:
2014-15 Teaching Assistant, University of California, Los Angeles, CA
Course: M101C. Neuroscience: From Molecules to Mind -- Molecular and Developmental Neuroscience (Undergraduate Course)

Certifications:
2016 UCLA Mentoring Training Program
2010 Flow Cytometry course, UC Davis Biotechnology program

Research Grants and Fellowships Received
2013-04 National Institute of General Medical Sciences (NRSA Training Grant 2T32GM065823-11)

Lectures and Presentations
2015 Misaligned feeding impairs hippocampal-dependent memories, MCIP *Student Seminar*
2018 Pyramidal Cell Excitability and Long-Term Portentiation Across Dorsal-Ventral Axis of Mouse Hippocampus. MCIP *Annual Retreat*

Research Papers: Peer Reviewed

Cain, C. K., Godsil, B. P., **Jami, S.**, & Barad, M. (2005). The L-type calcium channel blocker nifedipine impairs extinction, but not reduced contingency effects, in mice. *Learning & Memory*, *12*(3), 277-284.

Jami, S. A., Wright, W. G., & Glanzman, D. L. (2007). Differential classical conditioning of the gill-withdrawal reflex in Aplysia recruits both NMDA receptor-dependent enhancement and NMDA receptor-dependent depression of the reflex. *Journal of Neuroscience*, *27*(12), 3064-3068.

Fernandez, C., **Jami, S.**, Loredo, G., Ko, F., Hahn, T., McDougall, S., & Peters, J. H. (2010). Recognition of the alternatively spliced segments of fibronectin by the RCJ 3.1 C5. 18 chondrocytic rat cell line. *Osteoarthritis and cartilage*, *18*(2), 228-239.

Babiec, W. E., Guglietta, R., **Jami, S. A.**, Morishita, W., Malenka, R. C., & O'Dell, T. J. (2014). Ionotropic NMDA receptor signaling is required for the induction of long-term depression in the mouse hippocampal CA1 region. *Journal of Neuroscience*, *34*(15), 5285-5290. (**Featured Article, F1000 Prime Recommended**)

Lee, K. H., Mathews, P. J., Reeves, A. M., Choe, K. Y., **Jami, S. A.**, Serrano, R. E., & Otis, T. S. (2015). Circuit mechanisms underlying motor memory formation in the cerebellum. *Neuron*, *86*(2), 529-540.

Loh, D. H., **Jami, S. A.**, Flores, R. E., Truong, D., Ghiani, C. A., O'Dell, T. J., & Colwell, C. S. (2015). Misaligned feeding impairs memories. *Elife*, *4*, e09460.

Babiec, W. E., **Jami, S. A.**, Guglietta, R., Chen, P. B., & O'Dell, T. J. (2017). Differential Regulation of NMDA Receptor-Mediated Transmission by SK Channels Underlies Dorsal-Ventral Differences in Dynamics of Schaffer Collateral Synaptic Function. *Journal of Neuroscience*, *37*(7), 1950-1964.

Papers in Preparation (Research Completed)

Jami S. A., Gray E., O'Dell T. J., (*in preparation*) Role of p38MAPK in synaptic plasticity at the excitatory synapse of CA1 region of hippocampus in MAGUK mutant mice.

Jami S. A., O'Dell T. J., (*in preparation*) Cholinergic muscarinic neuromodulation of pyramidal cell excitability and Long Term Potentiation across Dorsal-Ventral axis of mouse hippocampus.

Selected Abstracts

Mathews, P., Lee, K.H., **Jami, S**., Serrano, R., Otis, T. "High speed video and optrode monitoring of the effects of optogenetic manipulation of Purkinje neurons" Society for Neurosence, 2013.

Mathews P.J., Lee K-H., **Jami S**., Serrano R.E., Otis T.S. "Behavioral and electrophysiological effects of optogenetically manipulating Purkinje Neurons " Gordon Conference. 2013.

Loh D., Floris R., Truong D., **Jami S. A.**, Ghiani C., O'dell T., Colwell C., "Pronounced impact of out of phase food intake on learning and memory" No. 454.30/RR27. 2014 Washington, DC: Society for Neuroscience, 2014

Babiec W., Guglietta R., **Jami S. A.**, O'Dell T., "Regulation of spontaneous synaptic transmission by extracellular calcium at excitatory synapses onto hippocampal CA1 pyramidal cells" No. 599.18/D33. 2014 Washington, DC: Society for Neuroscience, 2014

Babiec W., **Jami S. A.**, Guglietta R., O'Dell T., "Differences in theta-pulse stimulation induced LTP between dorsal and ventral hippocampus may rely on network properties" No. 194.09. 2015 Chicago: Society for Neuroscience, 2015 ***(Selected Nanosymposium Presentation)***

Jami S.A., Babiec W., Guglietta R., O'Dell T., Region-specific properties of schaffer collateral synapses in dorsal and ventral hippocampus. *UCLA Annual MCIP Retreat (**Invited Presentation**)*

Introduction

The ability of excitatory synapses to undergo long-lasting changes in strength following certain patterns of synaptic activity is thought to provide a cellular mechanism for storing new information during memory formation. This phenomenon is an especially prominent feature of excitatory synaptic transmission in regions of the brain involved in learning and memory, such as the hippocampus. For example, in the CA1 region of the hippocampus brief periods of high-frequency synaptic activity and subsequent increases in intracellular Ca^{2+} induce a robust and persistent increase in the strength of synaptic transmission known as long-term potentiation (LTP). Although the mechanisms responsible for LTP are not completely understood, activation of protein kinases (such as αCamKII and ERK2) that potentiate synaptic strength by enhancing the activity of postsynaptic AMPA type glutamate receptors (AMPAR) is thought to have a central role (Malenka and Bear, 2004; Brigman et al., 210). In contrast, bouts of low-frequency synaptic activity induce a lasting inhibition of synaptic transmission known as long-term depression (LTD) and, like LTP, the induction of LTD requires NMDAR activation and increases in postsynaptic calcium (Collingride et al., 2010; Dudet et al., 2009; Mulkey et al., 1992). Genetic and pharmacological manipulations that disrupt LTP and LTD have profound effects on learning and memory, supporting the notion that these forms of synaptic plasticity serve as cellular mechanisms involved in memory formation.

In the hippocampus, LTP and LTD are induced by activation of postsynaptic NMDA type glutamate receptors. Traditionally, these receptors were thought of in very simple terms, i.e. once activated by glutamate, NMDA receptors were thought to signal simply by allowing the influx of Ca^{2+} ions into the postsynaptic cell. Our view of NMDA receptors has changed over the last few

years, however, with the realization that these receptors are in fact part of a much larger complex of proteins. Within the postsynaptic density of excitatory synapses, NMDARs are associated with a large number of adaptor proteins and downstream signaling molecules through protein interactions mediated by the C-terminal tails of their GluN2 subunits. These protein interactions might provide a mechanism whereby conformational changes associated with glutamate binding could activate downstream signaling pathways. A recent study found that LTD is not inhibited by MK-801, an uncompetitive antagonist that blocks NMDAR channels (Nabavi et al, 2013). This suggests that LTD involves a metabotropic form of NMDAR signaling where, in a manner similar to mGluR signaling, conformational changes in NMDARs induced by glutamate binding can directly activate downstream signaling pathways. Thus, the notion that NMDARs are capable of metabotropic-like signaling and that this form of NMDAR signaling might have an important role in synaptic plasticity is an intriguing possibility. Consistent with a large body of previous results, all of which support a crucial role for NMDAR-mediated Ca^{2+} signaling in LTD our results in Chapter I indicate that ionotropic, rather than metabotropic, NMDA receptor signaling is required for the induction of LTD in the mouse hippocampus CA1 region.

Hippocampus plays an important role in commonly used associative learned behaviors such as hippocampal-dependent contextual fear conditioning and novel object recognition (Philips et al., 1992; Clark et al., 2000). In fear conditioning the animal is placed in a novel environment, allowed to acclimate, and then presented with a brief tone (CS). At the termination of this non-aversive tone (CS), an aversive footshock (US) is presented through a grid at the bottom of the cage. Obviously, if in a conditioning context one administers a foot shock that is paired with a tone, there will be learning not only to the tone, but also to the context. When tested a time later the previously non-aversive tone or context will elicit defensive fear response such as freezing

(CR). Pre and post training lesion of the hippocampus disrupt acquisition and recall of contextual fear conditioning whereas cued fear conditioning depends upon both the hippocampus and amygdala (Clark et al., 2000, Phillips et al., 1992).

Novel object recognition is another hippocampus dependent task that exploits the natural tendency of rodents to explore novel items and depending on the amount of time that rodents spend exploring the presented objects. Data indicate that temporary inactivation of hippocampus or permanent lesion of the hippocampus disrupts object memory in novel object recognition test (de Lima et al., 2006).

Robust sleep/wake rhythms are important for health and cognitive function. Unfortunately, many people are living in an environment where their circadian system is challenged by inappropriate meal- or work-times. In Chapter II we scheduled food access to the sleep time and examined the impact on learning and memory in mice by examining hippocampus dependent tasks such as fear conditioning and novel object recognition. Under these conditions, we demonstrate that the molecular clock in the master pacemaker, the suprachiasmatic nucleus (SCN), is unaltered while the molecular clock in the hippocampus is synchronized by the timing of food availability. This chronic circadian misalignment causes reduced hippocampal long term potentiation and CREB expression. Importantly this mis-timed feeding resulted in dramatic deficits in hippocampal-dependent learning and memory. Our findings suggest that both learning and synaptic plasticity is regulated by the circadian rhythm and find that misaligning the hippocampal oscillator from the SCN oscillator by misaligning mealtime is detrimental to learning and memory.

Although the hippocampus has been intensively studied because of its crucial role in spatial navigation as well as learning and memory, hippocampal lesions also have profound effects on

innate fear and anxiety (Deacon et al., 2002; Kjelstrup et al., 2002; Bannerman et al., 2003; Pentkowski et al., 2006). Intriguingly, these different aspects of hippocampal function are segregated into distinct anatomical zones, with the dorsal hippocampus having a key role in memory formation, whereas, the ventral hippocampus is more importantly involved in emotions and anxiety (Moser and Moser, 1998; Kjelstrup et al., 2002; Bannerman et al., 2003; Fanselow and Dong, 2010; Strange et al., 2014). Consistent with this functional segmentation along the dorsal-ventral axis of the hippocampus, both direct and indirect connections link the dorsal hippocampus to brain regions with roles in spatial information processing and memory, while the ventral hippocampus has prominent connections with brain regions involved in emotions and anxiety (see Fanselow and Dong, 2010 and Strange et al., 2014). It remains unclear whether there are important differences in how synapses, cells, and/or networks within the dorsal and ventral hippocampus process different patterns of synaptic activity.

In Chapter III, I investigated the mechanisms underlying dorsal-ventral differences in the LTP induction using theta pulse stimulation (TPS) patterns of SC fiber stimulation (Thomas et al., 1998 and find that dorsal and ventral SC synapses exhibit markedly distinct responses to TPS and, in contrast to dorsal hippocampus, TPS fails to induce LTP at ventral synapses. Excitatory postsynaptic potential (EPSP) amplification is also strongly reduced at ventral synapses and, as a result, both EPSP-spike (E-S) coupling and EPSP-evoked complex spike (CS) bursting are significantly weaker in ventral pyramidal cells. Our results indicate that all of these differences in postsynaptic function arise from a common mechanism: an enhanced activation of Ca^{2+}-activated SK-type K^+ channels that strongly inhibits NMDA receptor (NMDAR) activation at ventral SC synapses. Together, these findings indicated that a dorsal-ventral difference in SK channel regulation of NMDAR activation has a profound effect on the transmission, processing and storage

of information at SC synapses and thus likely contributes to the distinct roles of the dorsal and ventral hippocampus in different behaviors. Interestingly, SK channel activity at dendritic spines is strongly down-regulated by β-adrenergic (Carter et al. 2012) and muscarinic receptor activation (Buchanan et al. 2010; Giessel and Sabatini 2010). Thus, in addition to coincident pre- and postsynaptic activity, the induction of LTP at SC synapses in the ventral hippocampus may be highly state-dependent and require the release of modulatory neurotransmitters, such as norepinephrine or acetylcholine, to overcome the SK channel inhibition of NMDAR activation.

In Chapter IV, I examined the postsynaptic effects of muscarinic receptor activation in CA1 pyramidal neurons in dorsal and ventral hippocampus in presence of different sub-type selective, mAchR agonists and antagonists. Consistent with our previous results I found that although theta-frequency patterns of synaptic stimulation induce robust LTP at SC synapses in the dorsal CA1 region but not in ventral CA1 region, activation of acetylcholine receptors by non-selective cholinergic agonist and more selective muscarinic M1 agonist facilitates TPS-induced LTP at SC synapses in the ventral hippocampus. I also show that EPSP-spike coupling and NMDAR dependent EPSP amplification is enhanced in ventral SC synapses. These findings confirm and extend these earlier observations by demonstrating that regional differences in muscarinic receptor activity provide a mechanism for generating functionally distinct types of synapses where theta-frequency patterns of synaptic activity can have profoundly different effects on both synaptic transmission and long-term synaptic plasticity.

References

Bannerman, D. M., et al. "Ventral hippocampal lesions affect anxiety but not spatial learning." Behavioural brain research 139.1 (2003): 197-213.

Brigman, Jonathan L., et al. "Loss of GluN2B-containing NMDA receptors in CA1 hippocampus and cortex impairs long-term depression, reduces dendritic spine density, and disrupts learning." Journal of Neuroscience 30.13 (2010): 4590-4600.

Buchanan, Katherine A., et al. "Facilitation of long-term potentiation by muscarinic M 1 receptors is mediated by inhibition of SK channels." Neuron68.5 (2010): 948-963.

Carter, Brett C., et al. "Transient sodium current at subthreshold voltages: activation by EPSP waveforms." Neuron 75.6 (2012): 1081-1093.

Clark, Robert E., Stuart M. Zola, and Larry R. Squire. "Impaired recognition memory in rats after damage to the hippocampus." *Journal of Neuroscience* 20.23 (2000): 8853-8860.

Collingridge GL, Peineau S, Howland JG, and Wang YT (2010) Long-term depression in the CNS. Nat Neurosci. Rev 11: 459-473.

Deacon, Robert MJ, David M. Bannerman, and J. Nicholas P. Rawlins. "Anxiolytic effects of cytotoxic hippocampal lesions in rats." Behavioral neuroscience 116.3 (2002): 494.

de Lima, Maria Noemia, et al. "Temporary inactivation reveals an essential role of the dorsal hippocampus in consolidation of object recognition memory." *Neuroscience Letters* 405.1 (2006): 142-146.

Dudek SM and Bear MF (1992) Homosynaptic long-term depression in area CA1 of hippocampus and effects of N-methy-D-aspartate receptor blockade. Proc natl Acad Sci USA 89: 4363-4367.

Fanselow MS, Dong HW (2010) Are the dorsal and ventral hippocampus functionally distinct structures? Neuron 65:7-19.

Giessel, Andrew J., and Bernardo L. Sabatini. "M1 muscarinic receptors boost synaptic potentials and calcium influx in dendritic spines by inhibiting postsynaptic SK channels." Neuron 68.5 (2010): 936-947.

Kjelstrup KG, Tuvnes FA, Steffenach H-A, Murison R, Moser EI, Moser M-B (2002) Reduced fear expression after lesions of the ventral hippocampus. PNAS 99:10825-10830.

Malenka RC and Bear MF (2004) LTP and LTD: An embarrassment of riches. Neuron 30: 5-21.

Mulkey RM and Malenka RC (1992) Mechanisms underlying induction of homosynaptic long-term depression in area CA1 of the hippocampus. Neuron 9: 967-975.

Moser MB, Moser EI (1998) Functional differentiation in the hippocampus. Hippocampus 8:608-619.

Nabavi S, Kessels HW, Alfonso S, Aow J, Fox R, Malinow R (2013) Metabotropic NMDA receptor function is required for NMDA receptor-dependent long-term depression. Proc Natl Acad Sci USA 110:4027–4032.

Phillips, R. G., and J. E. LeDoux. "Differential contribution of amygdala and hippocampus to cued and contextual fear conditioning." *Behavioral neuroscience* 106.2 (1992): 274.

Pentkowski, Nathan S., et al. "Effects of lesions to the dorsal and ventral hippocampus on defensive behaviors in rats." European Journal of Neuroscience 23.8 (2006): 2185-2196.

Strange, Bryan A., et al. "Functional organization of the hippocampal longitudinal axis." Nature Reviews Neuroscience 15.10 (2014): 655-669.

Thomas, Mark J., et al. "Postsynaptic complex spike bursting enables the induction of LTP by theta frequency synaptic stimulation." Journal of Neuroscience 18.18 (1998): 7118-7126.

1 CHAPTER I: Ionotropic NMDA Receptor Signaling is Required for the Induction of LTD in the Mouse Hippocampal CA1 Region

1.1 Introduction

Excitatory synapses in many brain regions undergo long-lasting, activity-dependent changes in synaptic strength. For example, increases in intracellular Ca^{2+} mediated by NMDAR activation during brief periods of high-frequency synaptic activity induces long-term potentiation (LTP), a long-lasting enhancement of synaptic strength (Lüscher and Malenka, 2012). In contrast, long-term depression (LTD), a persistent decrease in synaptic strength, is induced by periods of low-frequency synaptic activity. Although activation of G protein-coupled, metabotropic glutamate receptors (mGluRs) can induce LTD, at many synapses the induction of LTD is dependent on NMDAR activation and increases in intracellular Ca^{2+} (Collingridge et al., 2010).

The notion that Ca^{2+} signaling has a crucial role in NMDAR-dependent forms of synaptic plasticity is widely accepted. However, although the induction of LTD is blocked by competitive NMDAR antagonists (Dudek and Bear, 1992; Mulkey and Malenka, 1992), a recent study found that LTD is not inhibited by MK-801, an uncompetitive antagonist that blocks NMDAR channels (Nabavi et al, 2013). This suggests that LTD involves a metabotropic form of NMDAR signaling where, in a manner similar to mGluR signaling, conformational changes in NMDARs induced by glutamate binding can directly activate downstream signaling pathways. Interestingly, the NMDAR-dependent inhibition of excitatory synaptic transmission induced by amyloid-β (Aβ) peptides is also MK-801 insensitive, suggesting that NMDAR metabotropic signaling contributes to Aβ-induced synaptic dysfunction in Alzheimer's disease (Tamburri et al., 2013; Kessels et al., 2013). In addition, metabotropic NMDAR signaling may mediate activation of p38-MAPK

(Nabavi et al., 2013), a protein kinase implicated in both LTD (Zhu et al., 2002) and the synaptotoxic effects of Aβ peptides (Li et al., 2011; Chen et al., 2013).

NMDAR-mediated ionotropic signaling undergoes pronounced changes during early postnatal development, in part due to developmental changes in the expression of different GluN2 type NMDAR subunits (Paoletti et al., 2013). Whether metabotropic signaling by NMDARs is also developmentally regulated is unclear, however. To examine this question we compared the effects of MK-801 on LTD induction and NMDA-induced changes in protein phosphorylation in hippocampal slices obtained from young and adult mice. We find that MK-801 blocks LTD in the hippocampal CA1 region of adult and, surprisingly, young mice. Moreover, LTD induction in the adult hippocampus is highly sensitive to extracellular Ca^{2+} levels. Thus, ionotropic, rather than metabotropic, NMDAR signaling is responsible for the induction of LTD during postnatal development and in the mature hippocampus.

1.2 Materials and Methods

Slice preparation and extracellular recording

Standard methods approved by the University of California, Los Angeles and Stanford University Institution Animal Care and Use Committees were used to prepare 400 μm-thick hippocampal slices. In experiments done at UCLA slices were obtained from adult (8-12 week old, male) or young (14-21 day old, male or female) C57BL/6N mice and maintained (at 30^{o}C) in interface-type chambers perfused (2 – 3 ml/min) with oxygenated (95% O_2/5% CO_2) ACSF containing (in mM): 124 NaCl, 4 KCl, 25 $NaHCO_3$, 1 NaH_2PO_4, 2 $CaCl_2$, 1.2 $MgSO_4$, and 10

glucose. Slices were allowed to recover for ≥ 2 hours prior to an experiment and fEPSPs evoked by Schaffer collateral/commissural fiber stimulation in the CA1 region were recorded using techniques described elsewhere (Delgado et al., 2007). Because of the use-dependent nature of the blockade of NMDARs by MK-801 (Huettner and Bean, 1988), slices were exposed to ACSF containing MK-801 (10 μM) for ≥ 2 hours prior to the start of an experiment and MK-801 was present throughout the experiment. To facilitate the induction of LTD in slices from adult mice the extracellular concentration of Ca^{2+} was increased to 4 mM (Norris et al., 1996; Delgado et al., 2007).

In experiments done at Stanford, hippocampal slices obtained from CD1 mice (18-21 days old, male or female) were prepared in a similar manner to C57BL/6N mice. Slices (300 μm thick) were allowed to recover in oxygenated (95% O_2/5% CO_2) ACSF maintained at 30°C for 1 hr and then transferred to a holding chamber containing ACSF or ACSF with MK-801 (50 μM) at room temperature for a minimum of 2 hrs before being transferred to the recording chamber (at 30°C). To maximize the number of synaptic NMDARs blocked by MK-801 slices were pre-stimulated at 0.2 Hz for 5 min at approximately twice the intensity used to elicit baseline fEPSPs. Picrotoxin (50 μM) was present in the perfusion solution in all experiments.

Three different synaptic stimulation protocols were used to examine the effect of MK-801 on activity-dependent changes in synaptic strength: (1) 1 Hz low-frequency stimulation (LFS) (900 pulses); (2) 2 Hz LFS (900 pulses); (3) high frequency stimulation (HFS) (4 trains of 100 Hz stimulation, 1 second in duration, inter-train interval = 20 seconds). We also examined the effect of MK-801 on LTD using a chemical induction protocol (chem-LTD) (Lee et al., 1998; Delgado

et al., 2007). In these experiments slices were maintained in a submerged-slice recording chamber and LTD was induced by a 3 minute bath application of 20 μM NMDA.

Western Immunoblotting

Hippocampal slices or CA1 mini-slices (where CA3 and dentate gyrus were removed during dissection to isolate the CA1 region) were prepared and maintained as described above. Slices were then placed into two separate interface type chambers and allowed to recover for 2 hours. During this time one chamber was perfused with ACSF, while slices in the second chamber were exposed to ACSF containing 10 μM MK-801. Several slices from both chambers were then collected to serve as untreated controls and the remaining slices were collected immediately after a 3 minute bath application of 20 μM NMDA. Slice homogenates were prepared using techniques described elsewhere (Delgado et al., 2007) and proteins were resolved on 12% SDS-PAGE gels and then transferred onto nitrocellulose membranes. Following incubation in primary and secondary antibodies immunoreactive bands were visualized using enhanced chemiluminesence. For quantification, all blots were probed with anti-tubulin antibodies and the optical density of bands of interest were normalized to tubulin levels in each lane to control for variations in loading.

Reagents and Antibodies

NMDA (Sigma-Aldrich, St. Louis, MO, USA), MK-801, and D-APV (both from Abcam, Cambridge, MA USA) were prepared as concentrated stock solutions in ddH_2O. Anti-phospho-Thr840 GluA1 (1:2,000) and total GluA1 (1:4,000) antibodies were from Abcam. Anti-phospho-Ser845 GluA1 (1:1,000) was from Millipore (Billerica, MA USA). Anti-phospho-p38 MAPK (1:1,000) antibody was from Cell Signaling Technology (Danvers, MA USA). Anti-βIII-tubulin

(1:20,000) was from Sigma. HRP conjugated secondary antibodies (1:2,000) were obtained from GE Healthcare.

Statistics

All results are presented as mean ± sem. Statistical significance was determined using paired and unpaired t-tests, one-way ANOVAs or, where appropriate, one-way ANOVAs on ranks. Student-Newman-Keuls tests were used for *post hoc* comparisons.

1.3 Results

MK-801 blocks LTD and LTP in hippocampal slices from adult mice.

Blocking NMDAR ionotropic signaling with MK-801 provides a useful approach for examining ion channel-independent, metabotropic forms of NMDAR signaling (Yang et al., 2004; Nabavi et al., 2013; Kessels et al., 2013; Tamburri et al, 2013). Thus, to determine whether metabotropic NMDAR signaling underlies LTD in the CA1 region of the adult hippocampus we first examined whether MK-801 fails to inhibit LTD induced by 1 Hz LFS in slices obtained from 8-12 week old mice. In control experiments fEPSPs were depressed to 77 ± 4% of baseline 45 minutes post-LFS ($n = 6$, $p < 0.005$ compared to pre-LFS baseline) (**Fig. 1-1A**). In contrast, LFS in the presence of the competitive NMDAR antagonist D-APV had no lasting effect on synaptic strength (fEPSPs were 102 ± 4% of baseline, $n = 6$), indicating that the induction of LTD is NMDAR dependent (**Fig. 1-1A**). LTD was also blocked, however, in slices where LFS was

delivered in the presence of MK-801 (10 μM) (**Fig. 1-1A**, fEPSPs were 100 ± 12% of baseline, n = 8). Consistent with previous reports (Norris et al., 1996; Delgado et al., 2007), the induction of LTD in slices from adult animals was sensitive to extracellular Ca^{2+} levels as LTD was not induced by LFS in slices bathed in ACSF containing 2 mM $CaCl_2$ (**Fig. 1-1B**). Thus Ca^{2+}-dependent, ionotropic NMDAR signaling is required for the induction of LTD in hippocampal CA1 region of adult mice.

In the CA1 region of hippocampal slices from young animals HFS in the presence of MK-801 induces LTD (Nabavi et al., 2013). Thus, we also examined the effect of MK-801 on HFS-induced changes in synaptic strength in slices from adult mice. Although MK-801 significantly inhibited HFS-induced LTP, it did not enable the induction of LTD (**Fig. 1-1C**, 45 minutes post-HFS fEPSPs were 164 ± 6% of baseline in control experiments, n = 9 and were 111 ± 4% of baseline in MK-801 experiments, n = 8, $p < 0.001$ compared to control). The small potentiation of synaptic transmission induced by HFS in the presence of MK-801 was also seen in experiments where NMDARs were blocked with D-APV (**Fig. 1-1C**). Together, these data suggest that the HFS protocol used in these experiments induces a small NMDAR-independent form of potentiation and that blocking NMDAR channels with MK-801 does not enable HFS-induced LTD in slices from adult mice.

As a final test for the potential role of metabotropic NMDAR signaling in LTD in the adult hippocampus we examined whether chem-LTD can still be induced in the presence of MK-801. Although a 3-minute bath application of 20 μM NMDA induced significant LTD in control experiments (fEPSPs were 52 ± 7% of baseline 50 minutes post NMDA application, n = 6), NMDA had no effect on synaptic transmission in slices incubated in ACSF containing MK-801 (**Fig. 1-**

1D, fEPSPs were 101 ± 1% of baseline, n = 4, $p < 0.001$ compared to control). Thus, like LFS-induced LTD, chem-LTD is also dependent on ionotropic NMDAR signaling. Indeed, bath application of NMDA in Ca^{2+}-free ACSF failed to induce LTD (**Fig. 1-1E**, 50 minutes post NMDA application in Ca^{2+}-free ACSF fEPSPs were 112 ± 8% of baseline, n = 6, compared to 53 ± 8% of baseline in interleaved control experiments, n = 6, $p < 0.001$).

MK-801 blocks LTD in hippocampal slices from young mice.

Because MK-801 readily blocked LTD in hippocampal slices from adult animals we reexamined the effects of MK-801 on LTD induction in slices obtained from young mice to test whether LTD is MK-801 insensitive in the hippocampus of young animals (Nabavi et al., 2013). Surprisingly, MK-801 completely blocked LFS-induced LTD in slices obtained from young C57BL/6 mice (**Fig. 1-2A**, fEPSPs were 78 ± 5% of baseline 50 minutes post-LFS in interleaved control experiments, n = 7, but were 99 ± 6% of baseline following LFS in the presence of MK-801, n = 6, $p < 0.05$ compared to control). Similarly, MK-801 also blocked LTD induced by a different LFS protocol (900 pulses at 2 Hz) in slices obtained from young CD1 mice (**Fig. 1-2B**, fEPSPs were 104 ± 6% of baseline following LFS in MK-801, n = 8, compared to 81 ± 5% of baseline in interleaved control experiments, n = 8 $p < 0.05$). Thus, as in adult animals, our results indicate that NMDAR channel ion flux is crucial for inducing LTD in the hippocampal CA1 region of young mice.

MK-801 blocks NMDAR-mediated changes in protein phosphorylation at sites implicated in LTD.

Because dephosphorylation of AMPAR GluA1 subunits and activation of p38-MAPK are thought to contribute to LTD induction (Zhu et al., 2002; Lee et al., 1998, 2000; Delgado et al., 2007), we also used MK-801 to examine whether metabotropic signaling by NMDARs regulates p38-MAPK and GluA1 phosphorylation. Although a 3-minute application of 20 μM NMDA induced a nearly 2-fold increase in p38-MAPK phosphorylation in control, CA1 mini-slices from adult mice, it had no effect on p38-MAPK phosphorylation in mini-slices incubated in ACSF containing MK-801 (**Fig. 1-3A**). NMDA induced increases in p38-MAPK phosphorylation in slices from young mice were also blocked by MK-801 (Fib. 1.3B). Similarly, MK-801 blocked NMDA induced dephosphorylation of GluA1 subunits in slices from adult (**Fig. 1-3A**) and young mice (**Fig. 1-3B**). Thus, ionotropic NMDAR signaling is required for activation of downstream signaling pathways implicated in LTD in the hippocampus of young and adult mice.

1.4 Discussion

Within the postsynaptic density of excitatory synapses NMDARs are associated with a large number of adaptor proteins and downstream signaling molecules through protein interactions mediated by the C-terminal tails of their GluN2 subunits (Husi et al., 2000; Paoletti et al., 2013). These protein interactions might provide a mechanism whereby conformational changes associated with glutamate binding could activate downstream signaling pathways. Thus the notion that NMDARs are capable of metabotropic-like signaling is an intriguing possibility. Moreover, kainate receptors, another type of ionotropic glutamate receptor, are capable of metabotropic signaling (Lerma and Marques, 2013). However, until recently there have been only a few reports suggesting that NMDARs might be capable of metabotropic signaling (Yang et al., 2004; Vissel et al., 2001). Thus, the recent suggestion that a Ca^{2+}-independent, metabotropic form of signaling by NMDARs underlies the induction of LTD represents a potentially important advance in our understanding of both synaptic plasticity and NMDAR signaling (Nabavi et al., 2013). However, in contrast to these findings we find that the induction of LTD is sensitive to extracellular Ca^{2+} levels and that blocking NMDAR channels with MK-801 blocks LTD. MK-801 also abolished activation of p38-MAPK and changes in AMPAR GluA1 subunit phosphorylation induced by NMDAR activation. Thus, our results are consistent with the view that Ca^{2+}-dependent, ionotropic NMDAR signaling underlies the induction of LTD at Schaffer collateral fiber synapses onto CA1 pyramidal cells in both the adult and young hippocampus.

The reasons for the discrepancy between our findings and those reported by Nabavi et al. (2013) are unclear. Because of the use-dependent nature of the MK-801 block of NMDAR channels (Huettner and Bean, 1988), one possibility is that the MK-801 resistant LTD seen in the

experiments of Nabavi et al. (2013) is due to incomplete block of NMDARs. This explanation seems unlikely however as we find that LTD is blocked by 2-10 fold lower concentrations of MK-801 than those used by Nabavi et al. (2013). Moreover, MK-801 completely prevents the inhibition of synaptic transmission induced by bath application of NMDA (**Fig. 1-1D**) suggesting that spontaneous glutamate release produces sufficient levels of receptor activation to enable inhibition of NMDARs during prolonged exposures to MK-801. An alternative, albeit unlikely, explanation is that even if NMDAR-mediated currents and NMDAR-triggered changes in intracellular Ca^{2+} are undetectable following application of MK-801 (Nabavi et al., 2013), these assays may have been unable to detect very small currents and more importantly, small increases in Ca^{2+} levels at the intracellular mouths of the NMDAR channels during LTD induction protocols.

Because our experiments were done using hippocampal slices obtained from mice while rat hippocampal slices were used in the previous studies (Nabavi et al., 2013) another possibility is that the role of metabotropic NMDAR signaling in LTD is species dependent. It would be surprising, however, if such a fundamental property of LTD induction was so different in two closely related species. Moreover, previous findings have shown that MK-801 not only inhibits LTD in the mouse visual cortex (Crozier et al., 2007) but also blocks LFS-induced LTD and chem-LTD in the CA1 region of rat hippocampus (Raymond et al., 2003; Kollen et al., 2008). Our observation that MK-801 blocks NMDA-induced activation of p38-MAPK also contradicts the role of metabotropic NMDAR signaling in LTD induction (Nabavi et al., 2013), but is consistent with previous studies showing that MK-801 inhibits NMDA-induced increases in p38-MAPK phosphorylation in hippocampal neurons (Waxman and Lynch, 2005; Xiao et al., 2011).

The ability of MK-801 to inhibit LTD induction is consistent with a number of previous findings suggesting that LTD induction requires ionotropic NMDAR signaling. For example, patterns of synaptic stimulation that normally have no effect on synaptic strength can induce LTD when paired with modest postsynaptic depolarization (Oliet et al., 1997; Ngezahayo et al., 2000) or dendritic spikes (Holthoff et al., 2004). This property of LTD induction can be readily explained by the voltage-dependent Mg^{2+} block of NMDAR ion channels but is difficult to understand if LTD induction involves an ion channel-independent form of NMDAR signaling. In addition, LTD is blocked by postsynaptic infusions of Ca^{2+} chelators (Bröcher et al., 1992; Mulkey and Malenka, 1992; Debanne et al., 1994) and is dependent on Ca^{2+}-activated signaling mechanisms, such as activation of protein phosphatase 2B (Mulkey et al., 1994) and the neuronal Ca^{2+} sensor hippocalcin (Palmer et al., 2005). Although the mechanism underlying the block of LTD by Ca^{2+} chelators has been questioned (Nabavi et al, 2013), it is unclear how a Ca^{2+}-independent form of NMDAR signaling could account for the key role of Ca^{2+}-dependent signaling pathways in LTD. Indeed, activation of voltage-dependent Ca^{2+} channels alone can induce a form of LTD that occludes NMDAR-triggered LTD (Cummings et al., 1996) and the induction of LTD by LFS occludes the persistent depression of synaptic transmission induced by photolysis of caged Ca^{2+} chelators (Neveu and Zucker, 1996). Thus, our results are consistent with a large body of previous results, all of which support a crucial role for NMDAR-mediated Ca^{2+} signaling in LTD. Although our results do not rule out the possibility that NMDARs are capable of metabotropic signaling, they do indicate that this form of signaling is unlikely to have an important role in NMDAR-dependent LTD at excitatory synapses on hippocampal CA1 pyramidal neurons.

1.5 Figures

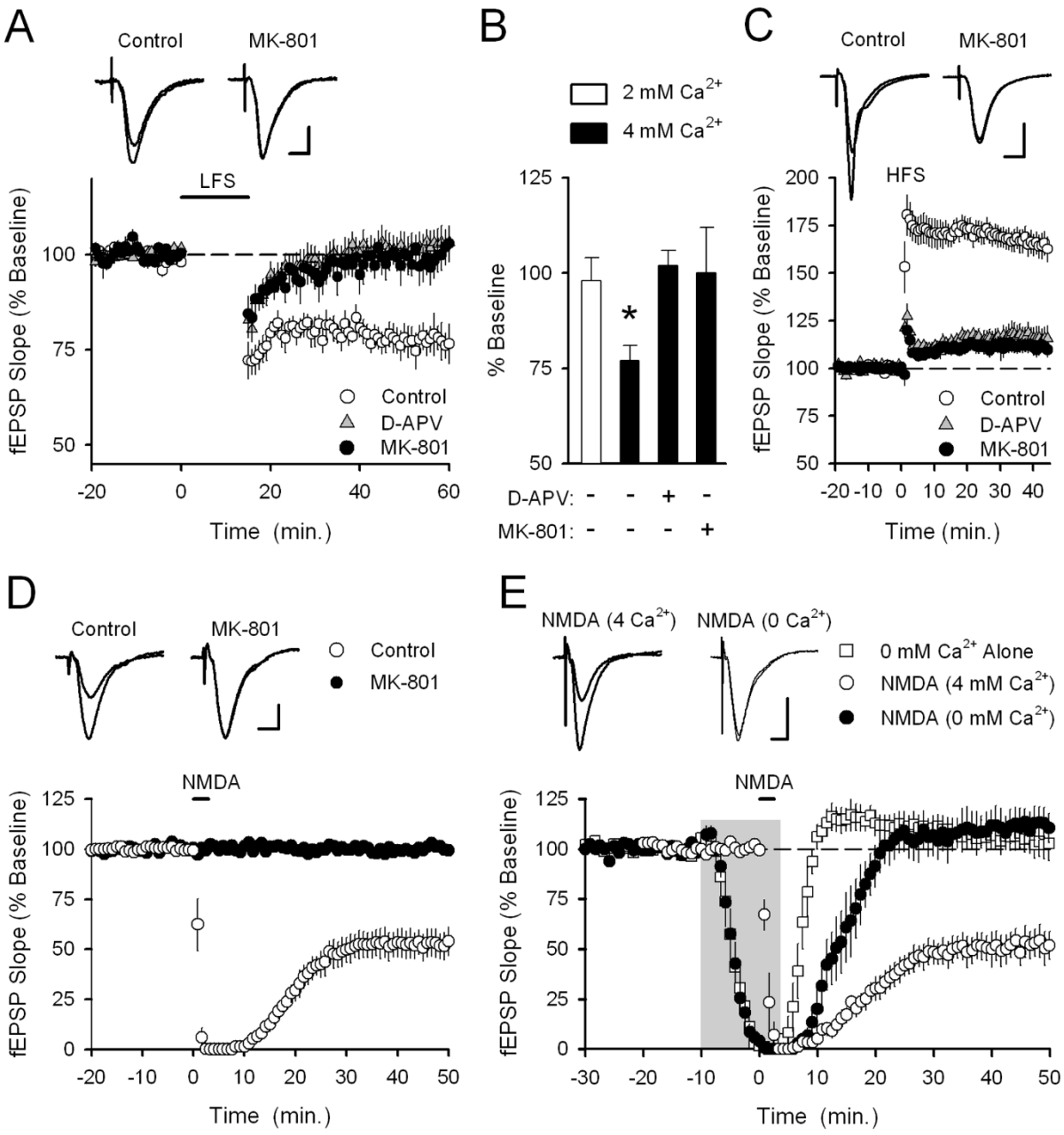
A
Control
MK-801
LFS
fEPSP Slope (% Baseline)
Control
D-APV
MK-801
Time (min.)
B
2 mM Ca2+
4 mM Ca2+
% Baseline
D-APV:
MK-801:
C
Control
MK-801
HFS
fEPSP Slope (% Baseline)
Time (min.)
D
Control
MK-801
NMDA
fEPSP Slope (% Baseline)
Time (min.)
E
NMDA (4 Ca2+)
NMDA (0 Ca2+)
0 mM Ca2+ Alone
NMDA (4 mM Ca2+)
NMDA (0 mM Ca2+)
NMDA
fEPSP Slope (% Baseline)
Time (min.)

Figure 1-1 MK-801 blocks LTD in the hippocampal CA1 region of adult mice.

A) LTD induced by 1 Hz LFS (open circles, n = 6) is blocked by 10 μM MK-801 (filled circles, n = 8) or 50 μM D-APV (triangles, n = 6). MK-801 or D-APV were present throughout the experiment. Traces are superimposed fEPSPs recorded during baseline and 45 minutes post LFS. **B)** Changes in synaptic strength induced by LFS in slices bathed in ACSF containing 2 mM $CaCl_2$ (open bar, n = 8) or 4 mM $CalCl_2$ (filled bars, * $p < 0.005$ compared to pre-LFS baseline). **C)** HFS-induced LTP (open circles, n = 9) is inhibited by MK-801 (filled circles, n = 8) or D-APV (triangles, n = 6). Traces show superimposed fEPSPs recorded during baseline and 45 minutes post HFS. **D)** Chem-LTD is blocked by MK-801. Bath application of 20 μM NMDA induced LTD in interleaved control experiments (open circles, n = 6) but had no effect on synaptic strength in MK-801 treated slices (filled circles, n = 4, $p < 0.001$ compared to control). Traces are superimposed fEPSPs recorded during baseline and 50 minutes post NMDA application. **E)** Chem-LTD is blocked when NMDA is applied in Ca^{2+}-free ACSF (no added $CaCl_2$). A 15 min bath application of Ca^{2+}-free ACSF alone (shaded region) transiently abolished synaptic transmission but had no lasting effect on synaptic strength (squares, n = 8). Bath application of NMDA induced LTD in interleaved control experiments (open circles, n = 6) but had no lasting effect on synaptic strength when applied in Ca^{2+}-free ACSF (filled circles, n = 6). Traces show superimposed fEPSPs recorded during baseline and 50 minutes post NMDA application in Ca^{2+}-free ACSF (right) in control experiments (left). Calibration bars are 1 mV and 5 msec (A, D, and E) and 2 mV and 5 msec (C).

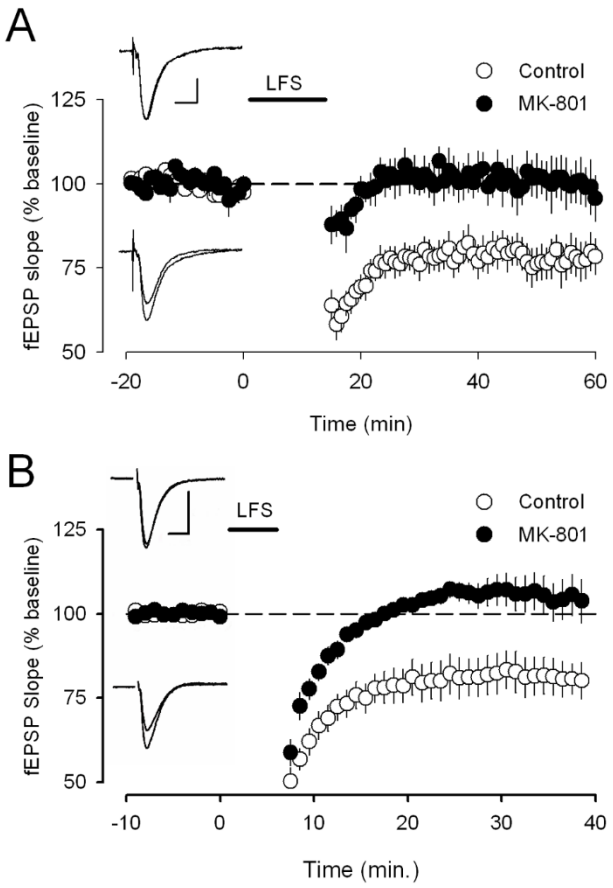

Figure 1-2 MK-801 blocks LTD induction in hippocampal CA1 region of slices from young animals.

A) MK-801 blocks 1 Hz LFS-induced LTD in slices from young C57BL/6 mice (open circles: interleaved control experiments, n = 7; filled circles: LFS in 10 μM MK-801, n = 6, $p < 0.05$ compared to control). **B)** MK-801 blocks 2 Hz LFS-induced LTD in slices obtained from young CD1 mice. Slices were incubated in ACSF containing 50 μM MK-801 for 2-6 hours prior to 2 Hz LFS and MK-801 was washed out following LFS (filled symbols, n = 8, $p < 0.05$ compared to control). Open symbols: results from interleaved control experiments (n = 8). Traces in A and B show superimposed fEPSPs recorded during baseline and post LFS in control (bottom) and MK-801 (top) experiments. Calibration bars are 1 mV and 10 msec (A) and 0.5 mV and 10 msec (B).

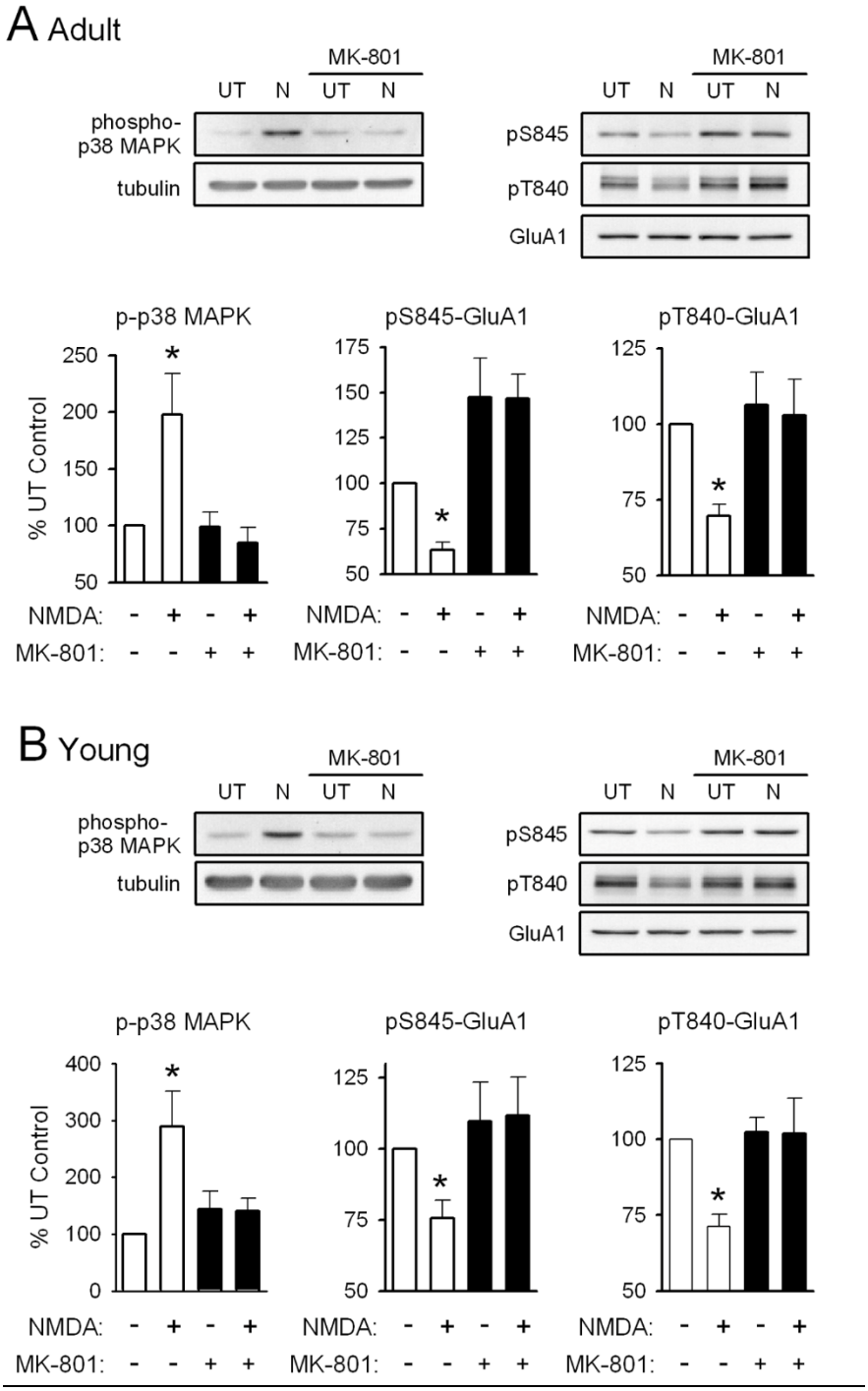
A Adult
MK-801
UT N UT N
phospho-
p38 MAPK
tubulin
pS845
pT840
GluA1
p-p38 MAPK
pS845-GluA1
pT840-GluA1
% UT Control
NMDA:
MK-801:
B Young

Figure 1-3 MK-801 blocks activation of p38-MAPK and AMPAR GluA1 subunit dephosphorylation induced by NMDAR activation.

A) MK-801 blocks NMDA-induced increases in p38-MAPK phosphorylation and GluA1 dephosphorylation at serine 845 and threonine 840 in CA1 mini-slices from adult mice ($[Ca^{2+}]_o$ = 4.0 mM, n = 6). Although basal levels of GluA1 S845 phosphorylation tended to be elevated in MK-801 treated slices, this difference was not statistically significant ($p = 0.065$). **B)** NMDA-induced increases in p38-MAPK phosphorylation and GluA1 phosphorylation are blocked by MK-801 in hippocampal slices from young mice ($[Ca^{2+}]_o$ = 2.0 mM, n = 5). *$p < 0.05$ compared to untreated control slices.

1.6 References

Bröcher S, Artola A, Singer W (1992) Intracellular injection of Ca^{2+} chelators blocks induction of long-term depression in rat visual cortex. Proc Natl Acad Sci USA 89:123–127.

Chen X, Lin R, Chang L, Xu S, Wei X, Zhang J, Wang C, Anwyl R, Wang Q (2013) Enhancement of long-term depression by soluble amyloid β protein in rat hippocampus is mediated by metabotropic glutamate receptor and involves activation of p38MAPK, STEP and caspase-3. Neuroscience 253:435–443.

Collingridge GL, Peineau S, Howland JG, Wang YT (2010) Long-term depression in the CNS. Nat Rev Neurosci 11:459–473.

Crozier RA, Wany Y, Liu CH, Bear MF (2007) Deprivation-induced synaptic depression by distinct mechanisms in different layers of mouse visual cortex. Proc Natl Acad Sci USA 104:1383–1388.

Cummings JA, Mulkey RM, Nicoll RA, Malenka RC (1996) Ca^{2+} signaling requirements for long-term depression in the hippocampus. Neuron 16:825–833.

Debanne D, Gähwiler BH, Thompson SM (1994) Asynchronous pre- and postsynaptic activity induces associative long-term depression in area CA1 of the rat hippocampus in vitro. Proc Natl Acad Sci USA 91:1148–1152.

Delgado JY, Coba M, Anderson CNG, Thompson KR, Gray EE, Heusner CL, Martin KC, Grant SGN, O'Dell TJ (2007) NMDA receptor activation dephosphorylates AMPA receptor glutamate receptor 1 subunits at threonine 840. J Neurosci 27:13210–13221

Dudek SM, Bear MF (1992) Homosynaptic long-term depression in area CA1 of hippocampus and effects of N-methyl-D-aspartate receptor blockade. Proc Natl Acad Sci USA 89:4363–4367.

Holthoff K, Kovalchuk Y, Yuste R, Konnerth A (2004) Single-shock LTD by local dendritic spikes in pyramidal neurons of mouse visual cortex. J Physiol 560:27–36.

Huettner JE, Bean BP (1988) Block of N-methyl-D-aspartate-activated current by the anticonvulsant MK-801: selective binding to open channels. Proc Natl Acad Sci USA 85:1307–1311.

Husi H, Ward MA, Choudhary JS, Blackstock WP, Grant SG (2000) Proteomic analysis of NMDA receptor-adhesion protein signaling complexes. Nat Neurosci 3:661–669.

Kessels HW, Nabavi S, Malinow R (2013) Metabotropic NMDA receptor function is required for β-amyloid-induced synaptic depression. Proc Natl Acad Sci USA 110:4033–4038.

Kollen M, Dutar P, Jouvenceau A (2008) The magnitude of hippocampal long term depression depends on the synaptic location of activated NR2-containing N-methyl-D-aspartate receptors. Neuroscience 154:1308–1317.

Lee HK, Barbarosie M, Kameyama K, Bear MF, Huganir RL (2000) Regulation of distinct AMPA receptor phosphorylation sites during bidirectional synaptic plasticity. Nature 405:955–959.

Lee HK, Kameyama K, Huganir RL, Bear MF (1998) NMDA induces long-term synaptic depression and dephosphorylation of the GluR1 subunit of AMPA receptors in hippocampus. Neuron 21:1151–1162.

Lerma J, Margues JM (2013) Kainate receptors in health and disease. Neuron 80: 292-311.

Li S, Jin M, Koeglsperger T, Shepardson NE, Shankar GM, Selkoe DJ (2011) Soluble Aβ oligomers inhibit long-term potentiation through a mechanism involving excessive activation of extrasynaptic NR2B-containing NMDA receptors. J Neurosci 31:6627–6638.

Lüscher C, Malenka RC (2012) NMDA receptor-dependent long-term potentiation and long-term depression (LTP/LTD). Cold Spring Harbor Perspectives in Biology 4: a005710.

Mulkey RM, Endo S, Shenolikar S, Malenka RC (1994) Involvement of a calcineurin/inhibitor-1 phosphatase cascade in hippocampal long-term depression. Nature 369:486–488.

Mulkey RM, Malenka RC (1992) Mechanisms underlying induction of homosynaptic long-term depression in area CA1 of the hippocampus. Neuron 9:967–975.

Nabavi S, Kessels HW, Alfonso S, Aow J, Fox R, Malinow R (2013) Metabotropic NMDA receptor function is required for NMDA receptor-dependent long-term depression. Proc Natl Acad Sci USA 110:4027–4032.

Neveu D, Zucker RS (1996) Postsynaptic levels of $[Ca^{2+}]_i$ needed to trigger LTD and LTP. Neuron 16: 619-629.

Ngezahayo A, Schachner M, Artola A (2000) Synaptic activity modulates the induction of bidirectional synaptic changes in adult mouse hippocampus. J Neurosci 20:2451–2458.

Norris CM, Korol DL, Foster TC (1996) Increased susceptibility to induction of long-term depression and long-term potentiation reversal during aging. J Neurosci 16:5382–5392.

Oliet SH, Malenka RC, Nicoll RA (1997) Two distinct forms of long-term depression coexist in CA1 hippocampal pyramidal cells. Neuron 18:969–982.

Palmer CL, Lim W, Hastie PGR, Toward M, Korolchuk VI, Burbidge SA, Banting G, Collingridge GL, Isaac JTR, Henley JM (2005) Hippocalcin functions as a calcium sensor in hippocampal LTD. Neuron 47:487–494.

Paoletti P, Bellone C, Zhou Q (2013) NMDA receptor subunit diversity: impact on receptor properties, synaptic plasticity and disease. Nat Rev Neurosci 14:383–400.

Raymond CR, Ireland DR, Abraham WC (2003) NMDA receptor regulation by amyloid-beta does not account for its inhibition of LTP in rat hippocampus. Brain Res 968:263–272.

Tamburri A, Dudilot A, Licea S, Bourgeois C, Boehm J (2013) NMDA-receptor activation but not ion flux is required for amyloid-beta induced synaptic depression. PLoS One 8:e65350.

Vissel B, Krupp JJ, Heinemann SF, Westbrook GL (2001) A use-dependent tyrosine dephosphorylation of NMDA receptors is independent of ion flux. Nat Neurosci 4:587–596.

Waxman EA, Lynch DR (2005) N-methyl-D-aspartate receptor subtype mediated bidirectional control of p38 mitogen-activated protein kinase. J Biol Chem 280:29322–29333.

Xiao L, Hu C, Feng C, Chen Y (2011) Switching of N-methyl-D-aspartate (NMDA) receptor-favorite intracellular signal pathways from ERK1/2 protein to p38 mitogen-activated protein kinase leads to developmental changes in NMDA neurotoxicity. J Biol Chem 286:20175–20193.

Yang L, Mao L, Tang Q, Samdani S, Liu Z, Wang JQ (2004) A novel Ca^{2+}-independent signaling pathway to extracellular signal-regulated protein kinase by coactivation of NMDA receptors and metabotropic glutamate receptor 5 in neurons. J Neurosci 24:10846–10857.

Zhu JJ, Qin Y, Zhao M, Van Aelst L, Malinow R (2002) Ras and Rap control AMPA receptor trafficking during synaptic plasticity. Cell 110:443–455.

2 CHAPTER II: Misaligned Feeding Impairs Hippocampus Dependent Memories

2.1 Introduction

The circadian system is a finely tuned network of central and peripheral oscillators headed by a master pacemaker, the suprachiasmatic nucleus (SCN), which governs daily rhythms in physiology and behaviour, including cognition. This network regulates cognitive processes (1, 2), and the neural circuits involved in learning and memory also exhibit circadian rhythms in gene expression and synaptic plasticity (3-6). Genetic disruption of these molecular oscillations has severe consequences on cognition (7-9). Environmental perturbations also have the capacity to disrupt synchrony and misalign this clock network (10-19) and are problematic as many people in our modern society extend their work and recreation into the night hours.

There has been mounting evidence that the timing of when we eat is critical for our metabolic health (20, 21). At this point, timing of food intake is well-established to have a major impact on the phase of the molecular oscillations in peripheral organs such as the liver and pancreas (22, 23). Mis-timed meals during the sleep phase accelerates weight gain compared with animals fed during their wake phase (24, 25), whereas wake-phase feeding has a protective effect against the cardiac and metabolic dysfunction caused by high fat diets (26, 27). Similar disruptive effects are seen in humans, where misaligned mealtimes produce cardiac and metabolic deficits, leading to a pre-diabetic state (28). We thus became interested in the possibility that these ill consequences of eating at inappropriate phases of the daily cycle may also be maladaptive for cognitive function. In this study, we sought to determine the effects of chronic but stable misalignment of the circadian network by scheduling access to food at an inappropriate phase of the daily cycle. We demonstrate that this simple manipulation has far-reaching consequences for learning and memory.

2.2 Results

Misaligned feeding alters diurnal rhythms of activity and sleep.

Mice were allotted a six hour window in which food was made available either during the middle of their active (aligned) or inactive (misaligned) phase (**Figure 2-1**). Mice adapted to the feeding protocol within 6 days ($P = 0.9$, **Fig. 2-2A**) and there were no significant differences in body weight between the two groups at the time of testing ($P = 0.5$, **Fig. 2-2B**). Daytime activity was increased in mice subjected to misaligned feeding ($P < 0.001$; **Fig. 2-3A, B**), and the strength of daily rhythms of activity was reduced by misaligned feeding ($P = 0.003$; **Fig. 2-3C**). Similarly, the temporal pattern of sleep was altered by misaligned feeding (**Fig. 2-3D**). Immobility-defined video monitoring of sleep behaviour of misaligned mice showed decreased time spent asleep during the day ($P < 0.001$) and a corresponding increase in sleep during the night ($P < 0.001$; **Fig. 2-3E**). Misaligned mice no longer exhibit a day vs night difference in sleep, sleeping equally during the day and night ($P = 0.5$). Crucially, the total time spent asleep over a 24 hr day was not reduced by misaligned feeding ($P = 0.2$). The change in temporal pattern of sleep quantity is also reflected in sleep fragmentation, where misaligned mice exhibit a greater number of sleep bouts ($P < 0.05$) with a corresponding decrease in average sleep bout duration ($P < 0.001$) during the day compared to aligned mice (**Fig 2-4**). This increased day-time sleep fragmentation is compensated by fewer ($P < 0.05$) and longer ($P < 0.001$) night sleep bouts in the misaligned animals, resulting in no significant change in the total number ($P = 0.9$) and average duration ($P = 0.6$) of sleep bouts over a 24 hr period.

Misaligned feeding alters phase of hippocampus without shifting the SCN.

Using *ex vivo* organotypic cultures of explants from PER2::LUC reporter mice subjected to aligned or misaligned feeding, we confirmed that daytime feeding shifts the phase of the liver oscillator ($P < 0.001$) without altering the phase of the SCN oscillator ($P = 0.07$; **Fig. 2.5A,C,D**). Importantly, we demonstrate that daytime feeding significantly misaligns the hippocampal oscillator by 14.1 hr ($P < 0.001$; **Fig. 2.5B, D**), with small but significant effects on the intrinsic properties of the oscillator, including period ($P = 0.05$; **Fig. 2.5E**) and damping rate ($P = 0.02$; **Fig 2.5F**).

Misaligned feeding blunts total CREB expression and reduces hippocampal long term potentiation.

We measured expression of phosphorylated CREB (pCREB) and total CREB (tCREB) in the hippocampus of aligned and misaligned mice at 6 hr intervals through a 24 hr day. pCREB protein levels were reduced in the misaligned animals at each time point, although significant differences were not detected (**Fig. 2-6A, B**). Strikingly, expression of tCREB was significantly reduced by misaligned feeding ($P < 0.01$; **Fig. 2-6A, C, D**), with the strongest effects in the day (*post hoc* $P < 0.05$ for ZT 2, 8, and 20). This decrease in tCREB levels was uniformly observed throughout the hippocampus (**Fig. 2-6D**).

Long term potentiation (LTP) responses of the dorsal hippocampus were measured during the day from mice subjected to aligned or misaligned feeding. LTP was significantly impaired in the misaligned group ($P < 0.05$; **Fig. 2-6E**), indicating significant deficits in synaptic plasticity in the misaligned hippocampus. This decrease in LTP is specific to the misaligned feeding treatment and not due to an LTP-boosting effect by aligned feeding (**Fig. 2-8**). To determine the impact of

misaligned feeding on presynaptic neurotransmitter release probability, paired pulse facilitation (PPF) experiments were performed at 25, 50, 100 and 250 msec intervals. There were no significant differences between the aligned and misaligned PPF ratios (P = 0.5; **Fig. 2-6F**), and EPSP profiles were similar.

Misaligned feeding affects hippocampal-dependent learning and memory.

To test our hypothesis that misaligning the hippocampal oscillator from the SCN oscillator is detrimental to learning and memory, we subjected aligned and misaligned mice to hippocampal-dependent contextual fear conditioning. Mice were trained to associate a specific novel context to a fearful stimulus in the form of a mild shock. Both aligned and misaligned mice acquired freezing behaviour during the training trial (**Fig. 2-9**). When tested 24 hr later by replacing the mice in the same context, the misaligned mice exhibited a significant reduction in fear-conditioned behaviour (ZT 2, $P < 0.0001$; **Fig. 2-9A, left**), indicating that circadian misalignment affects long term memory. Performance on the fear conditioning test is dependent on time of day and performance peaks in the early day (2, 3, 14). To test for the possibility that misaligned mice have an inverted peak performance time, we trained and tested a separate cohort of mice at the opposite time of day (night, ZT 14). Both aligned and misaligned groups acquired freezing behaviour (**Fig. 2-10**). Two way comparisons revealed a time of day effect on recall ($P < 0.001$) and an interaction between time of day and treatment ($P < 0.001$). Recall was significantly reduced in the aligned mice compared to the daytime tests (*post hoc* $P < 0.001$), but did not significantly change with time of day in misaligned mice (*post hoc* $P = 0.3$). Night-tested aligned and misaligned mice exhibited equally poor recall (*post hoc* $P = 0.4$; **Fig. 2.9A, right**), ruling out the possibility that the misaligned mice have an altered peak phase of cognition.

We applied the novel object recognition test to examine cognition that peaks during the night in nocturnal rodents (13). The misaligned mice exhibited significantly reduced novel object recognition (NOR) during night-time tests (ZT 21, $P < 0.001$; **Fig. 2-9B, right**), indicating decreased cognitive performance. Day-time tests of a separate cohort of aligned and misaligned found no differences between both groups (**Fig. 2-9B, left**), ruling out the possibility that peak performance of misaligned mice has shifted to the opposite phase. Two factor analysis revealed a significant effect of feeding condition ($P = 0.003$) and an interaction between time of day and feeding condition ($P = 0.02$). Specifically, aligned mice showed reduced NOR during the day (*post hoc* $P = 0.04$), and day-tested misaligned mice were not significantly different from aligned (*post hoc* $P = 0.6$).

2.3 Discussion

Many people in our society find themselves working or playing during their normal sleep times. Due to these schedules, we eat around the clock with well-established literature of metabolic consequences (21). In this study, we sought to determine if temporally restricted feeding schedules in mice could impact cognition. We found that time-restricted feeding had dramatic negative effects on commonly used learned behaviours such as hippocampal-dependent contextual fear conditioning and novel object recognition. Not all behavioural tests were similarly affected, as amygdala-dependent cued-fear conditioning was not altered by the misalignment. This implies that some learned behaviours are more vulnerable to the impact of misaligned feeding. Crucially, the total amount of sleep was not altered by the scheduled feeding and the mice did not lose weight as might be expected if their caloric intake was restricted. Hence, by simply adjusting the time of food access, we demonstrated that we can alter the cognitive performance of mice. We do not

know yet if this equally applies to humans but shift work has been associated with decreased performance on cognitive tests (29-31).

The importance of sleep for memory is well-documented, where both the amount of sleep and the quality of sleep have been found to be critical for memory consolidation (reviewed in 32). The misaligned feeding treatment did not result in an overall decrease in amount of sleep, but instead had a severe impact on the temporal pattern of sleep, suggesting that this treatment acts via disruption of the circadian timing of sleep. While sleep quality as assessed by polysomnography was not assessed in this study, we were able to examine the degree of sleep fragmentation as determined by the number and duration of individual sleep bouts. Misaligned feeding again has a greater impact on the temporal pattern of sleep fragmentation, where the misaligned mice appear to "catch up" on consolidated sleep during what should be their active phase.

Mechanistically, we used the clock-driven rhythms in bioluminescence to demonstrate that the altered feeding time not only shifted the peripheral clocks in the liver, but also altered the circadian clock in the hippocampus. This finding is consistent with earlier literature suggesting the phasing of the molecular clock in the corticolimbic system and hippocampus are strongly influenced by the time of food availability (33-35). We have thus created a situation in which the molecular clocks within the nervous system are running at different phases, *i.e.* internal desynchronisation of the circadian system. A consequence of this misalignment is altered synaptic plasticity within the hippocampal circuit (Schaffer Collaterals/CA1) as revealed by the reduction in LTP. This is the first demonstration that the time of eating can impact the physiological underpinning of learned behaviour. Importantly, our manipulation of feeding causes a significant decline in CREB in the hippocampus, which has been demonstrated to be critical for memory

allocation in mice (e.g. 36, 37). The levels of tCREB were reduced at all phases that we sampled (ZT 2, 8, 14, and 20). Although we did not carry out learning tests at each of these phases, the tCREB data indicates that memory would be impaired throughout the daily cycle. The reduction in tCREB provides a biochemical explanation for our finding, as well as providing a guidepost for future analysis of the effects of the misaligned feeding in the hippocampus. Therefore, this work raises the possibility that the timing of when we eat alters the physiological and biochemical events underlying learning and memory.

2.4 Methods

Animals

All experimental protocols used in this study were approved by the UCLA Animal Research Committee. UCLA Division of Laboratory animal recommendations for animal use and welfare, as well as National Institutes of Health guidelines were followed. Adult (2-4 month old) male C57BL/6N wild-type mice (UCLA) were housed in a 12:12-hour lighting (LD) cycle with *ad libitum* access to food and water. For the bioluminescence experiments, PER2::LUC knock-in homozygotes on the C57Bl/6J background were used (38). Mice were first entrained to a 12:12 LD cycle for a minimum of 2 weeks prior to further manipulations. For measurements of activity, sleep, and food consumption, mice were individually housed in cages. For bioluminescence measurements, learning and memory tests, hippocampal physiology, biochemistry and anatomy, mice were housed in groups of 3-5 mice per cage. Group-housed animals showed similar activity and food consumption patterns as singly housed animals.

Scheduled food access

Mice entrained to a 12:12 LD cycle were randomly sorted into two groups per experiment. Cages were topped with wire grids adapted to restrict access to the food chamber, which enabled us to provide access to food during specific times of day (**Fig. 2-1**). We visually verified that food pellets or powder were not being hoarded in nesting or bedding materials, but did not empty the cage bottoms to avoid excessive handling stress to the animals. Both groups were given a 6 hour window per 24 hr day to access the food chamber. Mice in one group were given access to the food chamber during the middle of the dark phase from Zeitgeber Time (ZT; ZT 0 equates to lights on) 15 to 21, aligned to their active phase. Mice in the second group were given automated access to the food chamber during the middle of the light phase from ZT 3 to 9, misaligned from what should have been their active phase. Scheduled food access was applied for 2 weeks prior to and for the entire duration of all experiments. The exceptions were for the data described in **Fig. 2-2** and **Fig. 2-3a**: food consumption and activity, for which we monitored the mice from day 1 of scheduled food access.

Activity monitoring

Mice were individually housed in automated feeding cages with a top-mounted passive infrared motion sensor (Honeywell IS-215T) to detect cage activity (aligned $n = 8$, misaligned $n = 8$). Data was collected using the Vital View system (Mini Mitter) and analysed as previously described for wheel running activity using the El Temps software (39). Specifically, nocturnality was calculated by determining the percentage of activity conducted during the dark phase (ZT 12-24) from 7 days of activity monitoring (days 8 to 14 of scheduled feeding). Power of diurnal

activity rhythms was determined from the same 7 days using fast fourier transform and reported as %V.

Immobility-defined sleep measurements

Following activity monitoring, sleep-wake behaviour from the same cohort of aligned (*n* = 8) and misaligned (*n* = 8) mice was measured using continuous video recording and automated mouse tracking as previously described (39). Mice were maintained in the same automated feeding cages under the same lighting cycle and feeding schedule, and continuous video recording was performed from days 15 to 17 of scheduled feeding. Side-on views of the cage were acquired using CCTV cameras (Gadspot, GS-335C, City of Industry, CA), and the ANY-maze software (Stoelting Co., Wood Dale, IL) was used to track the animals. Prior work by Fisher and colleagues established the parameters for immobility detection (95% immobility of the area of the animal, for a minimum of 40 sec) by correlation with EEG/EMG recordings (40). Immobility-defined sleep in 1 min bins from days 16 to 17 of scheduled feeding were averaged, and day (ZT 0-12) and night (ZT 12-24) sleep were compared. Average waveforms for display purposes were generated by smoothing the data using 1 hr running averages.

PER2-driven bioluminescence activity in ex vivo organotypic cultures

PER2::LUC male mice (2-3 mo) were subjected to either aligned (*n* = 8) or misaligned (*n* = 8) feeding for 2 weeks prior to sampling. Mice were sacrificed after anaesthesia (isoflurane) between ZT 10 and 11, and 1-2 mm^3 liver explants were immediately dissected in ice-cold Hanks' balanced salt solution (HBSS; Sigma) supplemented with 4.5 mM $NaHC0_3$, 10 mM HEPES and 100 U/ml penicillin-streptomycin as previously described (41). Brains were incubated in ice-cold slice solution (in mM: 26 $NaHCO_3$, 1.25 NaH_2PO_4, 10 glucose, 125 NaCl, 3 KCl, 5 $MgCl_2$, 1

$CaCl_2$) aerated with 95% O_2 / 5% CO_2 for 5 min, and 300 µm coronal sections were collected using a vibratome and further microdissected in HBSS under a 10X dissecting microscope. The SCN was cut away from the rest of the section using two cuts with a surgical scalpel (No. 21 blade, Fisher Sci.). To acquire the hippocampal explant, the dorsal-most section (Bregma -1.2 to -1.6 mm) was microdissected to liberate the hippocampus and dentate gyrus by gently teasing away the cortex with scalpels (No. 11 blade, Fisher Sci.). All explants were individually transferred to Millicell membranes (0.4µm, PICMORG50, Millipore, Bedford, MA) resting on 1.2 ml of recording media: (1X DMEM (Sigma), 1X B27 supplement (Gibco), 4.5 mM $NaHCO_3$, 10 mM HEPES, 40 mM Glutamax (Gibco), 4.5 mg/ml D-glucose, 25 U/ml penicillin, 25 U/ml streptomycin, 0.1 mM sodium salt monohydrate luciferin (Biosynth, Staad, Switzerland)) in a 35 mm dish sealed with autoclaved vacuum grease (Dow Corning, Midland, MI). SCN, hippocampus and liver explants were inserted into the Lumicycle photometer (Actimetrics, Wilmette, IL), incubated at 37 ºC, and bioluminescence was continuously monitored for 7 consecutive days. Raw bioluminescence values were normalized by baseline subtraction (24 hr running average) and smoothed with 2 hr windows to prepare the representative bioluminescence traces. The phase and damping rate of each explant were determined as previously described (41). Period was determined using the sine-wave fit function in Lumicycle Analysis (Actimetrics).

Western immunoblotting

Hippocampi were rapidly dissected and homogenized in lysis buffer (50mM Tris-HCl, 0.25% (w/v) sodium deoxycholate, 150mM NaCl, 1mM EDTA, 1% Nonidet P40, 1mM sodium vanadate, 1mM AEBSF, 10ug/ml Aprotinin, 10ug/ml Leupeptin, 10ug/ml Pepstatin, and 1 mM sodium fluoride). Total protein concentration in cleared extracts was estimated using Pierce's BCA

(bicinchoninic acid) Protein Assay Kit (Thermo Fisher Scientific) using bovine serum albumin as a standard. Western blots were performed as previously described (42, 43). Each extract was analysed for relative protein levels of phosphoCREB by using an antibody directed against the phosphorylated form at Ser133 (rabbit polyclonal, Millipore) and then for tCREB (rabbit polyclonal, Millipore). Equal protein loading was verified by Ponceau S solution (Sigma) reversible staining of the blots and each extract was also analysed for relative protein levels of β-actin (Sigma). Relative intensities of the protein bands were quantified by scanning densitometry using the NIH Image Software (Image J, http://rsb.info.nih.gov/ij/), and each value background-corrected. Data are shown as arbitrary units and are the average ± SEM of 4-5 animals/group. We confirmed by two way ANOVA comparisons that levels of β-actin do not vary with time of day in either group (P = 0.9) and is no different between aligned and misaligned mice (P = 0.9; **Fig. 2-7**).

Immunohistochemistry

Mice were perfused intracardially with 4% paraformaldehyde (PFA). Brains were dissected out, post-fixed in 4% PFA at 4°C overnight, cryoprotected in 15% sucrose. Immunolabelling of frozen sections (30 μm) was performed as previously described(44). Briefly, sections were blocked in carrier solution (1% BSA and 0.3% Triton X-100) containing 20% normal goat serum for 1 hr and incubated for 48h at 4°C with primary antibodies against tCREB (1:500 rabbit polyclonal, Millipore) diluted in carrier solution containing 5% normal goat serum. Sections were incubated with a goat anti-rabbit secondary antibodies conjugated to Cy3 (Jackson ImmunoResearch Laboratories) and mounted with Vectashield medium with DAPI (4′,6-diamidino-2-phenylindole; Vector Laboratories). Immunostained sections were visualized using a

Zeiss Axio Imager 2 with an AxioCam MRm and the ApoTome imaging system. Images were acquired using a 5X objective, in order to visualize the entire hippocampus.

Hippocampal slice preparation and electrophysiology

Hippocampal slice preparation and electrophysiological recordings were performed as previously described (45). Briefly, slices (400 µm) were maintained in oxygenated (95% O_2 / 5% CO_2), warmed (30 °C) artificial cerebrospinal fluid (ACSF) containing 124 mM NaCl, 4.4 M KCl, 25 mM $NaHCO_3$, 1.0 mM NaH_2PO_4, 2.0 mM $CaCl_2$, 1.2 mM $MgSO_4$, and 10 mM glucose, and allowed to recover for at least 2 hr prior to the start of an experiment. A bipolar, nichrome wire stimulating electrode was placed in stratum radiatum of the hippocampal CA1 region to activate Schaffer collateral–commissural fibre synapses and an extracellular glass microelectrode filled with ACSF (resistance = 5–10 MΩ) was used to record evoked field excitatory postsynaptic potentials (fEPSPs). Extracellular recordings were done under interface conditions. The intensity of presynaptic fibre stimulation was adjusted to evoke fEPSPs with amplitude approximately 50% of the maximal fEPSP amplitude that could be elicited in each slice. fEPSPs were then elicited at 0.02 Hz throughout the experiment. LTP was induced by high-frequency stimulation (HFS, 2 trains of 100 Hz stimulation, 1 sec duration, inter-train interval = 10 sec). The average slope of fEPSPs normalized to baseline measured between 55 and 60 min post-HFS was used for statistical comparisons (two tailed *t* tests). The paired pulse stimulation pulses were delivered with interpulse intervals of 25, 50, 100 and 200ms.

Fear conditioning (FC)

Contextual fear conditioning was performed as previously described (2, 8, 14) with minor modifications. In brief, aligned and misaligned mice were tested and trained either in the day (ZT

2) or the night (ZT 14). Mice were trained and tested only once to avoid effects of prior manipulation. Results reported for daytime and night-time tests are from distinct cohorts of animals. Mice were habituated to the testing room for 30 min under the relevant lighting conditions (dim red light, 2 lux, at night). The animals were individually introduced to the novel environment (shock chamber) and allowed to familiarize to context for 3 min, after which the mice were trained to associate the context with a fearful unconditioned stimulus (US): foot-shock (0.2 mA). The training protocol consisted of 2 US with an inter-trial interval of 64 sec. At the end of the last US, mice were left in the chamber for a further 64 sec, after which they were returned to their home cages. 24 hr later, mice were placed individually into the same conditioning chamber for 6 min. Video recordings of the acquisition and recall tests were done with CCTV (Gadspot) cameras with supplemental infrared lighting during both times of day. Freezing behaviour was scored as previously described (2). Cued fear conditioning was performed as previously described (8). Using the same stimulus protocol as contextual FC, 30 sec of white noise (80 dB; conditioned stimulus, CS) preceded the presentation of US1 and US2. 24 hr later, mice were placed individually into a novel testing chamber. Following 2 min of baseline, the cued tone was presented for 2 min; mice were left in the chamber for a further 2 min. Freezing behaviour was scored as previously described.

Novel object recognition (NOR)

Habituation to the testing arena, object familiarization, and testing for NOR over 5 consecutive days were performed in the active phase at ZT 21 (n = 8 per feeding condition) for night-time tests under dim red light (2 lux), with day tests at ZT 9 (n = 8 per feeding condition). Mice were habituated to the testing arena (60 x 48 x 30 cm) in 10 min trials on 2 consecutive days.

During familiarization trials, two identical objects were placed equidistant from each other and the walls of the arena, and mice were allowed to explore the arena for 10 min on 2 consecutive days. Mice that failed to travel 20 m or interact with objects for more than 20 sec in the second familiarization trial were eliminated from further analysis. On the day of testing for NOR, one familiar object was replaced with a novel object with a different shape and made of a different material (plastic or glass). The testing trial was 5 min in duration. Arenas and objects were wiped between animals with 10% Windex and dried using paper towels. Video feeds of each arena from an overhead CCTV camera supplemented with infrared lighting were fed to the ANY-maze software. The arena and object maps were defined in ANY-maze, and allowed for automated tracking of the animal's area, with the ability to distinguish between the head and tail. Entry of the animal's head to the defined object's area was scored for time interacting with the object. An experimenter watched the recorded videos and overlaid tracking in real-time to verify that tracking of the animal's area and head/tail orientation was consistent and that scoring of object interaction was accurate. Performance on the NOR test is indicated by a discrimination index calculated of time spent with the novel object (T_{novel}) divided by the sum of time spent with both objects ($T_{novel}+T_{familiar}$). One animal from the misaligned group (out of 8) tested during the day failed to sufficiently explore both objects (< 10 sec during the second familiarization trial) and was eliminated from further analysis. For all novel object recognition experiments, mice were trained and tested only once to avoid effects of prior manipulation. Results reported for daytime and night-time tests are from distinct cohorts of animals.

Statistical analysis

All statistical analysis was performed using Sigma Stat (ver. 12). Effects of misaligned feeding on activity, sleep, PER2-driven bioluminescence, and LTP were determined using unpaired *t*-tests in comparison to the aligned group. In cases of unequal variance, the Mann-Whitney rank sum test was applied. To determine the effects and interaction of time of day and scheduled feeding condition on protein expression, and hippocampal-dependent learning and memory, we applied two factor analysis of variance (ANOVA) tests. The Holm-Sidak *post hoc* test was used to distinguish differences due to misaligned feeding. Differences with $P < 0.05$ were deemed significant in all analyses. Where appropriate (**Fig. 2-3, 2-5, 2-9**), box plots indicate the 25^{th} and 75^{th} percentiles, with error whiskers indicating the 10^{th} and 90^{th} percentiles. Values in the text, line graphs, and bar graphs are reported as mean ± standard error mean (SEM).

2.5 Figures

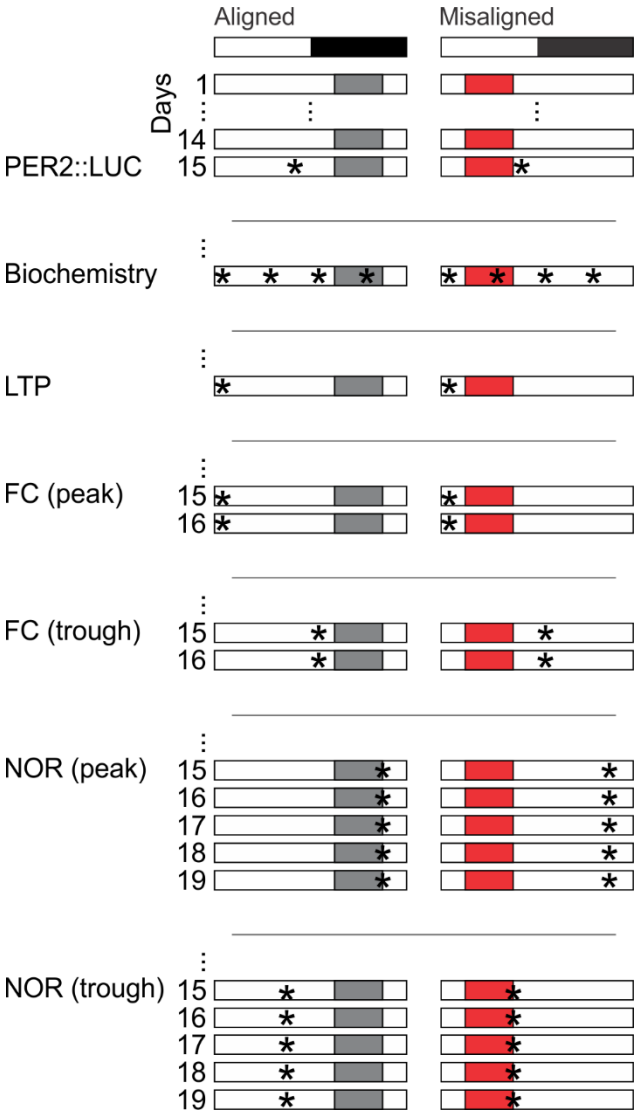

Figure 2-1 Cartoon schematic of experimental design.

Standard mouse cages were modified to restrict access to the food chamber. Access was controlled by a motorized gate controlled by timed relay switches. Mice could only access food pellets when the gate was lifted (6 hr), and positive drive of the motor kept the gate closed for the remaining 18 hr. The scheduled feeding protocol was maintained for a minimum of 2 weeks prior to and during sample collections and behavioural tests, indicated by *.

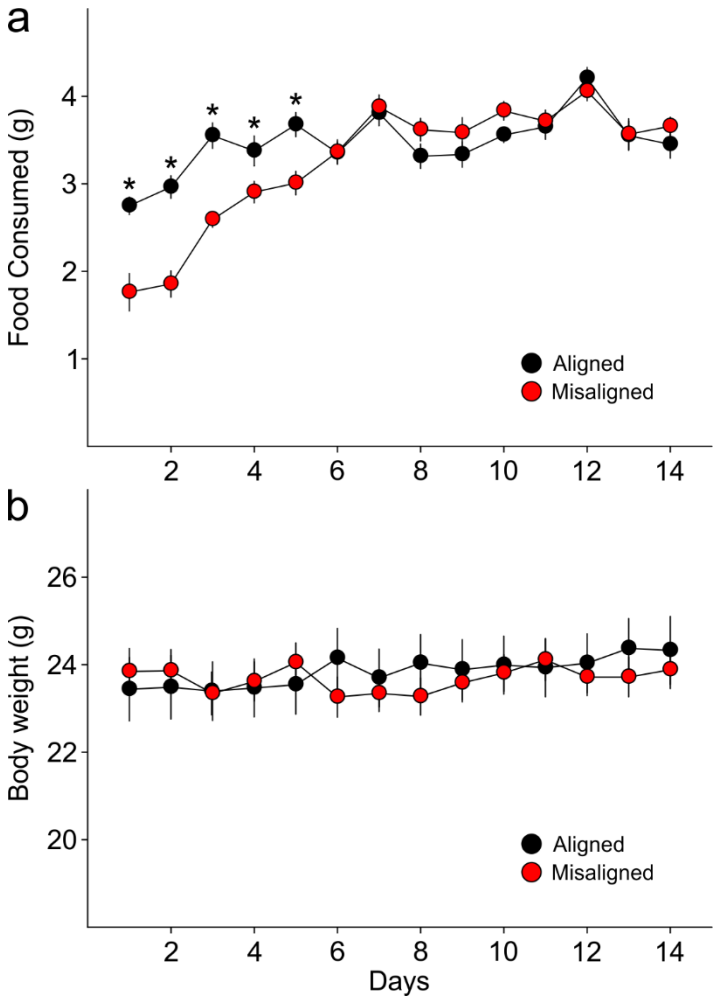

Figure 2-2 Food pellets in the automated feeding chambers were weighed daily to determine the amount of food consumed.

(**A**) Misaligned mice caught up with aligned mice in daily food consumption by day 6 of scheduled feeding ($P = 0.9$) and did not differ in food consumption subsequently (day 6-14 *post hoc* $P > 0.2$). (**b**) Mice were weighed daily prior to food access. Body weights between treatment groups did not differ significantly through the duration of scheduled feeding (two way ANOVA $P = 0.3$). Line graphs represent the mean ± SEM ($n = 16$ per treatment).

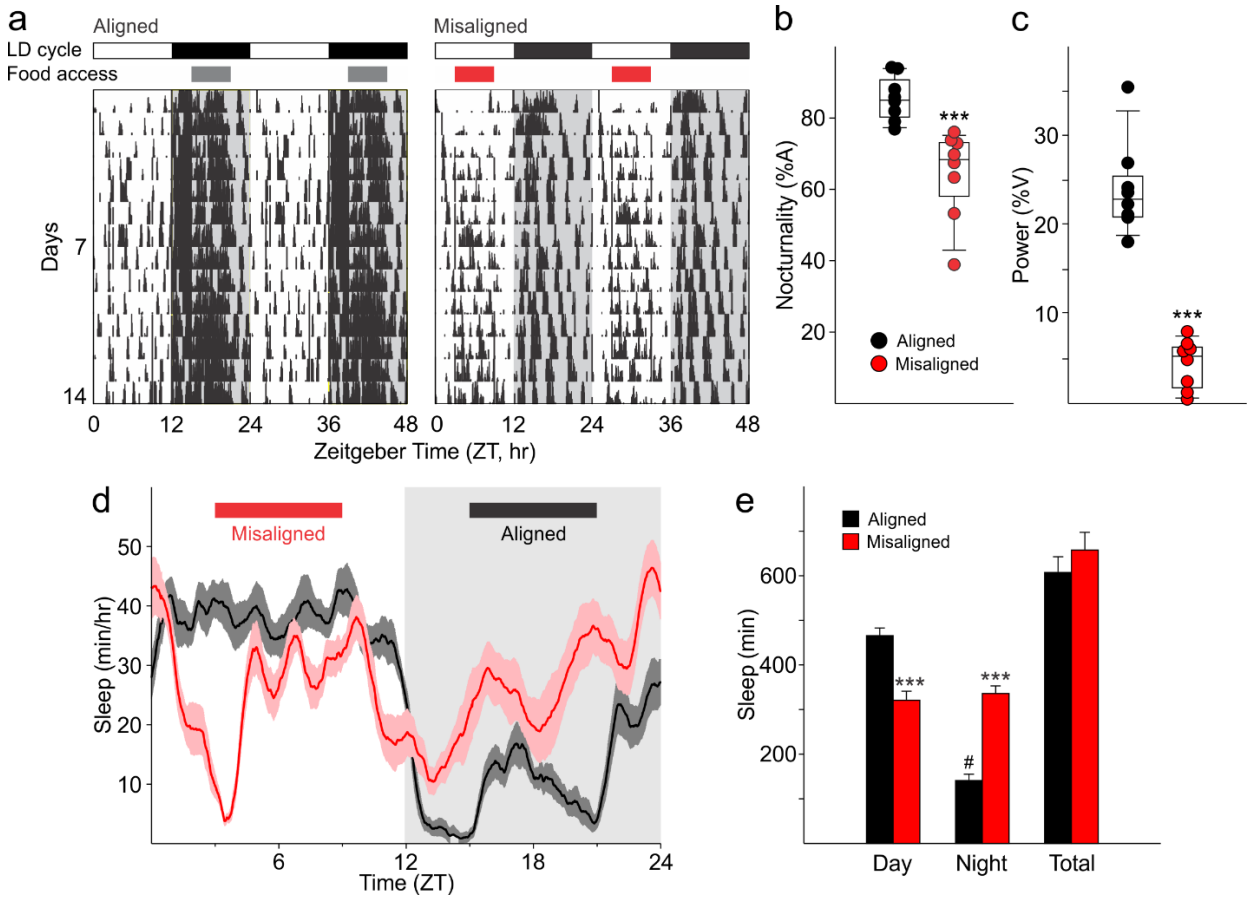

Figure 2-3 Altered temporal patterns of activity and sleep in mice subjected to misaligned feeding.

(**A**) Mice (*n* = 8 per treatment) were given 6 hr windows of food access during the middle of the night (aligned, grey) or day (misaligned, red). Representative double-plotted actograms show the increased daytime activity of the misaligned mice throughout the treatment in a 12 hr:12hr light:dark (LD) cycle. Grey shading in the actograms indicates lights off. (**b**) Nocturnality (% activity in the night) is reduced in misaligned mice (***$P < 0.001$). (**c**) Rhythm strength measured by the amplitude of a chi-square periodogram (%V) is reduced in misaligned mice (**$P < 0.01$). Box and whisker plots display the 25th to 75th percentiles, and the 10th to 90th percentiles respectively, with the median indicated by a line. (**d**) Sleep was measured by video monitoring after 2 weeks of scheduled food access (*n* = 8 per treatment). Running averages of immobility-defined sleep are shown for mice given aligned (black) and misaligned (red) access to food. The grey shading indicates lights off in a 12:12 LD cycle. (**e**) Total time spent asleep during the day

(12 hr), night (12 hr), or over 24 hr are shown. ***$P < 0.001$ as determined by *t*-tests of aligned vs misaligned groups; # $P < 0.001$ day vs night within treatment. Bar graphs represent the mean ± SEM.

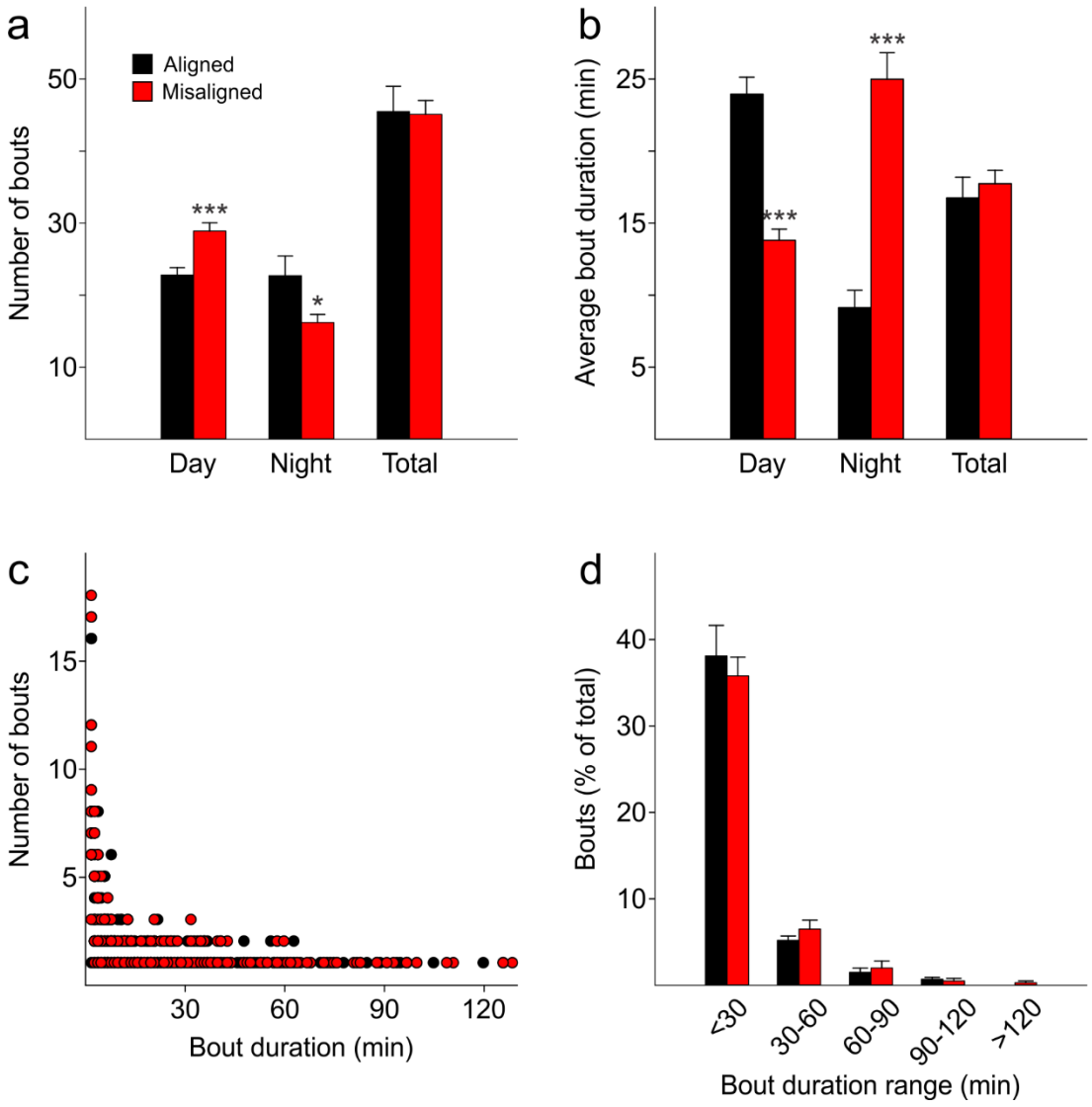

Figure 2-4 The temporal pattern of sleep fragmentation is altered by misaligned feeding without affecting overall sleep fragmentation over the 24 hr period.

(**a**) The number of sleep bouts during the day is increased in misaligned mice, decreased at night, and unchanged between groups when considered over 24 hr (total). (**b**) The average duration of a sleep bout is shorter in misaligned mice during the day, longer at night, and unchanged between groups over 24 hr (total). (**c,d**) The distribution of sleep bout lengths is similar between groups ($P = 0.3$). *$P < 0.05$, ***$P < 0.001$ as determined by *t*-tests of aligned vs misaligned groups. Bar graphs represent the mean ± SEM. Circles represent individual sleep bouts rounded to an integer minute.

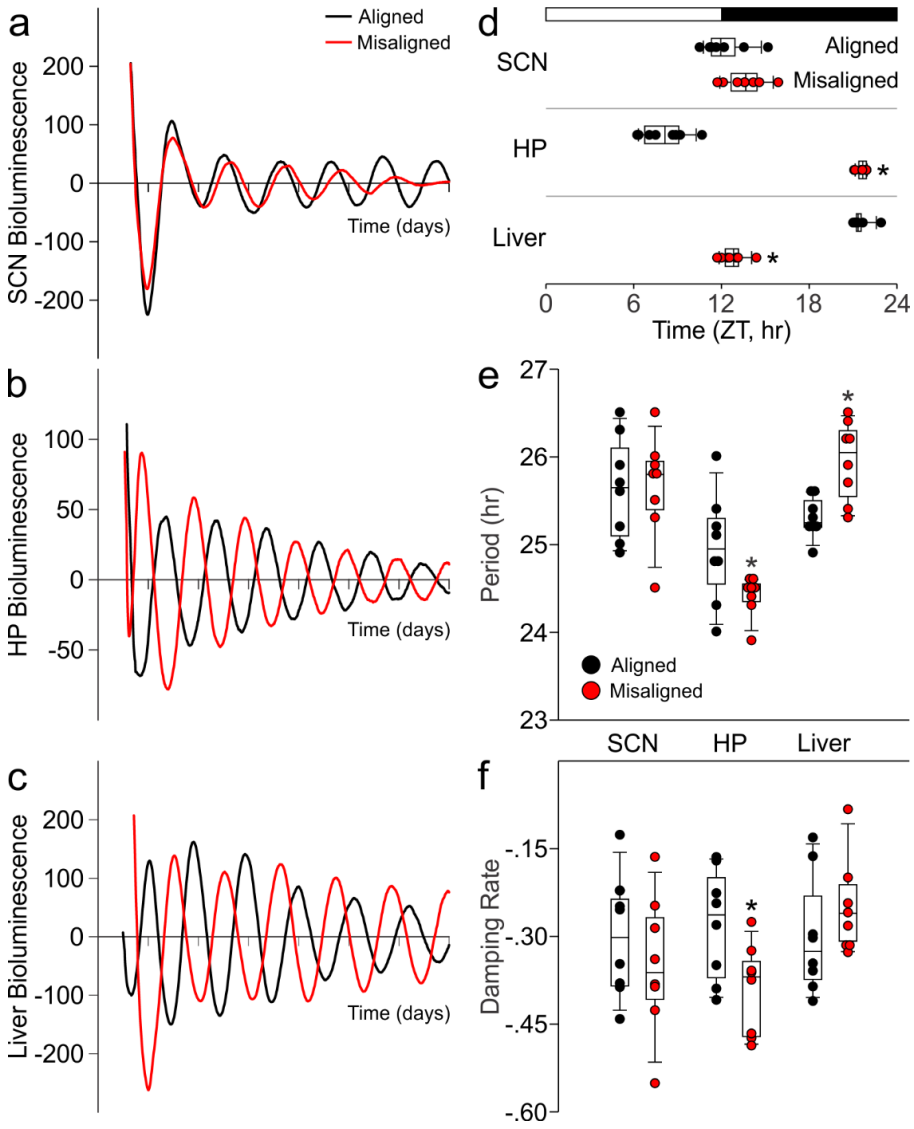

Figure 2-5 Differential impact of misaligned feeing on PER2-driven rhythms in bioluminescence of the SCN, hippocampus and liver (n = 8 per treatment).

Representative examples of baseline-subtracted traces of PER2-driven bioluminescence in the SCN (**a**), hippocampus (HP; **b**), and liver (**c**) explants from aligned (black) and misaligned (red) mice. (**d**) Phase relationship between the first calculated peaks of *ex vivo* bioluminescence plotted against time of the prior lighting cycle (ZT) shows a significant phase change in the HP and liver. (**e**) Period of bioluminescence rhythms were determined by sine wave fitting. (**f**) Damping rates were determined from 6 days in culture. * denotes significant differences (P < 0.05) between

aligned and misaligned samples. Box and whisker plots display the median as a line, the 25^{th} to 75^{th} percentiles, and the 10^{th} to 90^{th} percentiles respectively.

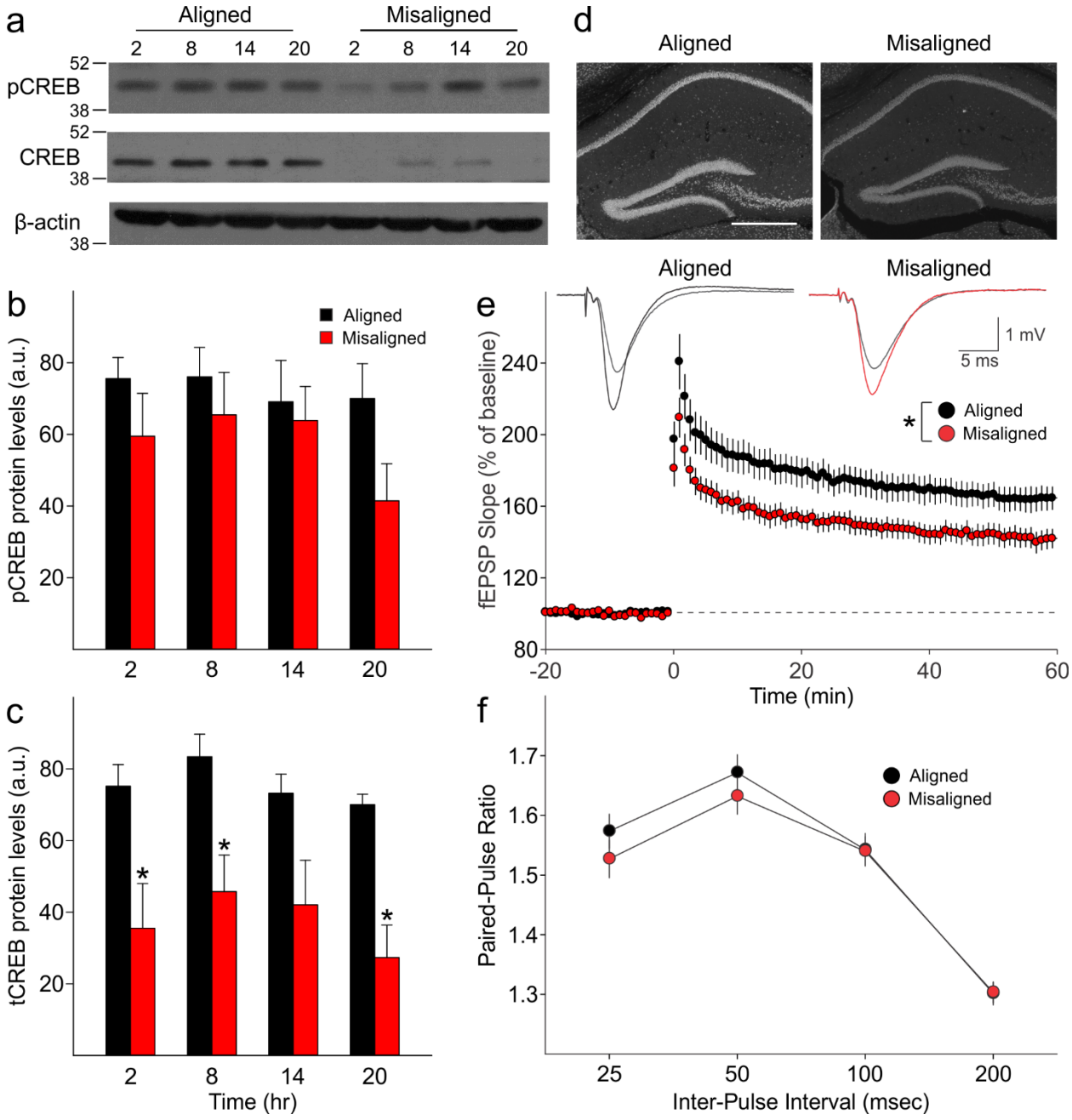

Figure 2-6 Reduced magnitude of hippocampal tCREB expression with a corresponding reduction in long term potentiation (LTP) in misaligned mice.

(**a**) Representative immunoblots show the decrease in tCREB expression levels in misaligned vs. aligned mice, sampled at 6 hr intervals through the daily cycle (ZT). (**b**) pCREB levels are not significantly altered. (**c**) Misaligned feeding led to significant decreases in the amount of tCREB

($P < 0.01$). * indicates significant differences between groups at each time point (*post hoc* $P < 0.05$). Protein levels are expressed as arbitrary units (a.u.). Bar graphs represent the mean ± SEM of aligned ($n = 4$) and misaligned ($n = 5$) animals per time point. (**d**) tCREB immunoreactivity is decreased throughout the hippocampus in misaligned mice. Scale bar = 500 µm. (**e**) LTP was induced by high-frequency stimulation of the Schaffer collateral fibres, 2 x 100 Hz, 1 sec duration, 10 sec inter-train interval, delivered at time = 0. Daytime LTP responses recorded from the CA1 region were significantly decreased in misaligned mice ($n = 6$; $P < 0.05$) compared to aligned mice ($n = 6$). The inset shows fEPSPs recorded during baseline and 55-60 min post-HFS in aligned (left) and misaligned slice (right). (**f**) Paired-pulse facilitation ratios changed with intervals ($P < 0.001$), but were not significantly different between aligned and misaligned mice ($P = 0.5$) and no interactions between both factors were detected ($P = 0.8$). Line graphs represent the mean ± SEM ($n = 6$ per treatment).

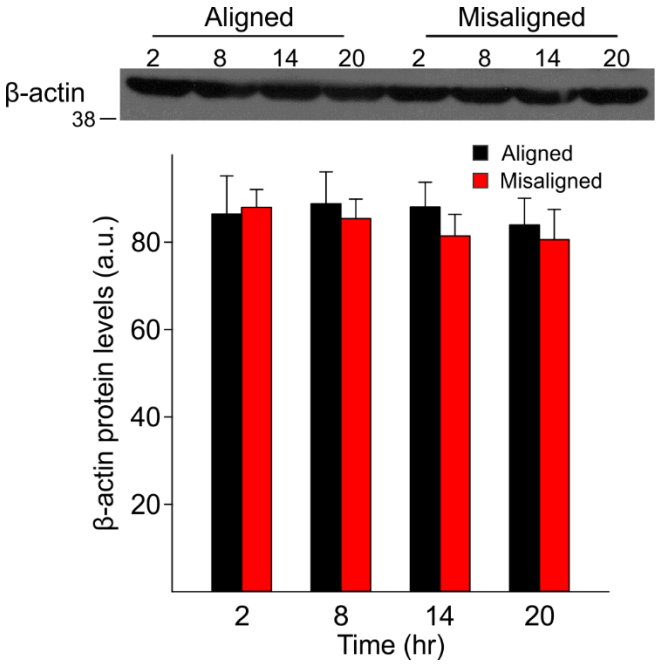

Figure 2-7 Expression of β-actin does not vary with time of day in both aligned and misaligned mice.

There are no differences in expression between aligned and misaligned mice ($P = 0.9$). Bar graphs represent the mean ± SEM of aligned ($n = 4$) and misaligned ($n = 5$) animals per time point.

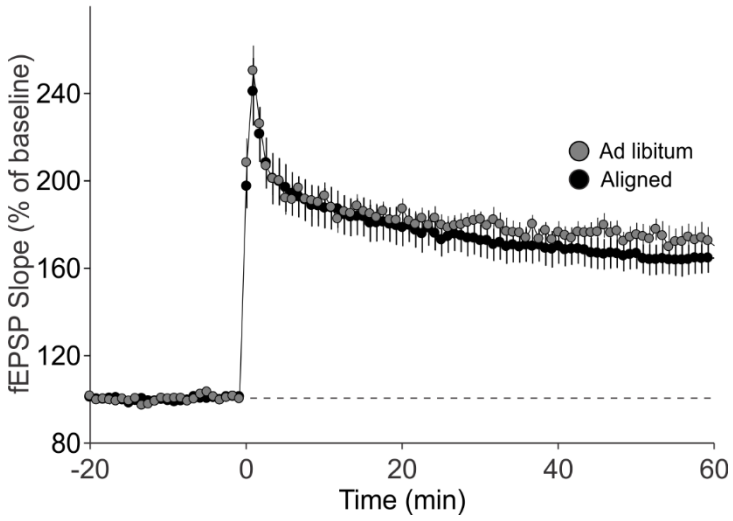

Figure 2-8 Aligned feeding does not significantly alter LTP magnitude compared to mice under *ad libitum* feeding ($P = 0.4$).

LTP was induced in both groups using the same protocol; data from aligned mice is the same as reported in **Fig. 2-6e**.

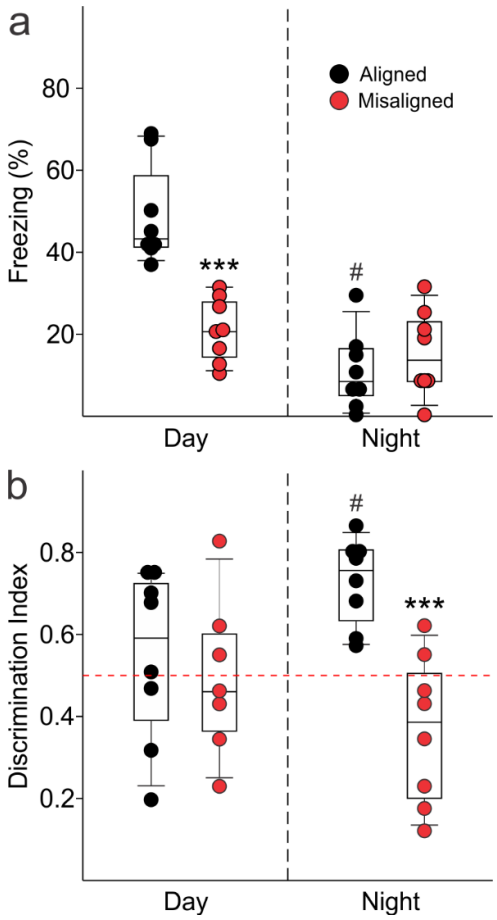

Figure 2-9 Memory deficits arise from misaligned feeding in mice.

(**a**) Recall of the fear conditioned (FC) context is measured by the percentage of freezing when re-exposed to the fearful context. Misaligned mice (n = 8) show significant deficits in recall of contextual (FC) compared to aligned mice (n = 8;***P < 0.001) when trained and tested during the day (ZT 2). Circadian regulation of learning and memory is demonstrated by the decreased recall in aligned mice trained and tested at night (ZT 14; n = 8; #P < 0.001). This time of day effect is lost in misaligned mice (n = 8), which perform equally poorly at both times. (**b**) Novel object recognition (NOR) is reported using a discrimination index of $T_{novel}/(T_{novel}+T_{familiar})$, and mice are considered to exhibit NOR at values of 0.5 and above (dotted red line). NOR is impaired in misaligned mice trained and tested at night (ZT 21; n = 8) compared to aligned mice (n = 8; ***P < 0.001). Time of day effects were also found for NOR in aligned mice (n = 8; #P < 0.01), which perform better during the night than day (ZT 9). Misaligned mice fail to show a time of day effect

(n = 7), again showing equally poor performance at both times. Box and whisker plots display the median as a line, the 25^{th} to 75^{th} percentiles, and the 10^{th} to 90^{th} percentiles respectively.

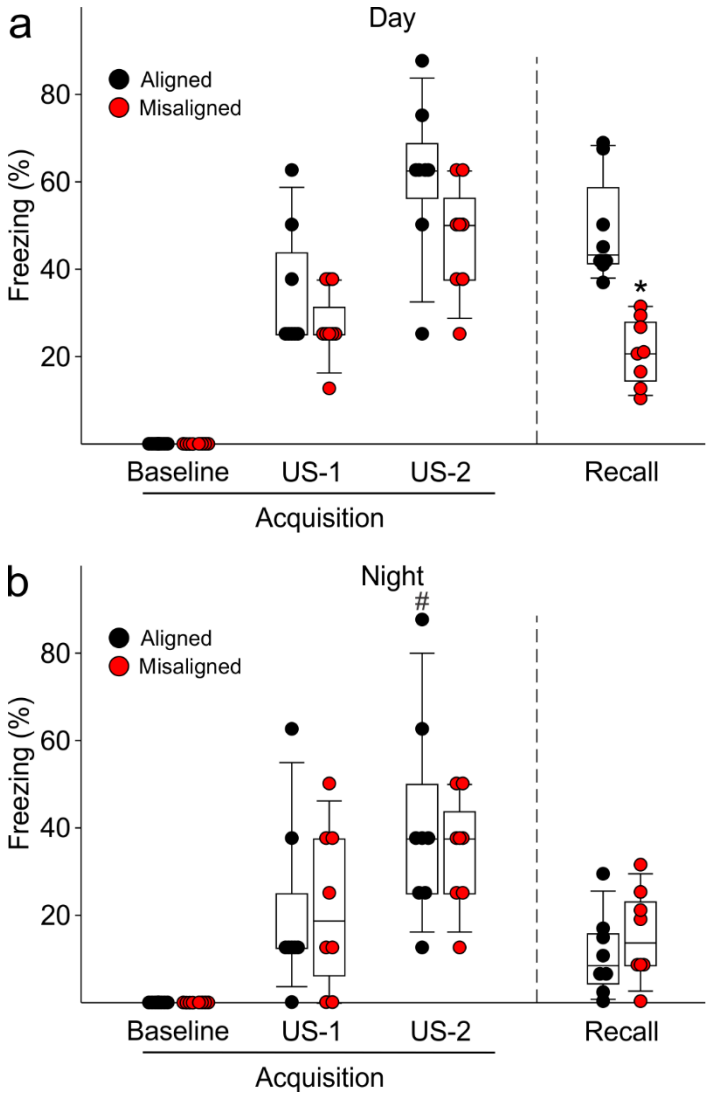

Figure 2-10 Acquisition of FC freezing in the day (ZT 2, *n* = 8/group) and night (ZT 14; *n* = 8/group) are unaltered by misaligned feeding.

(**a**) Misaligned mice did not show significant changes in baseline freezing (*P* = 0.3), freezing in response to the first foot shock (US-1; *P* = 0.9), or freezing in response to the second foot shock (US-2; *P* = 0.1). Recall was significantly reduced in misaligned mice as reported in the main text and **Fig. 2-9**. (**b**) Misaligned feeding did not cause differences in baseline freezing (*P* = 1.0), nor in acquisition of freezing in response to US-1 (*P* = 0.9) and US-2 (*P* = 0.5). There was a time of day effect on freezing in response to US-2 (# *P* < 0.05), as previously reported (2).

2.6 References

1. Holloway FA, Wansley R. Multiphasic retention deficits at periodic intervals after passive-avoidance learning. Science. 1973;180(4082):208-10
2. Chaudhury D, Colwell CS. Circadian modulation of learning and memory in fear-conditioned mice. Behav Brain Res. 2002;133(1):95-108
3. Eckel-Mahan KL, Phan T, Han S, Wang H, Chan GC, Scheiner ZS, et al. Circadian oscillation of hippocampal MAPK activity and cAmp: implications for memory persistence. Nat Neurosci. 2008;11(9):1074-82
4. Fropf R, Zhang J, Tanenhaus AK, Fropf WJ, Siefkes E, Yin JC. Time of day influences memory formation and dCREB2 proteins in Drosophila. Front Syst Neurosci. 2014;8:43. doi: 10.3389/fnsys.2014.00043
5. Lamont EW, Robinson B, Stewart J, Amir S. The central and basolateral nuclei of the amygdala exhibit opposite diurnal rhythms of expression of the clock protein Period2. Proc Natl Acad Sci U S A. 2005;102(11):4180-4. doi: 10.1073/pnas.0500901102
6. Lyons LC, Collado MS, Khabour O, Green CL, Eskin A. The circadian clock modulates core steps in long-term memory formation in Aplysia. J Neurosci. 2006;26(34):8662-71. doi: 10.1523/JNEUROSCI.2307-06.2006
7. Van der Zee EA, Havekes R, Barf RP, Hut RA, Nijholt IM, Jacobs EH, et al. Circadian time-place learning in mice depends on Cry genes. Curr Biol. 2008;18(11):844-8. doi: 10.1016/j.cub.2008.04.077
8. Wang LM, Dragich JM, Kudo T, Odom IH, Welsh DK, O'Dell TJ, et al. Expression of the circadian clock gene Period2 in the hippocampus: possible implications for synaptic plasticity and learned behaviour. ASN Neuro. 2009;1(3). doi: 10.1042/AN20090020
9. Wardlaw SM, Phan TX, Saraf A, Chen X, Storm DR. Genetic disruption of the core circadian clock impairs hippocampus-dependent memory. Learn Mem. 2014;21(8):417-23. doi: 10.1101/lm.035451.114
10. Fekete M, van Ree JM, Niesink RJ, de Wied D. Disrupting circadian rhythms in rats induces retrograde amnesia. Physiol Behav. 1985;34(6):883-7
11. Cho K, Ennaceur A, Cole JC, Suh CK. Chronic jet lag produces cognitive deficits. J Neurosci. 2000;20(6):RC66

12. Devan BD, Goad EH, Petri HL, Antoniadis EA, Hong NS, Ko CH, et al. Circadian phase-shifted rats show normal acquisition but impaired long-term retention of place information in the water task. Neurobiol Learn Mem. 2001;75(1):51-62. doi: 10.1006/nlme.1999.3957

13. Ruby NF, Hwang CE, Wessells C, Fernandez F, Zhang P, Sapolsky R, et al. Hippocampal-dependent learning requires a functional circadian system. Proc Natl Acad Sci U S A. 2008;105(40):15593-8. doi: 10.1073/pnas.0808259105

14. Loh DH, Navarro J, Hagopian A, Wang LM, Deboer T, Colwell CS. Rapid changes in the light/dark cycle disrupt memory of conditioned fear in mice. PLoS One. 2010;5(9). doi: 10.1371/journal.pone.0012546

15. Gibson EM, Wang C, Tjho S, Khattar N, Kriegsfeld LJ. Experimental 'jet lag' inhibits adult neurogenesis and produces long-term cognitive deficits in female hamsters. PLoS One. 2010;5(12):e15267. doi: 10.1371/journal.pone.0015267

16. Karatsoreos IN, Bhagat S, Bloss EB, Morrison JH, McEwen BS. Disruption of circadian clocks has ramifications for metabolism, brain, and behavior. Proc Natl Acad Sci U S A. 2011;108(4):1657-62. doi: 10.1073/pnas.1018375108

17. Fonken LK, Kitsmiller E, Smale L, Nelson RJ. Dim nighttime light impairs cognition and provokes depressive-like responses in a diurnal rodent. J Biol Rhythms. 2012;27(4):319-27. doi: 10.1177/0748730412448324

18. LeGates TA, Altimus CM, Wang H, Lee HK, Yang S, Zhao H, et al. Aberrant light directly impairs mood and learning through melanopsin-expressing neurons. Nature. 2012;491(7425):594-8. doi: 10.1038/nature11673

19. Fernandez F, Lu D, Ha P, Costacurta P, Chavez R, Heller HC, et al. Circadian rhythm. Dysrhythmia in the suprachiasmatic nucleus inhibits memory processing. Science. 2014;346(6211):854-7. doi: 10.1126/science.1259652

20. Bass J. Circadian topology of metabolism. Nature. 2012;491(7424):348-56. doi: 10.1038/nature11704

21. Mattson MP, Allison DB, Fontana L, Harvie M, Longo VD, Malaisse WJ, et al. Meal frequency and timing in health and disease. Proc Natl Acad Sci U S A. 2014;111(47):16647-53. doi: 10.1073/pnas.1413965111

22. Damiola F, Le Minh N, Preitner N, Kornmann B, Fleury-Olela F, Schibler U. Restricted feeding uncouples circadian oscillators in peripheral tissues from the central pacemaker in the suprachiasmatic nucleus. Genes Dev. 2000;14(23):2950-61

23. Stokkan KA, Yamazaki S, Tei H, Sakaki Y, Menaker M. Entrainment of the circadian clock in the liver by feeding. Science. 2001;291(5503):490-3. doi: 10.1126/science.291.5503.490

24. Arble DM, Bass J, Laposky AD, Vitaterna MH, Turek FW. Circadian timing of food intake contributes to weight gain. Obesity (Silver Spring). 2009;17(11):2100-2. doi: 10.1038/oby.2009.264

25. Bray MS, Ratcliffe WF, Grenett MH, Brewer RA, Gamble KL, Young ME. Quantitative analysis of light-phase restricted feeding reveals metabolic dyssynchrony in mice. Int J Obes (Lond). 2013;37(6):843-52. doi: 10.1038/ijo.2012.137

26. Hatori M, Vollmers C, Zarrinpar A, DiTacchio L, Bushong EA, Gill S, et al. Time-restricted feeding without reducing caloric intake prevents metabolic diseases in mice fed a high-fat diet. Cell Metab. 2012;15(6):848-60. doi: 10.1016/j.cmet.2012.04.019

27. Gill S, Le HD, Melkani GC, Panda S. Time-restricted feeding attenuates age-related cardiac decline in Drosophila. Science. 2015;347(6227):1265-9. doi: 10.1126/science.1256682

28. Scheer FA, Hilton MF, Mantzoros CS, Shea SA. Adverse metabolic and cardiovascular consequences of circadian misalignment. Proc Natl Acad Sci U S A. 2009;106(11):4453-8. doi: 10.1073/pnas.0808180106

29. Wright KP, Jr., Hull JT, Hughes RJ, Ronda JM, Czeisler CA. Sleep and wakefulness out of phase with internal biological time impairs learning in humans. J Cogn Neurosci. 2006;18(4):508-21. doi: 10.1162/jocn.2006.18.4.508

30. Marquie JC, Tucker P, Folkard S, Gentil C, Ansiau D. Chronic effects of shift work on cognition: findings from the VISAT longitudinal study. Occup Environ Med. 2015;72(4):258-64. doi: 10.1136/oemed-2013-101993

31. Zhou X, Ferguson SA, Matthews RW, Sargent C, Darwent D, Kennaway DJ, et al. Sleep, wake and phase dependent changes in neurobehavioral function under forced desynchrony. Sleep. 2011;34(7):931-41. doi: 10.5665/SLEEP.1130

32. Diekelmann S, Born J. The memory function of sleep. Nat Rev Neurosci. 2010;11(2):114-26. doi: 10.1038/nrn2762

33. Amir S, Lamont EW, Robinson B, Stewart J. A circadian rhythm in the expression of PERIOD2 protein reveals a novel SCN-controlled oscillator in the oval nucleus of the bed nucleus of the stria terminalis. J Neurosci. 2004;24(4):781-90. doi: 10.1523/JNEUROSCI.4488-03.2004

34. Angeles-Castellanos M, Mendoza J, Escobar C. Restricted feeding schedules phase shift daily rhythms of c-Fos and protein Per1 immunoreactivity in corticolimbic regions in rats. Neuroscience. 2007;144(1):344-55. doi: 10.1016/j.neuroscience.2006.08.064

35. Wakamatsu H, Yoshinobu Y, Aida R, Moriya T, Akiyama M, Shibata S. Restricted-feeding-induced anticipatory activity rhythm is associated with a phase-shift of the expression of mPer1 and mPer2 mRNA in the cerebral cortex and hippocampus but not in the suprachiasmatic nucleus of mice. Eur J Neurosci. 2001;13(6):1190-6

36. Sano Y, Shobe JL, Zhou M, Huang S, Shuman T, Cai DJ, et al. CREB regulates memory allocation in the insular cortex. Curr Biol. 2014;24(23):2833-7. doi: 10.1016/j.cub.2014.10.018

37. Zhou Y, Won J, Karlsson MG, Zhou M, Rogerson T, Balaji J, et al. CREB regulates excitability and the allocation of memory to subsets of neurons in the amygdala. Nat Neurosci. 2009;12(11):1438-43. doi: 10.1038/nn.2405

38. Yoo SH, Yamazaki S, Lowrey PL, Shimomura K, Ko CH, Buhr ED, et al. PERIOD2::LUCIFERASE real-time reporting of circadian dynamics reveals persistent circadian oscillations in mouse peripheral tissues. Proc Natl Acad Sci U S A. 2004;101(15):5339-46. doi: 10.1073/pnas.0308709101

39. Loh DH, Kudo T, Truong D, Wu Y, Colwell CS. The Q175 mouse model of Huntington's disease shows gene dosage- and age-related decline in circadian rhythms of activity and sleep. PLoS One. 2013;8(7):e69993. doi: 10.1371/journal.pone.0069993

40. Fisher SP, Godinho SI, Pothecary CA, Hankins MW, Foster RG, Peirson SN. Rapid assessment of sleep-wake behavior in mice. J Biol Rhythms. 2012;27(1):48-58. doi: 10.1177/0748730411431550

41. Loh DH, Dragich JM, Kudo T, Schroeder AM, Nakamura TJ, Waschek JA, et al. Effects of vasoactive intestinal peptide genotype on circadian gene expression in the suprachiasmatic nucleus and peripheral organs. J Biol Rhythms. 2011;26(3):200-9. doi: 10.1177/0748730411401740

42. Ghiani C, Gallo V. Inhibition of cyclin E-cyclin-dependent kinase 2 complex formation and activity is associated with cell cycle arrest and withdrawal in oligodendrocyte progenitor cells. J Neurosci. 2001;21(4):1274-82

43. Ghiani CA, Starcevic M, Rodriguez-Fernandez IA, Nazarian R, Cheli VT, Chan LN, et al. The dysbindin-containing complex (BLOC-1) in brain: developmental regulation, interaction with SNARE proteins and role in neurite outgrowth. Mol Psychiatry. 2010;15(2):115, 204-15. doi: 10.1038/mp.2009.58

44. Ghiani CA, Mattan NS, Nobuta H, Malvar JS, Boles J, Ross MG, et al. Early effects of lipopolysaccharide-induced inflammation on foetal brain development in rat. ASN Neuro. 2011;3(4). doi: 10.1042/AN20110027

45. Carlisle HJ, Fink AE, Grant SG, O'Dell TJ. Opposing effects of PSD-93 and PSD-95 on long-term potentiation and spike timing-dependent plasticity. J Physiol. 2008;586(Pt 24):5885-900. doi: 10.1113/jphysiol.2008.163469

3 CHAPTER III: Differential Regulation of NMDA Receptor-Mediated Transmission by SK Channels Underlies Dorsal-Ventral Differences in Dynamics of Schaffer Collateral Synaptic Function

3.1 Introduction

Although the hippocampus has been intensively studied because of its crucial role in spatial navigation as well as learning and memory, hippocampal lesions also have profound effects on innate fear and anxiety (Deacon et al., 2002; Kjelstrup et al., 2002; Bannerman et al., 2003; Pentkowski et al., 2006). Intriguingly, these different aspects of hippocampal function are segregated into distinct anatomical zones, with the dorsal hippocampus having a key role in memory formation, whereas, the ventral hippocampus is more importantly involved in emotions and anxiety (Moser and Moser, 1998; Kjelstrup et al., 2002; Bannerman et al., 2003; Fanselow and Dong, 2010; Strange et al., 2014). Consistent with this functional segmentation along the dorsal-ventral axis of the hippocampus, both direct and indirect connections link the dorsal hippocampus to brain regions with roles in spatial information processing and memory, while the ventral hippocampus has prominent connections with brain regions involved in emotions and anxiety (see Fanselow and Dong, 2010 and Strange et al., 2014).

In contrast to the extensive differences in afferent and efferent connections of the dorsal and ventral regions of the hippocampus, the general structure of the internal circuitry of the hippocampus (i.e., the trisynaptic circuit) is preserved throughout the dorsal-ventral axis. This suggests that along the dorsal-ventral axis, the hippocampus uses a stereotyped circuit to implement a common computational algorithm to process information. From this perspective, the distinct functions of the dorsal and ventral hippocampus are driven primarily by their unique

patterns of connectivity with different brain regions. This notion, however, is complicated by dorsal-ventral differences in the cellular and synaptic physiology of hippocampal neurons that likely alter how information is processed by the trisynaptic circuit. For example, a remarkable level of heterogeneity in gene expression exists in both CA1 and CA3 pyramidal cells along the dorsal-ventral axis of the hippocampus (Leonardo et al., 2006; Thompson et al., 2008; Dong et al., 2009; Cembrowski et al., 2016A). Moreover, a variety of ion channels are differentially expressed in dorsal and ventral CA1 pyramidal cells (Marcelin et al., 2012; Dougherty et al., 2013; Hönigsperger et al., 2015). Any role these differences have in determining how information processing varies in the trisynaptic circuit of dorsal and ventral hippocampus has yet to be established, however. Interestingly, both short-term facilitation and long-term potentiation (LTP) are reduced at Schaffer collateral (SC) synapses in the ventral hippocampus (Papatheodoropoulos et al., 2000; Maggio and Segal, 2007; Papatheodoropoulos, 2015). Although these differences could support important dorsal-ventral differences in information processing, the molecular mechanisms responsible for the divergent properties of synaptic plasticity in these regions are unclear. Furthermore, although theta oscillations in the ventral hippocampal CA1 region recorded in-vivo are significantly less regular, lower in amplitude, and sometimes absent during behavioral states associated with robust theta oscillations in the dorsal CA1 region (Patel et al. 2012), it remains unclear whether there are important differences in how synapses, cells, and/or networks within the dorsal and ventral hippocampus process theta-frequency patterns of activity.

Here, we investigated the mechanisms underlying dorsal-ventral differences in the LTP induction using theta pulse stimulation (TPS) patterns of SC fiber stimulation (Thomas et al., 1998). We find that dorsal and ventral SC synapses exhibit markedly distinct responses to TPS and, in contrast to dorsal hippocampus, TPS fails to induce LTP at ventral synapses. Excitatory

postsynaptic potential (EPSP) amplification is also strongly reduced at ventral synapses and, as a result, both EPSP-spike (E-S) coupling and EPSP-evoked complex spike (CS) bursting are significantly weaker in ventral pyramidal cells. Our results indicate that all of these differences in postsynaptic function arise from a common mechanism: an enhanced activation of Ca^{2+}-activated SK-type K^+ channels that strongly inhibits NMDA receptor (NMDAR) activation at ventral SC synapses. Together, our findings indicate that differences in the expression and/or activity of SK channels provides a potent mechanism for modulating multiple aspects of synaptic function involved in the transfer, processing and storage of information.

3.2 Material and Methods

Animals and slice preparation

Male C57Bl/6N mice (Charles River Laboratories, Cambridge, MA; 2-3 months old; housed in a 12/12 light/dark cycle) and *Syt7* knockout mice and wild type litter mates of both sexes (RRID: IMSR_JAX:004950, The Jackson Laboratory, Bar Harbor, ME; 2-3 months old; housed in a 12/12 light/dark cycle) were deeply anesthetized with isoflurane and following cervical dislocation the brain was rapidly removed and submerged in ice-cold, oxygenated (95% O_2/5% CO_2) ACSF containing (in mM) 124 NaCl, 4 KCl, 25 $NaHCO_3$, 1 NaH_2PO_4, 2 $CaCl_2$, 1.2 $MgSO_4$, and 10 glucose (Sigma-Aldrich, St. Louis, MO). On a cold plate, the brain hemispheres were separated, blocked, and the hippocampi removed. 400-µm-thick slices were then cut using a manual tissue chopper. Slices from the dorsal and ventral thirds of the hippocampus were used. Slices were maintained (at 30^{o}C) in interface-type chambers that were continuously perfused (2-3 ml/min) with ACSF and allowed to recover for at least 2 hours prior to recordings. All

experimental techniques were approved by the Institutional Care and Use Committee at the University of California, Los Angeles.

Electrophysiological recordings

A bipolar, nichrome wire stimulating electrode was placed in *stratum radiatum* of the CA1 region and used to activate Schaffer collateral/commissural fiber synapses. For extracellular recordings, evoked fEPSPs (basal stimulation rate = 0.02 Hz) were recorded in *stratum radiatum* using a glass microelectrode (A-M Systems, Carlsborg, WA) filled with ACSF (resistance ranged from 5–10 MΩ). Interface-type recording chambers were used for extracellular recordings while whole-cell current- and voltage-clamp recordings were done using slices maintained in submerged-slice type chambers. Whole-cell current-clamp recordings were used to examine pairing-induced LTP, intrinsic excitability, E-S coupling, and EPSP amplification. In these experiments recording electrodes (4–8 MΩ) were filled with a K^+-based electrode-filling solution containing (in mM) 122.5 K-gluconate, 17.5 KCl, 10 HEPES, 0.2 EGTA, 10 Na_2-phosphocreatine, 4 Mg-ATP, 0.3 Na-GTP (pH = 7.3, 290 mOsm). Whole-cell voltage-clamp recordings (evoked EPSCs and mEPSCs) were performed using a Cs^+-based electrode-filling solution containing (in mM) 102 mM Cs-gluconate, 20 mM CsCl, 10 K-gluconate, 10 mM TEA-Cl, 5 mM QX314, 20 HEPES, 0.2 EGTA, 4 Mg-ATP, 0.3 Na-GTP, and 20 mM HEPES (pH = 7.3, 290 mOsm). For experiments performed in picrotoxin (Sigma-Aldrich; 100 μM) the CA3 region was removed and, unless noted otherwise, the slices were bathed in a modified ACSF containing 2.4 mM KCl, 4.0 mM $CaCl_2$, and 2.4 mM $MgSO_4$. Series resistance compensation was used in all voltage-clamp recordings except in experiments examining miniature postsynaptic currents. All cells were allowed to equilibrate for ≥ 3 minutes after break-in before starting experiments. Recordings where

series resistance was ≥ 30 MΩ or unstable were discarded. Unless noted, reported membrane potentials are not adjusted for junction potentials.

LTP induction protocols

The induction of LTP by TPS was examined using a 30s long train of 5 Hz stimulation (150 pulses). At the start of each experiment the maximal fEPSP amplitude was determined and the intensity of presynaptic fiber stimulation was then adjusted to evoke fEPSPs with an amplitude ~50% of the maximal amplitude. Note that unlike more conventional theta-burst stimulation protocols, where bursts of presynaptic stimulation are delivered at 5 Hz, only single pulses of stimulation are delivered during TPS. The average slope of fEPSPs evoked between 40 and 45 min post-TPS (normalized to pre-TPS baseline) was used for statistical comparisons. In experiments using whole-cell current-clamp recordings, LTP was induced by pairing EPSPs evoked by SC fiber stimulation with tonic postsynaptic depolarization. Slices were bathed in modified ACSF containing picrotoxin and the strength of SC fiber stimulation was adjusted to evoke approximately 15 mV EPSPs (V_m = -80 mV). Following a 10-minute baseline (basal stimulation rate = 0.05 Hz), 100 pulses of presynaptic fiber stimulation delivered at 2 Hz were paired with postsynaptic depolarization to -10 mV. The average slope of EPSPs elicited 25-30 min post-pairing (normalized to baseline) was used for statistical comparisons.

Basal properties of excitatory and inhibitory synaptic transmission

Basal synaptic strength at SC synapses was determined by comparing presynaptic fiber volleys and fEPSP slopes elicited by different intensities of presynaptic fiber stimulation. Quantal size and release probability were determined from the amplitude and frequency (Prange and Murphy, 1999), respectively, of miniature EPSCs (mEPSCs) recorded at −80 mV in pyramidal

cells bathed in standard ACSF containing TTX (1 µM; Alomone Labs, Jerusalem, Israel) and picrotoxin. A template-based event detection routine in pClamp 10 (Molecular Devices) was used to identify mEPSCs. Detected events smaller than 6 pA were excluded from the analysis. The use-dependent inhibition of NMDAR-mediated EPSCs by MK-801 (Huettner and Bean, 1988) was also used to examine basal release probability (Hessler et al. 1993; Rosenmund et al. 1993). In these experiments slices were bathed in CNQX (Alomone Labs; 20 µM) and picrotoxin and pyramidal cells were voltage-clamped at 40 mV. Evoked currents were set at ~300 pA and a baseline was established. Synaptic stimulation was stopped for 10 minutes during bath application of MK-801 (Abcam, Cambridge, MA; 40 µM) and then 100 pulses of synaptic stimulation were delivered at 0.1 Hz. For each cell, the activity-dependent, MK-801 inhibition of NMDAR-mediated EPSCs was measured using a weighted decay time constant (τ_w) calculated from double exponential fits to the time course of the inhibition using the equation: $\tau_w = \tau_f \times \left[a_f/(a_f + a_s)\right] + \tau_s \times \left[a_s/(a_f + a_s)\right]$ where τ_f and τ_s are the time constants of the fast and slow components and a_f and a_s are the amplitudes of fast and slow components.

The ratio of NMDAR to AMPAR-mediated EPSCs was measured by adjusting the strength of presynaptic fiber stimulation to elicit EPSCs with a peak amplitude of ~-200 pA at V_m = -80 mV and then recording EPSCs at V_m = 40 mV. The AMPAR and NMDAR-mediated components of the synaptic currents were estimated by measuring the EPSC amplitude at 5 and 50 ms after EPSC onset, respectively, from the average 40 mV waveform for each cell. To determine the NMDA current decay time constant, the decay of the average EPSC waveform at 40 mV for each cell was fit with a double exponential and a weighted decay time constant was calculated for comparison.

EPSP-spike (E-S) coupling was measured using whole-cell current-clamp techniques to record postsynaptic responses elicited by different intensities of SC fiber stimulation (membrane potential was set to -70 mV using current injection). Five responses were elicited at each stimulation intensity and the size of EPSPs was measured using the average EPSP slope. To examine EPSP amplification, current through the recording electrode was used to set V_m = -80 mV and the strength of SC fiber stimulation was adjusted to evoke ~5 mV EPSPs. Steady-state current injection was then used to examine the effect of membrane depolarization (up to -40 mV) on EPSP amplitude and duration. For each cell, the average of 5 EPSPs recorded at each membrane potential tested was used for analysis. D-APV and apamin were acquired from Alomone Labs.

Inhibitory synaptic transmission was assessed in the following ways. The ratio of excitation to inhibition was measured by voltage clamping and holding cells at the reversal potential for GABA (-42 mV) and for glutamate (15 mV) receptors, which had been measured in this preparation and was not different between dorsal and ventral pyramidal cells. Charge transfer at each reversal potential was computed and the ratio taken for comparison. The recording electrode solution used in these experiments contained (in mM): 115 Cs-gluconate, 10 K-gluconate, 13 TEA-Cl, 0.2 EGTA, 20 HEPES, 5 QX314, 5 Na-posphocreatine, 0.3 Na-GTP, and 4 Mg-ATP (pH = 7.3, 290 mOsm). Spontaneous and miniature IPSCs (mIPSCs) were recorded in cells voltage-clamped at -70 mV using recording electrodes filled with a solution containing (in mM): 140 CsCl, 4 NaCl, 1 $MgCl_2$, 0.1 EGTA, 4 Mg-ATP, 0.3 Na-GTP, 5 QX314, and 10 HEPES (pH = 7.3). The external solution contained kynurenate (Abcam; 3 mM) to block AMPAR and NMDAR-mediated currents and TTX was also present during mIPSC recordings. The very high frequency of spontaneous and mIPSCs made it difficult to resolve single events and thus total charge transfer during 10-second-long recording intervals was measured. The TPS-induced depression of evoked

IPSCs (V_m = -70) was also measured using CsCl-based electrode solutions and kynurenate to block excitatory synaptic transmission. Bath application of picrotoxin (100 µM) or bicuculline (Abcam; 40 µM) completely blocked currents recorded in the presence of kynurenate, confirming that the responses are $GABA_A$ receptor-mediated.

Intrinsic excitability

Resting membrane potential was the steady-state membrane voltage with no current injection measured ≥ 3 min after break-in but before any kind of current injection to the neuron. All other intrinsic properties were measured with steady-state current injected to hold cells at -57 mV (~ -70 mV after correction for calculated junction potential), which was the approximate resting membrane potential for pyramidal cells (**Table 1**). All protocols were repeated three times per cell and averaged. For input resistance, 500 ms current steps of 0 pA to -200 pA were injected in -20 pA increments. Steady-state responses were measured as the average change in voltage in the last 100 ms of the pulse. The slope of a regression line fitted to the voltage versus current data was used to calculate input resistance. Current sag was also measured during these experiments and computed as the initial voltage trough during the -100 pA and -200 pA steps minus the steady-state voltage change. Rheobase was determined by injecting 1 ms square pulses in 100 pA steps and recording the strength of the first pulse to elicit an action potential. Action potential threshold, height, after-hyperpolarization, and after-depolarization were computed from these waveforms as described in Jensen et al. (1996) except for threshold, which was the average of the thresholds computed using Methods II, VI, VII from Sekerli et al. (2004). Firing frequency vs. injected current was measured as the number of spikes per 500 ms step in 25 pA increments from 0 pA to 150 pA.

Reverse transcription and quantitative PCR (RT-qPCR)

Isolated CA1 regions were micro-dissected from dorsal and ventral hippocampal slices, snap frozen on dry ice, and then stored at -80°C until use. RNA was then purified from samples (each containing 8 CA1 regions) using a combined Trizol (Invitrogen, Grand Island, NY) and column (Qiagen, Valencia, CA) purification protocol. 500 µL of Trizol was added to each sample, followed by the standard Trizol protocol until the phase separation step. The top aqueous layer was then removed, mixed 1:1 with 100% ethanol, and added to the column, followed by the manufacturer protocol for column purification.

Equal amounts of dorsal and ventral purified RNA (100 ng per RT reaction) were added into the reverse transcription reaction using the SuperScript III First Strand Synthesis System with random hexamer priming. qPCR was then carried out on the cDNA using SYBR Green-based PCR (Applied Biosystems, Waltham, MA) using primers specific for *Kcnn2*, *Kcnn3*, and *HPRT1* in technical triplicates per reaction. Normalization was done using ΔCt by first normalizing *Kcnn2/3* expression levels to HPRT of that sample, then by comparing the normalized *Kcnn2/3* ventral Ct values to dorsal Ct values.

Exon-spanning primers for *Kcnn2* were 5’ GTCGCTGTATTCTTTAGCTCTG, 3’ ACGCTCATAAGTCATGGC; and *Kcnn3* were 5’ GCTCTGATTTTTGGGATGTTTG, 3’ CGATGATCAAACCAAGCAGGATGA (both from Bond et al. (2004)). *Hprt1* primers were 5’ TGTTGTTGGATATGCCCTTG, 3’ GGCCACAGGACTAGAACACC.

Statistical analysis

Values are reported as mean ± SEM. After evaluating data for normality and homoscedasticity, Student's t tests or, where appropriate, Mann Whitney U tests were used to determine statistical significance between two groups. All other comparisons used either one-way or two-way ANOVAs. Student-Newman-Keuls *post hoc* tests were used in cases where multiple comparisons were required. Each test and sample sizes are documented in the figure legends.

3.3 Results

CS bursting and LTP deficits in ventral CA1 following theta-frequency stimulation

TPS protocols induce LTP at SC synapses by activating a rich set of circuit and synaptic temporal dynamics that lead to complex-spike (CS) bursting in CA1 pyramidal cells (Thomas et al. 1998; Fink and O'Dell 2009; Wójtowicz and Mozrzymas 2015), a pattern of action potential (AP) firing exhibited by pyramidal cells *in vivo* (Kandel and Spencer 1961; Rank 1973). Thus, understanding how these dynamics vary in the dorsal and ventral hippocampal CA1 region can provide insights into how dorsal-ventral differences in gene expression impact synaptic plasticity, neuronal excitability, and circuit function. Therefore, in our initial experiments we examined both the short-and long-term changes in synaptic transmission induced by a 150 pulse train of TPS. As expected from previous work (Thomas et al., 1998), TPS elicited complex, time-varying changes in both synaptic transmission and postsynaptic firing in dorsal slices (Fig. 1). Following an initial facilitation of synaptic transmission, EPSPs began to elicit bursts of multiple population spikes (**Fig. 3-1 A,B**), which are due to CS bursts of postsynaptic APs (Thomas et al., 1998). Although the facilitation gradually faded and synaptic transmission at later time points was depressed, EPSPs continued to elicit CS bursts for the remainder of the stimulation train (**Fig. 3-1B**). In stark contrast, the dynamics of synaptic transmission during TPS were less dramatic at SC synapses in the ventral hippocampus and, surprisingly, EPSPs failed to elicit postsynaptic CS bursts (**Fig. 3-1A,B**). Notably, CS bursting provides the postsynaptic depolarization needed for NMDAR activation and LTP induction by TPS (Thomas et al., 1998). Thus, this difference in EPSP-evoked CS bursting suggested that SC synapses in the dorsal and ventral hippocampus would exhibit an equally dramatic difference in their ability to undergo TPS-induced LTP. Indeed, TPS induced robust LTP

in dorsal hippocampal slices but had no lasting effect on synaptic strength in ventral slices (**Fig. 3-1C**). In contrast, similar amounts of potentiation were induced in dorsal and ventral pyramidal cells when low-frequency SC fiber stimulation was paired with strong postsynaptic depolarization during whole-cell current-clamp recordings (**Fig. 3-1D**). This indicates that the failure of TPS to induce LTP at SC synapses in the ventral hippocampus is not simply due to a reduced capacity for LTP. Instead, it suggests that dorsal-ventral differences in TPS-induced LTP are due to differences in pre- and/or postsynaptic properties that regulate the ability of SC EPSPs to evoke postsynaptic CS bursts.

Properties of basal synaptic transmission at dorsal and ventral SC fiber synapses

In addition to the weaker facilitation observed during TPS (**Fig. 3-1B**), ventral SC synapses also exhibited significantly reduced paired-pulse facilitation compared to dorsal synapses (**Fig. 3-2A**). In contrast, basal synaptic strength, determined by comparing the amplitudes of presynaptic fiber volleys and fEPSP slopes for responses elicited by different intensities of SC fiber stimulation, was the same (**Fig. 3-2B**). Moreover, there was no difference in the amplitude of miniature EPSCs (mEPSCs) in dorsal and ventral CA1 pyramidal cells (**Fig. 3-2C**), indicating that quantal size is similar at excitatory synapses in the dorsal and ventral hippocampus. The frequency of mEPSCs was also similar (**Fig. 3-2D**), suggesting that the probability of transmitter release is the same at dorsal and ventral synapses (Prange and Murphy, 1999). Consistent with this notion, the activity-dependent inhibition of NMDAR-mediated EPSCs by the channel blocker MK-801 (Huettner and Bean, 1988), which can be used to measure the probability of evoked release at SC synapses (Hessler et al., 1993; Rosenmund et al., 1993), was not significantly different in dorsal and ventral CA1 pyramidal cells (**Fig. 3-2F,G**). Thus, although SC synapses in the dorsal and

ventral hippocampus exhibit striking differences in activity-dependent forms of plasticity, basal transmission appears to be essentially identical at these synapses.

Assessing the importance of activity-dependent presynaptic facilitation in the induction of theta-frequency CS bursting and LTP

The robust initial facilitation of transmission at SC fiber synapses during TPS in the dorsal hippocampus and its near absence at ventral synapses (**Fig. 3-1B**) suggested that dorsal-ventral differences in short-term, presynaptic plasticity may have a central role in regulating CS bursting and LTP induced by theta-frequency stimulation. To examine this, we used mice lacking the *Syt7* gene that encodes synaptotagmin VII, a presynaptic Ca^{2+} sensor recently shown to have a crucial role in paired-pulse and frequency facilitation at SC fiber synapses (Jackman et al., 2016). Consistent with previous findings (Jackman et al., 2016), both paired-pulse facilitation (**Fig. 3-3A**) and the facilitation of synaptic transmission during the initial phase of TPS were almost completely abolished in slices from $Syt7^{-/-}$ mice (**Fig. 3-3B**). The ability of EPSPs to elicit CS bursts was also altered in $Syt7^{-/-}$ mutants, with the onset of EPSP-evoked bursting during TPS being significantly delayed (**Fig. 3-3C,D**). Moreover, TPS induced significantly less LTP in slices from $Syt7^{-/-}$ mice (**Fig. 3-3E**), most likely due to the reduction in EPSP-evoked bursting during the stimulation train (see Thomas et al 1998). Together, these findings indicate that, although not essential, frequency facilitation of EPSPs during TPS does contribute to LTP induction by significantly advancing the onset of CS bursting.

Therefore, we next tested whether enhancing stimulation strength during theta-frequency stimulation would induce CS bursting and LTP in ventral slices from wild type mice. In these experiments the intensity of presynaptic fiber stimulation during the first 50 pulses of stimulation

(the time period where CS bursting develops in dorsal slices) was increased to mimic (or exceed) the initial facilitation of transmission that occurs during TPS in dorsal slices (**Fig. 3-4A**). Despite more robust synaptic activation during TPS, CS bursting (**Fig. 3-4B**) and LTP (**Fig 3-4C**) failed to occur, suggesting that a lack of facilitation at ventral SC synapses is not primarily responsible for the absence of TPS-induced CS bursting and LTP at these synapses.

Previous studies have shown that another type of presynaptic plasticity, the short-term depression of feedforward inhibition that occurs during theta-frequency SC fiber stimulation, can have a crucial role in the induction of LTP (Davies et al., 1991; Mott and Lewis, 1991). Thus, we also examined whether there might be dorsal-ventral differences in both short-term plasticity and the basal properties of inhibitory synaptic transmission. We found, however, that the TPS-induced depression of inhibitory postsynaptic currents (IPSCs) was essentially identical in dorsal and ventral pyramidal cells (**Fig. 3-5A**). Moreover, spontaneous IPSCs (**Fig. 3-5B,C**) and IPSC/excitatory postsynaptic current (EPSC) ratios for synaptic currents evoked by SC fiber stimulation (**Fig. 3-5D,E**) were not different in dorsal and ventral pyramidal cells. Thus, there do not appear to be significant differences in inhibitory transmission that could contribute the distinct effects of TPS on LTP induction and CS bursting in dorsal and ventral CA1 regions.

Weaker EPSP-Spike coupling and EPSP amplification in ventral CA1

We next examined whether differences in postsynaptic excitability might contribute to dorsal-ventral differences in TPS-induced CS bursting and LTP. Although previous studies have found differences in intrinsic excitability in dorsal and ventral CA1 pyramidal cells (Dougherty et al., 2012; Marcelin et al., 2012; Dougherty et al., 2013; Hönigsperger et al., 2015; Malik et al., 2015), under our experimental conditions rheobase and threshold for APs elicited by somatic

current injection were not significantly different (**Table 1**). There was also no significant difference in the number of APs elicited by somatic injection of pulses of depolarizing current (**Fig. 3-6A,B**). Importantly, somatic current injection might fail to detect differences in ionic conductances present in dendritic spines that regulate depolarization mediated by excitatory synaptic inputs (Gu et al., 2008; Ngo-Anh et al., 2005; Bloodgood and Sabatini, 2007; Faber et al., 2008; Wang et al., 2014). Thus, we also examined intrinsic excitability by measuring the ability of different sizes of EPSPs, evoked by different intensities of presynaptic fiber stimulation, to elicit APs, a phenomenon known as E-S coupling. Although AP firing in response to somatic current injections was the same in dorsal and ventral pyramidal cells (**Fig. 3-6A,B**), E-S coupling was significantly weaker in ventral pyramidal cells (**Fig. 3-6C,D**).

To gain further insight into the mechanisms responsible for the dorsal-ventral difference in E-S coupling, we examined the voltage-dependent amplification of EPSPs that occurs with membrane depolarization in pyramidal cells (Stuart and Sakmann, 1995; Andreasen and Lambert, 1998; Fricker and Miles, 2000; Carter et al., 2012). In these experiments inhibitory synaptic transmission was blocked with picrotoxin (100 μM) to pharmacologically isolate EPSPs, and the strength of SC fiber stimulation was adjusted to evoke small, sub-threshold EPSPs (~5 mV at V_m = -80 mV). Synaptic responses were then recorded at postsynaptic membrane potentials between -80 and -40 mV (**Fig. 3-7A**). Although robust EPSP amplification was observed in dorsal pyramidal cells, there was little, if any, depolarization-induced amplification of EPSPs in ventral pyramidal cells (**Fig. 3-7A,B**).

Consistent with previous findings indicating that NMDAR activation significantly contributes to EPSP amplification in CA1 pyramidal cells (Fricker and Miles, 2000), bath

application of the NMDAR antagonist D-APV (50 μM) strongly inhibited EPSP amplification in dorsal CA1 pyramidal cells (**Fig. 3-7C,D**). Blocking NMDARs had no effect, however, on EPSPs in ventral pyramidal cells (**Fig. 3-7C,D**). These findings indicate that NMDAR activation is strongly down-regulated at ventral SC synapses. Moreover, because NMDAR activation has a crucial role in CS bursting in dorsal CA1 pyramidal cells *in vivo* (Grienberger et al., 2014), we hypothesized that the absence of robust NMDAR-mediated EPSP amplification in ventral pyramidal cells might account for the absence of CS bursting during TPS in the ventral hippocampus.

SK channel suppression of NMDAR-dependent EPSP amplification and CS bursting

Given the prominent role of NMDAR activation in EPSP amplification in dorsal CA1 pyramidal cells, one simple explanation for the absence of EPSP amplification in ventral CA1 pyramidal cells is that NMDAR expression is lower at ventral SC synapses. Indeed, the NMDAR-mediated component of fEPSPs measured using extracellular recording techniques is smaller at SC synapses in the ventral hippocampus (Maggio et al., 2015). Previous studies have found, however, that the presence of Ca^{2+}-activated, SK-type K^+ channels in dendritic spines can potently inhibit activation of NMDARs by sub-threshold EPSPs (Ngo-Anh et al., 2005; Bloodgood and Sabatini, 2007; Faber et al., 2005). Thus, another possibility was that differential expression of SK channels might underlie the differences in EPSP amplification between dorsal and ventral pyramidal cells. Consistent with this second possibility, the NMDAR-mediated component of EPSCs elicited by SC fiber stimulation was not significantly different in dorsal and ventral pyramidal cells when postsynaptic SK channels (and other K^+ channels) were blocked by intracellular perfusion of Cs^+ and TEA (**Fig. 3-8A**). This indicates that the absence of NMDAR-

mediated EPSP amplification in ventral CA1 pyramidal cells is not due to a dorsal-ventral difference in postsynaptic NMDAR content. In contrast, using quantitative RT-PCR we found that, although there was no dorsal-ventral difference in mRNA levels for the SK2 subunit of the SK channel, mRNA levels for SK3 subunits were approximately 1.6-fold higher in isolated CA1 regions obtained from ventral hippocampal slices (**Fig. 3-9A**). Although this suggests that SK3 subunit mRNA is more highly expressed in ventral pyramidal cells, measurements of mRNA levels in samples prepared from hippocampal slices reflect levels of SK channel subunit mRNA expression in multiple cell types. Thus, we also analyzed data generated from a recent RNA-Seq study specifically examining differences in gene expression in dorsal and ventral CA1 pyramidal cells (Cembrowski et al., 2016A). This analysis, performed using Hipposeq (Cembrowski et al., 2016B), revealed that SK3 subunit mRNA levels are 2 to 9-fold higher in ventral CA1 pyramidal cells (**Fig. 3-9B**). Based on these findings, we directly tested the potential impact of dorsal-ventral differences in SK channel expression and/or function on NMDAR-dependent EPSP amplification by examining the effects of the selective SK channel antagonist apamin. Blocking SK channels with apamin (100 nM) significantly enhanced EPSP amplification in ventral pyramidal cells, abolishing the dorsal-ventral difference in EPSP amplification observed previously (**Fig. 3-8B,C**). In addition, blocking NMDARs with APV prevented the apamin-induced enhancement of EPSP amplification in ventral pyramidal cells (**Fig. 3-8B,C**), indicating that SK channel activation suppresses EPSP amplification in ventral pyramidal cells by inhibiting NMDAR activation. Indeed, although APV had no effect on EPSPs evoked at -40 mV in ventral pyramidal cells under control conditions, an APV-sensitive component of EPSPs was present when SK channels were blocked with apamin (**Fig. 3-8D**).

Enabling CS bursting and LTP in ventral CA1 by SK channel inhibition

To determine how the lack of EPSP amplification in ventral pyramidal cells influences E-S coupling and CS bursting, we next examined its effect on EPSP-evoked AP firing in dorsal and ventral pyramidal cells. First, the intensity of SC stimulation was adjusted to evoke large EPSPs (~15 mV) that were below threshold for action potential generation at V_m = -70 mV, and the ability of EPSPs to elicit APs was then tested at membrane potentials between -70 and -50 mV. In addition, inhibitory synaptic transmission was suppressed with picrotoxin to mimic the activity-dependent depression of IPSCs that occurs during TPS (**Fig. 3-5A**). Under these conditions, EPSPs reliably elicited robust, CS bursts in dorsal pyramidal cells at membrane potentials depolarized to ≥ -60 mV, with little or no bursting observed in ventral pyramidal cells at all membrane potentials tested (Fig. 10A). Consistent with the notion that NMDAR activation facilitates CS bursting, bursts of postsynaptic APs were rarely seen in cells where NMDARs were blocked by intracellular application of MK-801 (40 μM) (**Fig. 3-10B**). To determine whether SK channel inhibition of the NMDAR-mediated component of EPSPs is responsible for the lack of EPSP-evoked bursting in ventral pyramidal cells, we next repeated these experiments in the presence of apamin. Although apamin had little effect on bursting in dorsal cells, it strongly facilitated EPSP-evoked CS bursting in ventral pyramidal cells (**Fig. 3-10C**). Importantly, apamin did not facilitate EPSP-evoked CS bursting in ventral pyramidal cells where intracellular perfusion of MK-801 was used to block NMDARs, demonstrating both the crucial role for NMDAR activation in EPSP-evoked CS bursting and the direct role of SK channels in suppressing NMDAR activation. Together, these findings indicate that NMDAR-mediated EPSP amplification has an important role in the ability of excitatory synaptic inputs to trigger CS-like bursting in CA1 pyramidal cells and that activation

of SK channels prevents EPSP-evoked bursting in ventral CA1 pyramidal cells by suppressing NMDAR activation and EPSP amplification.

Finally, we examined whether enhanced SK suppression of NMDAR-dependent amplification and resultant CS bursting at ventral SC synapses is responsible for the robust dorsal-ventral difference in TPS-induced LTP by examining the effects of apamin on TPS-induced CS bursting and LTP. As we observed in our initial experiments (**Fig. 3-1**), EPSPs failed to elicit CS bursting and LTP during TPS in ventral hippocampal slices under control conditions. However, inhibiting SK channels with apamin enabled robust CS bursting (**Fig. 3-11A,B**) and strongly facilitated the induction of LTP in ventral hippocampal slices (**Fig. 3-11C**), while having no effect on LTP induction in dorsal hippocampal slices (**Fig. 3-11D**).

3.4 Discussion

Results from numerous anatomical and behavioral studies provide strong support for the idea that the dorsal and ventral zones of the hippocampus have fundamentally distinct roles in spatial learning, anxiety, and emotions (Moser and Moser 1998; Fanselow and Dong 2010; Strange et al. 2014). It is unclear, however, whether the different functional roles of the dorsal and ventral hippocampus simply reflect the distinct connections of the dorsal and ventral hippocampus with other brain regions or whether the dorsal and ventral hippocampus also process information in different ways. The fact that the overall anatomical organization of the trisynaptic circuit is preserved along the entire dorsal-ventral axis suggests that a common, core algorithm is implemented throughout the hippocampus. Our results, however, challenge this view and suggest that, at least within the CA1 component of this circuit, the distinct functional roles of the dorsal

and ventral hippocampus are supported by pronounced differences in both pre- and postsynaptic function that can fundamentally influence the processing and storage of information.

Consistent with previous work (Papatheodoropoulos and Kostopoulos, 2000; Papatheodoropoulos, 2015), both paired-pulse facilitation (**Fig. 3-2A**) and the initial facilitation of transmission that occurs at the start of TPS (**Fig. 3-1B**) were significantly lower at ventral SC synapses. Surprisingly, although differences in short-term plasticity are often associated with differences in the basal probability of neurotransmitter release from presynaptic terminals, basal release probability at dorsal and ventral SC synapses was the same. This dissociation indicates that a difference in the efficacy of transmission at SC synapses in the dorsal and ventral hippocampus will only emerge during patterns of presynaptic activity that occur at frequencies high enough to engage the mechanisms underlying short-term plasticity. Thus, the distinct properties of short-term plasticity at dorsal and ventral SC fiber synapses likely give rise to profound dorsal-ventral differences in basic forms of synaptic computation, such as pattern detection and frequency filtering that are thought to be mediated by short-term plasticity (Abbott and Regehr 2004).

Our results indicate that differences in long-term plasticity can also support the segregation of hippocampal function along its dorsal-ventral axis. Specifically, we find that although theta-frequency patterns of synaptic stimulation induce robust LTP at SC synapses in the dorsal CA1 region, activation of SK-type K^+ channels potently suppresses NMDAR activation and prevents TPS-induced LTP at SC synapses in the ventral hippocampus. Consistent with our findings, both SK2 and SK3 subunits of SK channels are present in dendritic spines (Lin et al. 2008; Ballesteros-Merino et al. 2014) and activation of SK channels by increases in spine Ca^{2+} acts in a feedback fashion to limit membrane depolarization and inhibit NMDAR activation (Faber et al. 2005; Ngo-

Anh et al. 2005; Bloodgood and Sabatini 2007). Moreover, inhibiting SK channels with the selective blocker apamin facilitates LTP induction (Behnisch and Reymann 1998; Stackman et al. 2002; Faber et al. 2005; Buchanan et al. 2010). Our findings confirm and extend these earlier observations by demonstrating that regional differences in SK channel activity provide a mechanism for generating functionally distinct types of synapses where theta-frequency patterns of synaptic activity can have profoundly different effects on both synaptic transmission and long-term synaptic plasticity. Importantly, our findings also indicate that in addition to their canonical role as a detector of coincident pre- and postsynaptic activity, NMDARs also have a crucial role in EPSP-evoked CS bursting. Thus, differences in SK channel regulation of NMDAR activation at SC-CA1 pyramidal cell synapses also underlie the profound dorsal-ventral disparity in EPSP amplification and E-S coupling, processes that fundamentally impact input-output transformations at synapses.

Although our results suggest that dorsal-ventral differences in SK3 subunit expression contribute to increased SK channel activity at SC synapses in the ventral hippocampus, they do not rule out the possibility that a dorsal-ventral difference in the coupling between SK channels and sources of Ca^{2+} influx, such as NMDARs and voltage-activated Ca^{2+} channels, might also be involved. Moreover, the spine localization of SK channels is highly activity-dependent (Lin et al. 2008, 2010), suggesting that factors in addition to overall levels of expression may contribute. The specific increase in SK3 is of interest, though, as elevated SK3 subunit expression contributes to age-related deficits in both LTP and memory (Blank et al. 2003).

An important implication of our results is that differences in the susceptibility of dorsal and ventral SC synapses to LTP induction during theta-frequency stimulation are achieved by

placing differing inhibitory constraints on LTP induction. In dorsal CA1 pyramidal cells, even large EPSPs fail to induce AP bursting when inhibitory synaptic transmission is intact (**Fig. 3-4C,D**) but readily elicit CS bursts when inhibitory synaptic transmission is reduced (Fig. 7A). Thus, GABAergic inhibition acts as the sole inhibitory constraint that counteracts EPSP amplification and the activity-dependent suppression of IPSCs during TPS is sufficient to enable the EPSP-evoked CS bursting necessary for LTP induction. Although the suppression of IPSCs during TPS is similar in ventral pyramidal cells (**Fig. 3-5A**), ventral synapses have the additional potent inhibitory constraint of elevated SK channel activity that prevents theta-frequency patterns of presynaptic activity from engaging the cellular and molecular machinery necessary for LTP induction. Moreover, although we find that presynaptic facilitation does not appear to be either necessary or sufficient for TPS-induced LTP, the disruption of facilitation in Syt7-/- mutants was associated with a reduction in both EPSP-evoked CS bursting and LTP induction during TPS at dorsal SC synapses. Thus, it seems likely that the dorsal-ventral difference in facilitation also has an important role in regulating the ability of SC synapses in the dorsal and ventral hippocampus to undergo LTP in response to theta-frequency patterns of presynaptic activity. In contrast, the induction machinery for LTP, itself, appears to be unchanged between the dorsal and ventral CA1 regions (**Fig. 3-1D, 3-11C**). Thus, levels of postsynaptic phasic inhibition, presynaptic facilitation, and SK channel activity likely work together to confer differential pattern selectivity for LTP induction at dorsal and ventral SC synapses. This implies that LTP is used to store information at both dorsal and ventral SC synapses but is recruited by very different patterns of presynaptic activity.

Although the optimal activity patterns for inducing LTP at ventral SC synapses remain unclear, SK channels are inhibited by adrenergic receptor activation (Maingret et al., 2008) and

SK channel activity in dendritic spines is down-regulated by metabotropic glutamate receptor activation (Tigaret et al., 2016) as well as β-adrenergic (Faber et al., 2008) and muscarinic receptor activation (Buchanan et al. 2010; Giessel and Sabatini 2010). Thus, in addition to coincident pre- and postsynaptic activity, the induction of LTP at SC synapses in the ventral hippocampus may be highly state-dependent and require the release of modulatory neurotransmitters, such as acetylcholine or norepinephrine, to overcome the SK channel inhibition of NMDAR activation. Interestingly, a variety of neuromodulatory projections, including noradrengeric inputs from the locus coeruleus, are denser in ventral hippocampus (Haring and Davis, 1985; Strange et al. 2014). Neurons in the locus coeruleus exhibit elevated levels of tonic activity during heightened states of arousal and fire high frequency bursts of APs in response to stressful, noxious, and/or novel stimuli (Aston-Jones and Cohen, 2005; Sara and Bouret, 2012). Thus, norepinephrine, as well as other modulatory neurotransmitters that regulate SK channel activity, may serve as an essential trigger for plasticity in the ventral hippocampus during behaviors that contain greater emotional valence.

Our results also indicate a previously unappreciated strong interrelationship among several fundamental properties of synaptic transmission that have been studied for decades. These are NMDA receptor activation, EPSP amplification, and E-S coupling. As integrate-and-fire neurons, pyramidal cells are not only sensitive to the rising slope and peak of the EPSP but also the duration and magnitude of the EPSP envelope (Shadlen and Newsome, 1994; Sakai et al., 1999; Rauch et al., 2003). Because of this, the amplification of EPSP amplitude and duration due to NMDAR activation at depolarized membrane potentials strongly facilitates the ability of synaptic inputs to elicit postsynaptic APs (**Fig. 3-10**). This indicates that rather than acting as passive detectors of coincident pre- and postsynaptic activity, NMDARs also have an active role in regulating postsynaptic firing. Thus, low levels of NMDAR activation can act in a positive feedback manner

by promoting postsynaptic AP firing and bursting which, by helping to relieve the voltage-dependent Mg^{2+} block of NMDAR ion channels, leads to even stronger NMDAR activation. This phenomenon, which our results indicate allows even low-frequency patterns of synaptic activity to produce the strong levels of NMDAR activation needed for LTP induction, is likely to be a common feature of NMDAR-mediated synaptic transmission at excitatory synapses throughout the brain. Moreover, by providing an activity-dependent, negative feedback mechanism to limit NMDAR activation, SK channel activation interacts with these phenomena to regulate multiple aspects of synaptic transmission and plasticity.

Tables:

Intrinsic Excitability in Dorsal and Ventral CA1 Pyramidal Cells

Parameter	Mean ± SEM [range]	*P* value	Test
Input resistance (mV)	D: 83.6 ± 3.4 [56.5 - 99.3] (n = 13) V: 87.5 ± 7.6 [51.7 - 128.9] (n = 12)	0.892	Mann Whitney
Resting membrane potential (mV)*	D: -75.2 ± 1.1 [-80 to -66] (n = 13) V: -72.9 ± 0.8 [-79 to -69] (n = 12)	0.052	Mann Whitney
Sag w/ -100 pA injection (mV)	D: -2.7 ± 0.2 [-0.9 to -4.0] (n = 13) V: -3.2 ± 0.4 [-0.9 to -5.8] (n = 12)	0.724	Mann Whitney
Sag w/ -200 pA injection (mV)	D: -5.2 ± 0.4 [-7.2 to -2.0] (n = 13) V: -6.1 ± 0.8 [-9.9 to -1.9] (n = 12)	0.724	Mann Whitney
Rheobase (pA)	D: 892 ± 136 [533 - 2433] (n = 13) V: 1072 ± 188 [300 - 2200] (n = 12)	0.956	Mann Whitney
AP Threshold (mV)*	D: -49.0 ± 1.0 [-52.6 to -38.3] (n=13) V: -46.4 ± 1.4 [-52.7 to -36.7] (n=11)	0.072	Mann Whitney
AP Height (mV)	D: 95.5 ± 1.5 [81.0 to 105.0] (n=13) V: 90.1 ± 2.4 [72.9 to 98.2] (n=11)	0.093	Mann Whitney
AP After-depolarization Peak (mV)	D: -44.7 ± 0.7 [-48.4 to -38.7] (n = 13) V: -42.8 ± 1.4 [-48.9 to -31.6] (n = 11)	0.224	Mann Whitney
AP After-hyperpolarization Peak (mV)	D: -45.8 ± 0.9 [-51.8 to -39.0] (n = 13) V: -44.1 ± 1.0 [-39.3 to -50.5] (n = 11)	0.214	Student's t

*adjusted for calculated junction potential of 13.4 mV

3.5 Figures

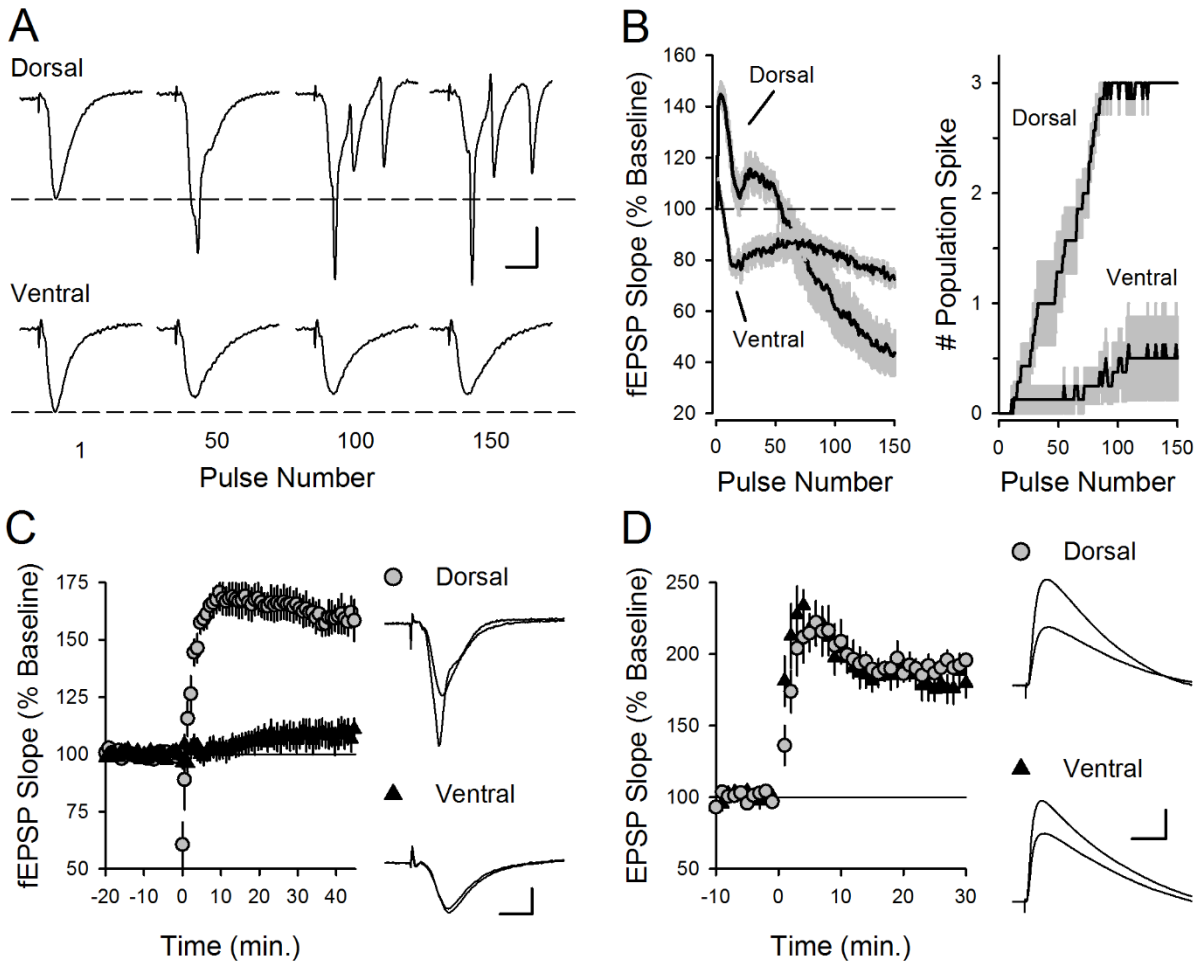

Figure 3-1 Theta-frequency modulation of transmission at SC synapses in the dorsal and ventral hippocampal CA1 regions.

A, Examples of fEPSPs evoked by TPS in dorsal (top) and ventral hippocampal slices (bottom). Note the prominent, multiple population spikes elicited during TPS in dorsal hippocampal slices. Calibration bars are 2 mV and 5 ms. ***B***, fEPSP slopes (left) and number of population spikes (right) elicited during TPS (n = 6 dorsal and 7 ventral slices, shading indicates SEM). ***C***, TPS fails to induce LTP at SC fiber synapses in ventral hippocampus. 45 minutes post-TPS (delivered at time = 0) fEPSPs were potentiated to 160 ± 8% of baseline in dorsal slices (n = 6) and were 109 ± 6% of baseline in ventral slices (n = 7, $P = 1.8 \times 10^{-4}$, Student's t-test: t(11) = 5.516). Traces at right

show superimposed fEPSPs recorded during baseline and 45 min post-TPS. Calibration bars are 2 mV and 5 ms. ***D,*** Pairing presynaptic fiber stimulation (100 pulses at 2 Hz) with postsynatpic depolarization (at time = 0) induces similar amounts of LTP in dorsal and ventral pyramidal cells. 30 minutes post-pairing EPSPs were 193 ± 4.6% of baseline in dorsal cells (n = 7) and 180 ± 10% of baseline in ventral cells (n = 6, P = 0.22, Student's t-test: t(11) = 1.291). Traces show superimposed EPSPs recorded during baseline and 30 minutes post-LTP induction. Calibration bars are 5 mV and 20 ms.

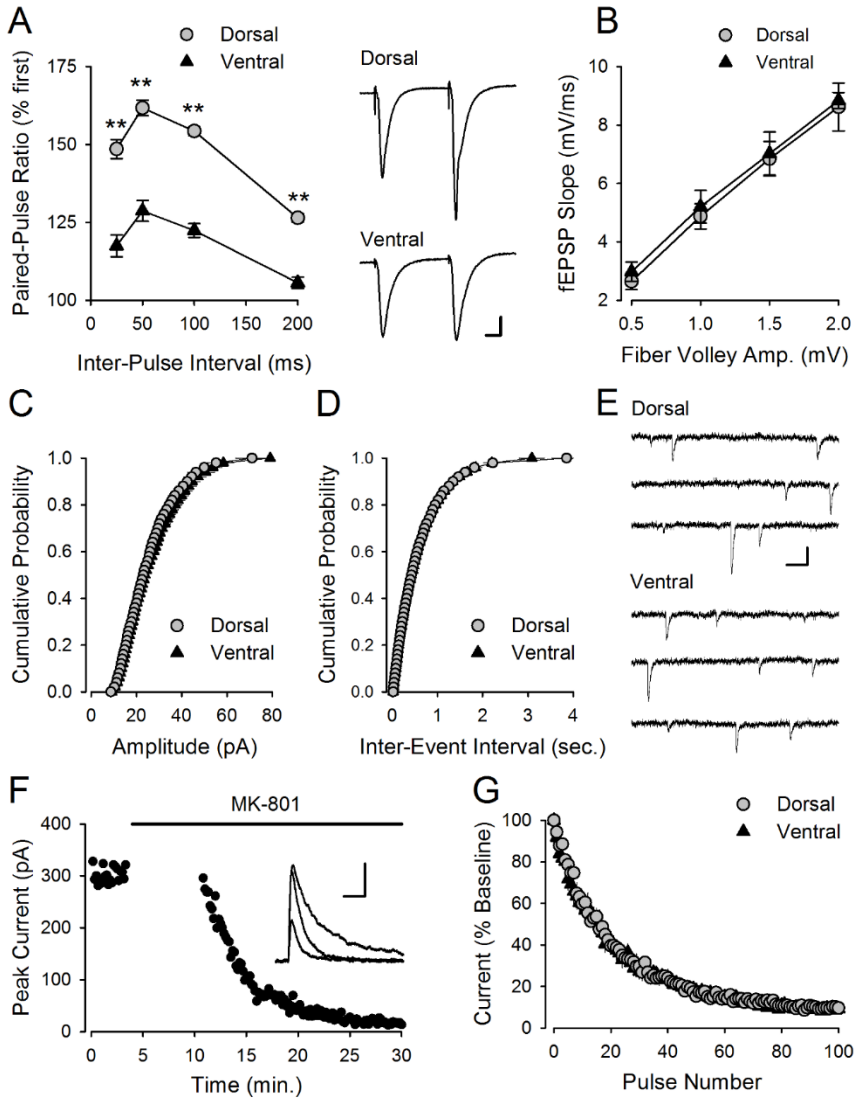

Figure 3-2 Paired-pulse facilitation, basal synaptic strength, and transmitter release probability at excitatory synapses in CA1 region of dorsal and ventral hippocampus.

A, Paired-pulse facilitation is significantly lower at ventral SC fiber synapses (**$P < 0.001$, two-way ANOVA with Student-Newman-Keuls post hoc multiple comparisons test: $P = 1.6 \times 10^{-14}$, $F_{(1,57)} = 104.7$, n = 12 dorsal and 9 ventral slices). Traces at right show fEPSPs evoked by stimulation pulses delivered with a 50 millisecond inter-pulse interval. Calibration bars are 1 mV and 10 ms. ***B,*** Comparison of presynaptic fiber volley amplitudes and postsynaptic fEPSP slopes for responses elicited by different intensities of SC fiber stimulation in dorsal (n = 17) and ventral (n = 18) hippocampal slices ($P = 0.982$, Student t-test: $t(33) = 0.022$). ***C and D***, Amplitude (C) and

frequency (D) of mEPSCs in dorsal and ventral CA1 pyramidal cells (n = 1,843 events from 7 dorsal cells and 1,815 events from 7 ventral cells). There was no significant difference in either the mean amplitude (dorsal: 23.0 ± 1.6 pA, ventral: 23.7 ± 1.0 pA, P = 0.71, Student t-test: t(11) = 0.378) or frequency of mEPSCs (dorsal: 1.7 ± 0.1 Hz, ventral: 1.7 ± 0.1 Hz, P = 0.94, Student t-test: t(11) = 0.076). ***E,*** Examples of mEPSCs recorded from dorsal and ventral pyramidal cells. Calibration bars are 20 pA and 100 ms. ***F,*** Plot shows an example of the use-dependent block of NMDAR-mediated EPSCs in the presence of 40 μM MK-801 in a dorsal CA1 pyramidal cell. Synaptic stimulation was omitted during the first 10 minutes of MK-801 application. Inset shows NMDAR-mediated currents recorded before, immediately after resuming synaptic stimulation in presence of MK-801, and after 20 stimulation pulses in presence of MK-801. Calibration bars are 100 pA and 50 ms. ***G***, The activity-dependent inhibition of NMDAR-mediated EPSCs by MK-801 is not significantly different in dorsal (n = 6) and ventral (n = 7) pyramidal cells. Weighted decay time contansts for the MK-801 inhibition of NMDAR EPSCs were 209 ± 10 ms and 214 ± 33 ms in dorsal and ventral cells, respectively (P = 0.88, Student t-test: t(11)=0.155).

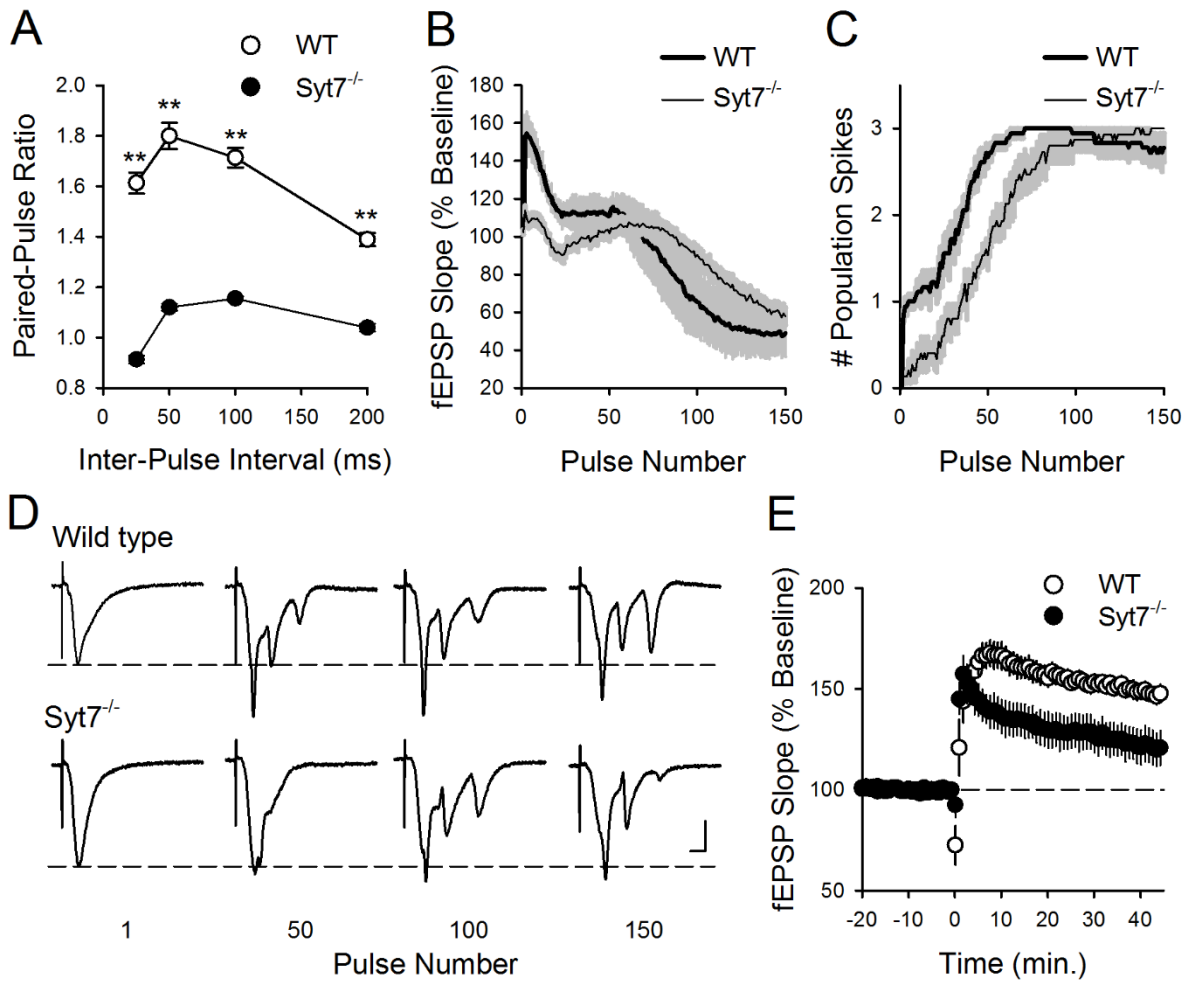

Figure 3-3 Faciliation, CS bursting, and LTP induction are reduced in dorsal hippocampal slices from Syt7$^{-/-}$ mutant mice.

A, Paired-pulse facilication is significantly reduced in dorsal hippocampal slices from Syt7$^{-/-}$ mice (**$P < 0.001$, two-way ANOVA with Student-Newman-Keuls *post hoc* multiple comparisons test: $P = 3.7\text{x}10^{-24}$, $F_{(1,36)} = 609.2$, n = 18 slices from 6 wild type and 15 slices from 5 Syt7$^{-/-}$ mutant mice). ***B*** *and* ***C***, fEPSP slopes (B) and number of population spikes (C) elicited during TPS in slices from wild type (n = 18 slices from 6 mice) and Syt7$^{-/-}$ mutants (n = 15 slices from 5 mice). Shading indicates SEM. The latency to first burst (first stimulation pulse to elicit 2 or more population spikes) was 28 ± 3.1 pulses in slices from wild type mice and 55 ± 6.7 pluses in slices from Syt7$^{-/-}$ mice ($P = 4.1\text{x}10^{-4}$, Student's t-test: t(9) = 5.445). ***D***, Examples of fEPSPs elicited during TPS in slices from wild type (top) and Syt7$^{-/-}$ mutant mice. Calibration bars are 2 mV and

5 ms. ***E***, TPS stimulation-induced LTP is reduced in Syt7$^{-/-}$ mutant mice (P = 0.014, Student's t-test: t(9) = 3.045). 45 minutes post-TPS (delivered at time = 0) fEPSPs were potentiated to 148 ± 4% of baseline in slices from wild type littermates ($P = 8.38 \times 10^{-7}$, Paired t-test: t(17) = 7.521) and were 121 ± 8% of baseline in slices from Syt7$^{-/-}$ mutants ($P = 1.86 \times 10^{-3}$, Paired t-test: t(14) = 3.824. Results from the same experiments shown in B and C.

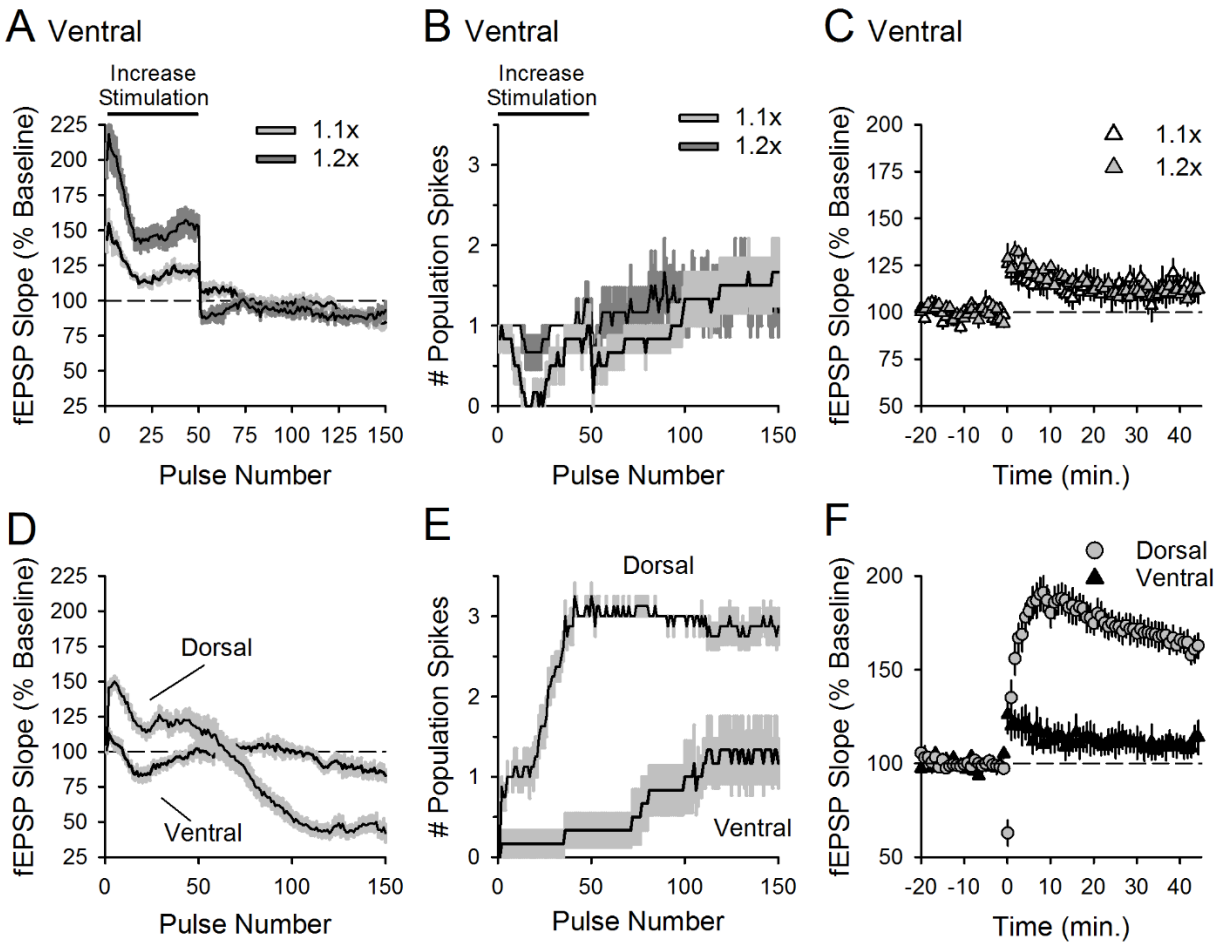

Figure 3-4 Increasing the strength of presynaptic fiber stimulation does not enable EPSP-evoked CS bursting and LTP induction in ventral hippocampus.

A** and **B, fEPSP slopes (A) and number of population spikes (B) elicited during TPS in ventral slices in experiments where the strength of presynaptic fiber stimulation during the first 50 pulses of TPS was increased to mimic (1.1x basal stimulation pulse duration, n = 6) or exceed (1.2x basal stimulation pulse duration, n = 6) the facilitation that occurs during the first 50 pulses of TPS in dorsal hippocampal slices. ***C***, Increasing the intensity of presynaptic fiber stimulation during TPS (delivered at time = 0) fails to enable LTP induction in ventral hippocampal slices. 45 minutes post-TPS fEPSPs were 112.7 ± 5.9% of baseline in experiments where stimulation strength was increased 1.1-fold at start of TPS and were 110 ± 2.5% of baseline in experiments where the stimulation strength was increased to 1.2-fold (P = 0.928, one-way ANOVA: $F_{(2,15)}$ = 0.075). ***D** and **E***, fEPSP slopes (D) and number of population spikes (E) elicited by TPS in interleaved

control experiments where the strength of presynaptic fiber stimulation was held constant throughout the experiment (n = 8 dorsal and 6 ventral slices). ***F***, TPS-induced LTP in interleaved control experiments. 45 minutes post-TPS fEPSPs were potentiated to 161 ± 5.7% of baseline in dorsal slices and were 111 ± 6% of baseline in ventral slices ($P = 6.6x10^{-5}$, Student's t-test: t(12) = 5.962).

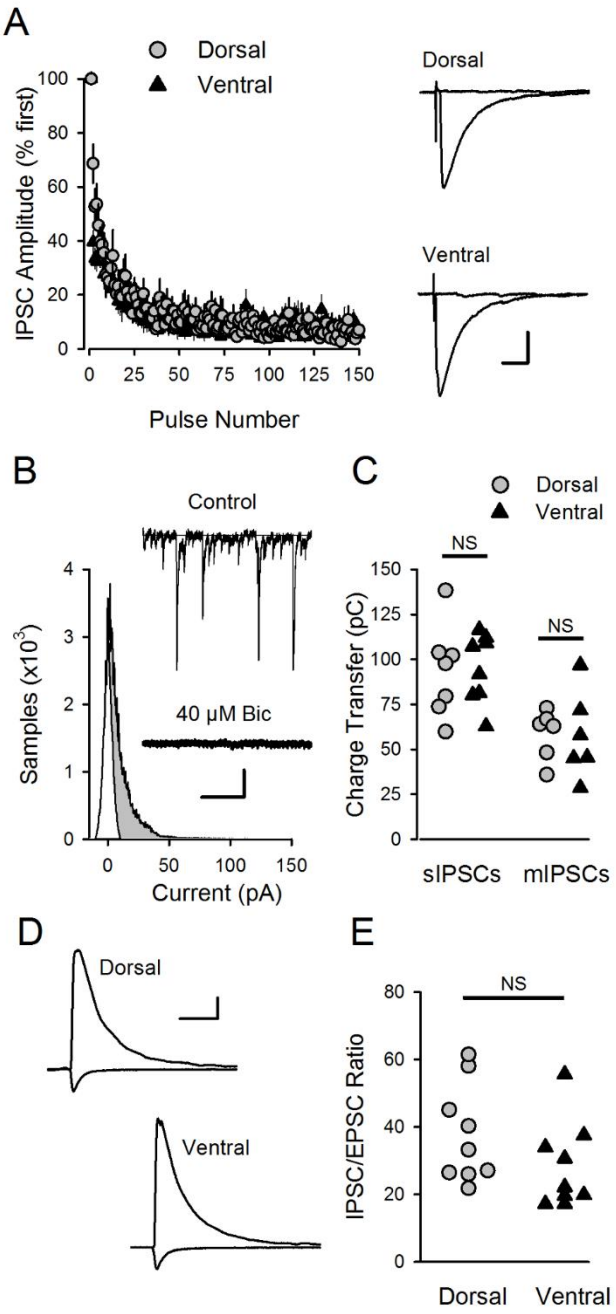

Figure 3-5 Inhibitory synaptic transmission in CA1 region of dorsal and ventral hippocampus.

A, Activity-dependent depression of IPSCs during TPS is similar in dorsal (n = 8) and ventral (n = 9) CA1 pyramidal cells. Traces show superimposed IPSCs evoked by the first and last pulse of TPS in dorsal and ventral CA1 pyramidal cells. Calibration bars are 15 ms and 100 pA. ***B***, All points histogram showing spontaneous IPSC current amplitudes in the presence and absence of

the $GABA_A$ receptor blocker bicuculline (40 μM). Shaded region corresponds to IPSC charge transfer. Traces show spontaneous IPSCs (sIPSCs) recorded from a dorsal CA1 pyramidal cell before (control) and after application of bicuculline. Calibration bars are 0.5 sec and 40 pA ***C***, Charge transfer for sIPSCs and mIPSCs (mIPSCs were recorded in presence of 1 μM TTX). Charge transfer for sIPSCs was 94.3 ± 8.4 pC in dorsal cells (n = 8) and 95.2 ± 6.8 pC in ventral cells (n = 8 ventral cells, $P = 0.937$, Student t-test: t(14) = 0.08). Charge transfer for mIPSCs was 58.5 ± 5.6 pC in dorsal cells (n = 6) and 57.6 ± 9.8 pC in ventral cells (n = 6, $P = 0.939$, Student t-test: t(10) = 0.078). ***D***, Examples of evoked IPSCs (V_m = +15 mV) and EPSCs (V_m = -42 mv) in dorsal and ventral pyramidal cells. Calibration bars are 40 ms and 250 pA. ***E***, IPSC/EPSC ratios in dorsal (37.7 ± 4.8, n = 9) and ventral pyramidal cells (27.6 ± 3.8, n = 10) were not significantly different ($P = 0.117$, Student t-test: t(17) = 1.651).

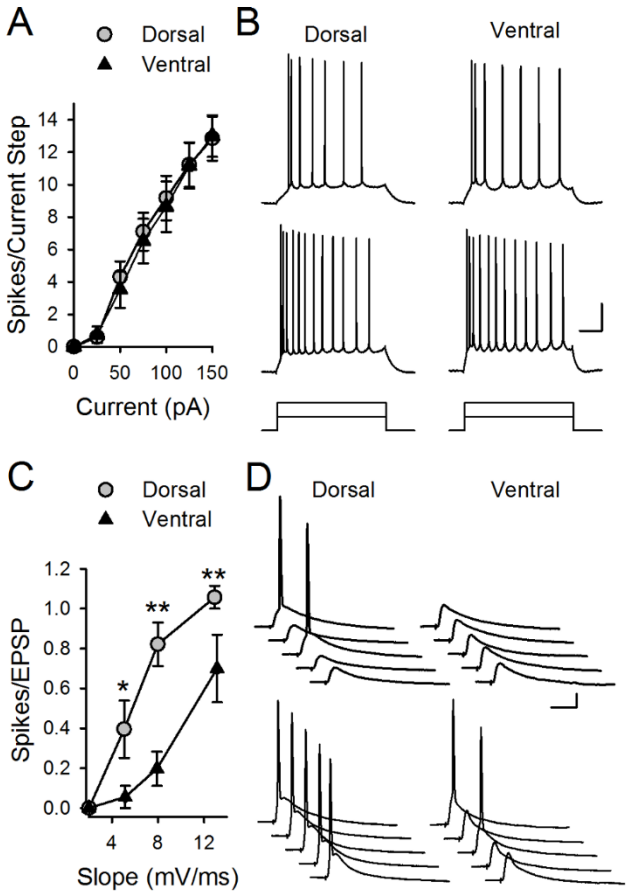

Figure 3-6 Weaker E-S coupling in ventral CA1 pyramidal cells.

A, Depolarization induced by somatic current injection elicits similar numbers of APs in dorsal and ventral pyramidal cells (n = 13 dorsal and 12 ventral cells, $P = 0.694$, two-way ANOVA: $F_{(1,138)} = 0.155$). ***B***, Traces show examples of APs elicited by 50 and 100 pA current injections in dorsal and ventral cells. Calibration bars correspond to 20 mV and 100 ms. ***C***, The ability of EPSPs to elicit postsynaptic APs is significantly reduced in ventral pyramidal cells ($*P < 0.01$, $**P < 0.001$, two-way ANOVA with Student-Newman-Keuls *post hoc* multiple comparisons test: $P = 2.3\text{x}10^{-7}$, $F_{(1,62)} = 33.794$, n = 10 dorsal and 7 ventral cells). ***D***, Traces show examples of postsynaptic responses evoked by small (top, EPSP slope ≈ 5 mV/ms) and larger EPSPs (bottom, EPSP slope ≈ 8 mV/ms). Calibration bars correspond to 10 mV and 20 ms.

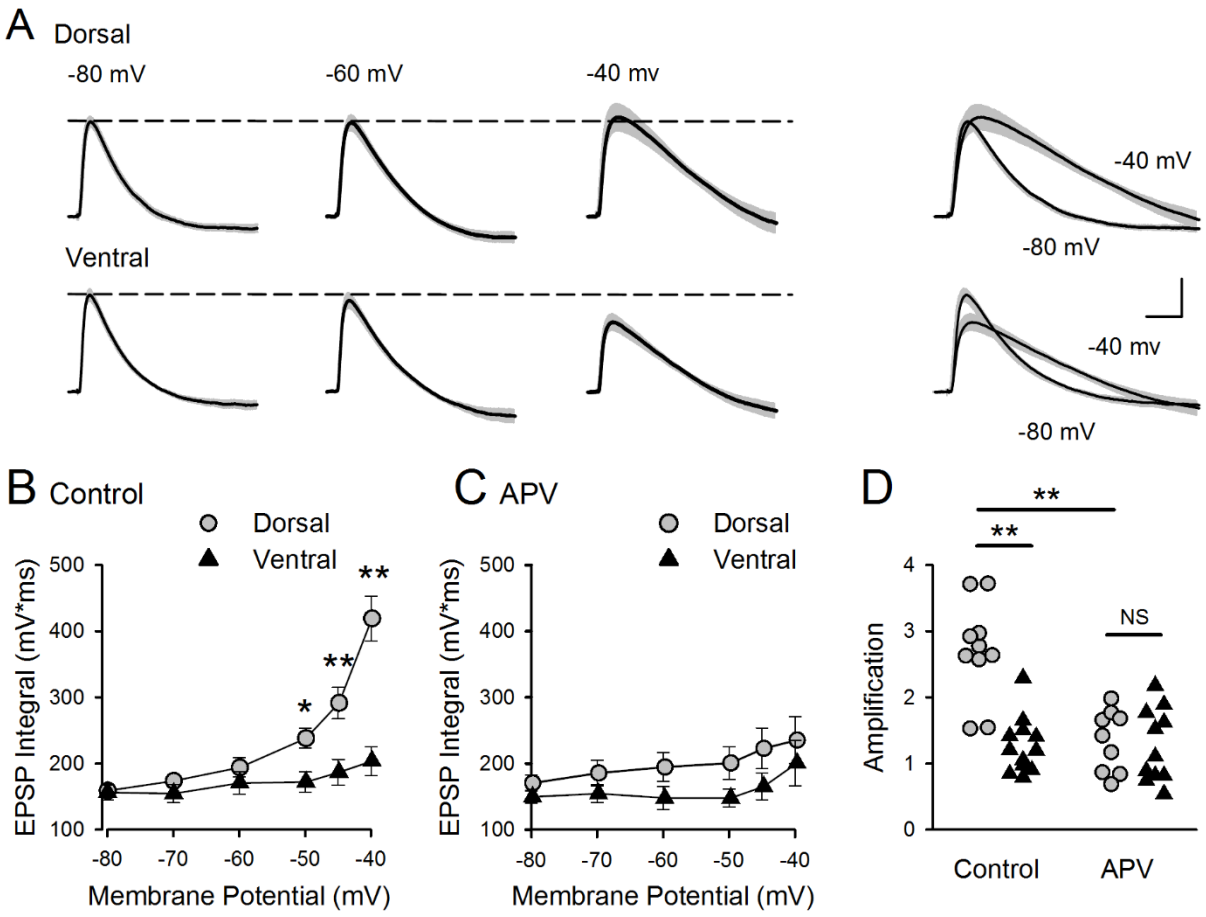

Figure 3-7 Dorsal-ventral difference in NMDAR-mediated EPSP amplification at SC synapses.

A, Average EPSPs recorded from 10 dorsal and 12 ventral cells at the indicated membrane potentials (shading indicates SEM). Traces at right show superimposed EPSPs recorded at -80 and -40 mV. Scale bars are 2 mV and 20 ms. ***B***, Increase in EPSP integrals with depolarization (EPSP amplification) is significantly smaller in ventral pyramidal cells (**P* < 0.05, ***P* < 0.001, two-way ANOVA with Student-Newman-Keuls *post hoc* multiple comparisons test: $P = 6.5 \times 10^{-8}$, $F_{(1,120)} = 33.23$). ***C***, EPSP amplification in the presence of the NMDAR blocker D-APV (50 μM) (n = 9 dorsal and 10 ventral cells). ***D***, Amplification determined from the ratio of EPSP integrals at -40 and -80 mV for all cells for results shown in (B) and (C). In control recordings the amplification in dorsal cells (2.7 ± 0.23) was significantly greater than that seen in ventral pyramidal cells (1.3 ± 0.12). Blocking NMDARs significantly reduced amplification in dorsal cells (1.3 ± 0.16) but had no effect on amplification in ventral pyramidal cells (1.3 ± 0.17). ***P* < 0.001, two-way

ANOVA with Student-Newman-Keuls *post hoc* multiple comparisons test: $P = 4.9 \times 10^{-7}$, $F_{(3,38)} = 16.544$.

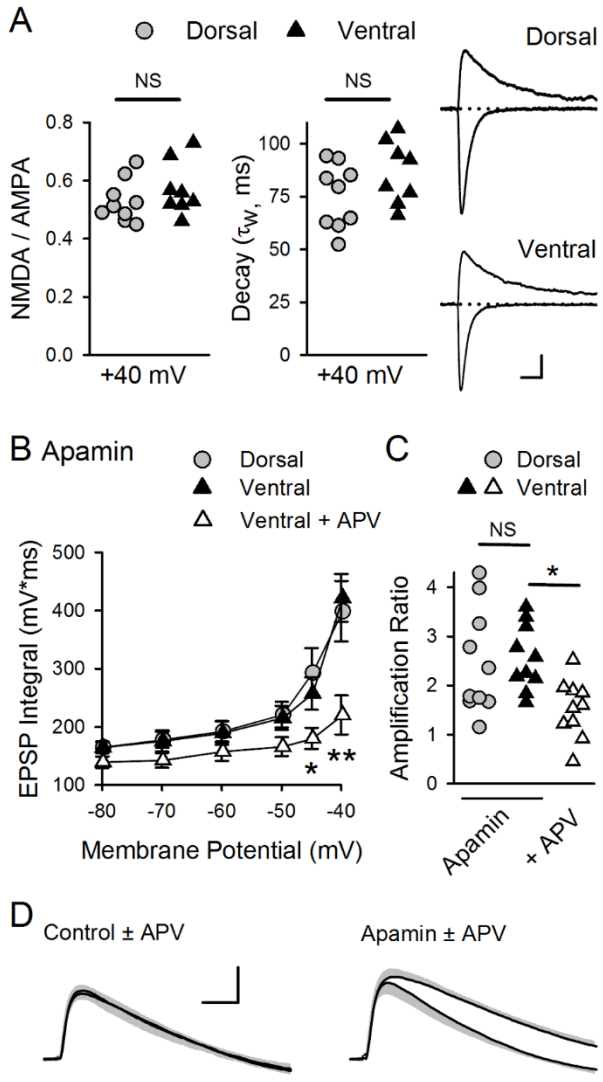

Figure 3-8 SK channel suppression of NMDAR activation and EPSP amplification at SC synapses in ventral hippocampus.

A, Ratio of NMDAR and AMPAR-mediated components (left) and decay time constants (middle) for EPSCs recorded at V_m = 40 mV in dorsal and ventral pyramidal cells (n = 9 dorsal and 8 ventral cells). Ratios were 0.52 ± 0.02 and 0.57 ± 0.03 in dorsal and ventral cells, respectively (*P* = 0.312, Student t-test: t(15) = 1.046). Decay time constants were 75 ± 5.1 ms in dorsal cells and 86 ± 5.2 ms in ventral cells (*P* = 0.15, Student t-test: t(15) = 1.517). Traces (right) show example EPSCs recorded at -80 and 40 mV. Calibration bars are 75 pA and 20 ms. ***B***, Blocking SK channels with 100 nM apamin enables NMDAR-mediated EPSP amplification in ventral pryamidal cells (**P* <

0.05, ***P* < 0.001, two-way ANOVA with Student-Newman-Keuls *post hoc* multiple comparisons test: $P = 4.1x10^{-7}$, $F_{(2,162)} = 16.12$, n = 10 dorsal and 10 ventral cells in apamin, n = 10 ventral cells in apamin plus D-APV). ***C***, Amplification for all cells in the presence of apamin or apamin plus D-APV. Amplification in the presence of apamin was 2.5 ± 0.34 and 2.6 ± 0.21 for dorsal and ventral pyramidal cells, respectively and 1.7 ± 0.17 for ventral cells in the presence of apamin + D-APV. **P* < 0.05, one-way ANOVA with Student-Newman-Keuls *post hoc* multiple comparisons test: *P* = 0.013, $F_{(2,27)} = 5.154$. ***D***, Traces show superimposed average EPSPs in ventral pyramidal cells elicited at V_m = -40 mV in the absence and presence of APV in control cells (left, from experiments shown in Fig. 7B,C) and in the presence of apamin (right). Shading indicates SEM. Calibration bars are 2 mV and 20 ms.

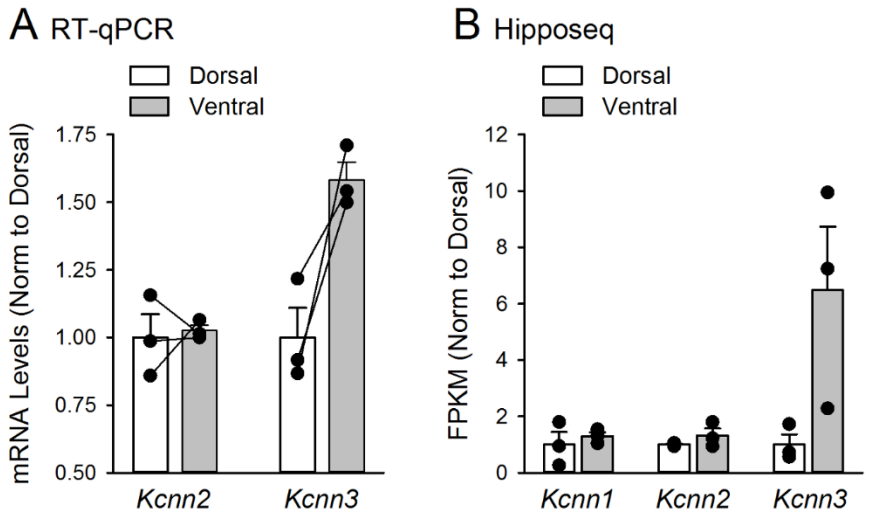

Figure 3-9 SK channel subunit expression in dorsal and ventral hippocampus.

A, Levels of *Kcnn2* (SK2) and *Kcnn3* (SK3) mRNA expression in isolated CA1 regions micro-dissected from dorsal and ventral hippocampal slices. Lines indicate values obtained from tissue samples from the same hippocampus. ***B***, Expression levels for SK channel subunit mRNA in dorsal and ventral CA1 pyramidal cells obtained using Hipposeq (Cembrowski et al., 2016B) analysis of hippocampal RNA-seq database generated by Cembrowski et al. (2016A).

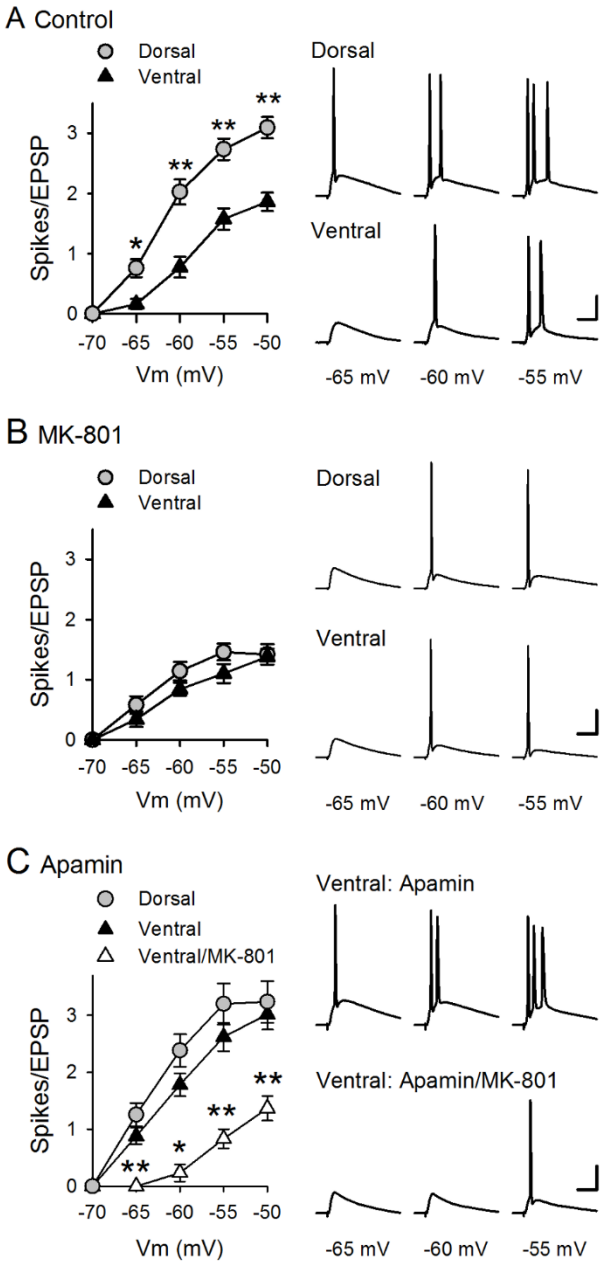

Figure 3-10 Enhancement of EPSP-evoked CS bursting by blockade of SK channels in ventral CA1 pyramidal cells.

A, Effect of membrane depolarization on EPSP-evoked AP firing in dorsal (n = 15) and ventral (n = 16) CA1 pyramidal cells. *P < 0.01, **P < 0.001, two-way ANOVA with Student-Newman-Keuls *post hoc* multiple comparisons test: $P = 1.8\text{x}10^{-15}$, $F_{(1,120)} = 83.715$. Traces show postsynaptic responses elicited at the indicated membrane potentials. ***B***, EPSPs fail to elicit

bursting when NMDARs are inhibited with intracellular application of 40 μM MK-801 (n = 10 dorsal and 10 ventral cells). ***C***, Inhibiting SK channels with 100 nM apamin enables NMDAR-dependent EPSP-evoked bursting in ventral CA1 pyramidal cells (n = 11 dorsal cells and 10 ventral cells in the presence of apamin and 6 ventral cells in the presence of apamin with intracellular application of MK-801). **P* < 0.05, ***P* < 0.001, two-way ANOVA with Student-Newman-Keuls *post hoc* multiple comparisons test: $P = 5.5 \times 10^{-14}$, $F_{(2,84)} = 44.902$. Traces show postsynaptic responses elicited in ventral pyramidal cells in the presence of apamin with and without intracellular MK-801. Calibration bars in A, B, and C are 20 mV and 20 ms.

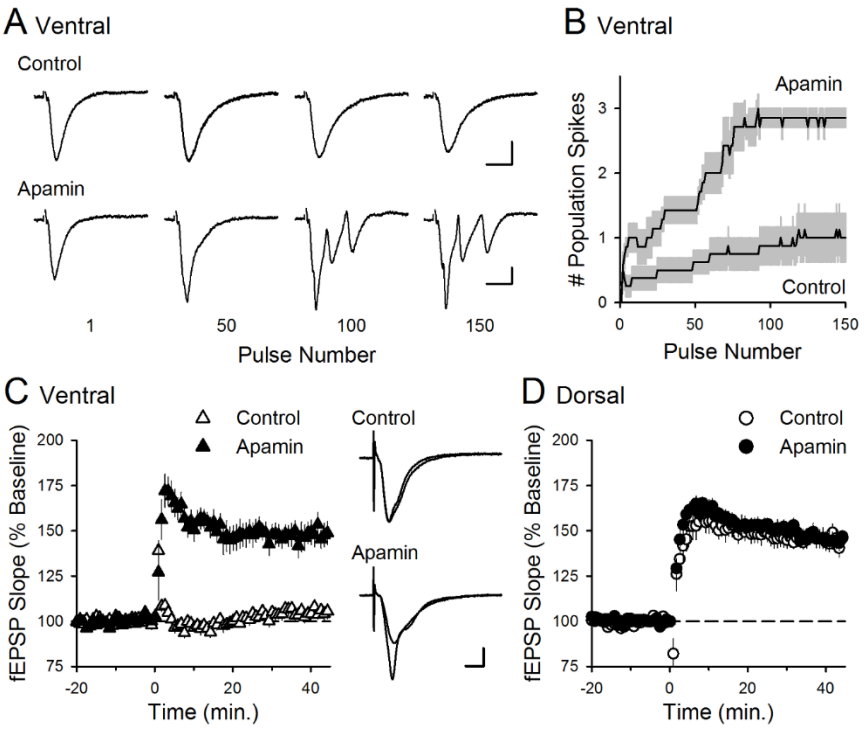

Figure 3-11 Inhibiting SK channels enables TPS-induced CS bursting and LTP in ventral hippocampal slices.

A, Traces show examples of fEPSPs elicited during TPS in ventral hippocampal slices during control experiments and in the presence of apamin. Calibration bars are 1 mV and 10 ms. ***B***, Summary of EPSP-evoked bursting during TPS in ventral hippocampal slices in the absence (control, n = 8) and presence of apamin (n = 7). Results are from same experiments shown in (C). ***C***, Apamin enables LTP induction by TPS (delivered at time = 0) in ventral hippocampal slices. 45 minutes post-TPS fEPSPs were potentiated to 149 ± 6.2% of baseline in the presence of apamin compared to 105 ± 2.9% of baseline in control experiments ($P = 1.6 \times 10^{-5}$, Students t-test: t(13) = 6.65). Traces show superimposed fEPSPs recorded during baseline and 45 minutes post-TPS in control experiments (top) and in experiments with apamin (bottom). Calibration bars are 1 mV and 5 ms. (*D*) Apamin has no effect on TPS-induced LTP in dorsal hippocampal slices. 45 minutes post-TPS fEPSPs were potentiated to 145 ± 3.8% of baseline in control experiments (n = 7) and 144 ± 4.2% of baseline in the presence of apamin (n = 7, $P = 0.85$, Student's t-test: t(12) = 0.199).

3.6 References

Abbott LF, Regehr WG (2004) Synaptic computation. Nature 431:796-803.

Andreasen M Lambert JC (1998) Somatic amplification of distally generated subthreshold EPSPs in rat hippocampal pyramidal neurones. J Physiol (Lond) 519:85-100.

Aston-Jones G, Cohen JD (2005) An integrative theory of locus coeruleus-norepinephrine function: Adaptive gain and optimal performance. Ann Rev Neurosci 28:403-450.

Ballesteros-Merino C, Watanabe M, Shigemoto R, Fukazawa Y, Adelman JP, Luján R (2014) Differential subcellular localization of SK3-containing channels in the hippocampus. Eur J Neurosci 39:883-892.

Bannerman DM, Grubb M, Deacon RMJ, Yee BK, Feldon J, Rawlins JNP (2003) Ventral hippocampal lesions affect anxiety but not spatial learning. Behav Brain Res 139:197-213.

Behnisch T, Reymann KG (1998) Inhibition of apamin-sensitive calcium dependent potassium channels facilitate the induction of long-term potentiation in the CA1 region of rat hippocampus in vitro. Neurosci Lett 253:91-94.

Blank T, Nijholt I, Kye MJ, Radulovic J, Spiess J (2003) Small-conductance, Ca^{2+}-activated K^+ channel SK3 generates age-related memory and LTP deficits. Nat Neurosci 6:911-912.

Bloodgood BL, Sabatini BL (2007) Nonlinear regulation of unitary synaptic signals by CaV(2.3) voltage-sensitive calcium channels located in dendritic spines. Neuron 53:249-260.

Bond CT, Herson PS, Strassmaier T, Hammond R, Stackman R, Maylie J, Adelman JP (2004) Small conductance Ca^{2+}-activated K^+ channel knock-out mice reveal the identity of calcium-dependent afterhyperpolarization currents. J Neurosci. 24:5301-5306.

Buchanan KA, Petrovic MM, Chamberlain SE, Marrion NV, Mellor JR (2010) Facilitation of long-term potentiation by muscarinic M(1) receptors is mediated by inhibition of SK channels. Neuron 68:948-963.

Carter BC, Giessel AJ, Sabatini BL, Bean BP (2012) Transient sodium current at subthreshold voltages: activation by EPSP waveforms. Neuron 75:1081-1093.

Cembrowski MS, Bachman JL, Wang L, Sugino K, Shields BC, Spruston N (2016A) Spatial gene-expression gradients underlie prominent heterogeneity of CA1 pyramidal neurons. Neuron 89:351-368.

Cembrowski MS, Wang L, Sugino K, Shields BC, Spruston N (2016B) Hipposeq: a comprehensive RNA-seq database of gene expression in hippocampal principal neurons. eLife 5 10.7554/eLife.14997.

Davies CH, Starkey SJ, Pozza MF, Collingridge GL (1991) GABA autoreceptors regulate the induction of LTP. Nature 349:609-11.

Deacon RMJ, Bannerman DM, Rawlins JNP (2002) Anxiolytic effects of cytotoxic hippocampal lesions in rats. Behav Neurosci 116:494-497.

Dong HW, Swanson LW, Chen L, Fanselow MS, Toga AW (2009) Genomic-anatomic evidence for distinct functional domains in hippocampal field CA1. PNAS. 106:11794-11799.

Dougherty KA, Islam T, Johnston D (2012) Intrinsic excitability of CA1 pyramidal neurones from the rat dorsal and ventral hippocampus. J Physiol. 590:5707-5722.

Dougherty KA, Nicholson DA, Diaz L, Buss EW, Neuman KM, Chetkovich DM, Johnston D (2013) Differential expression of HCN subunits alters voltage-dependent gating of h-channels in CA1 pyramidal neurons from dorsal and ventral hippocampus. J Neurophysiol 109:1940-1953.

Faber ES, Delaney AJ, Power JM, Sedlak PL, Crane JW, Sah P (2008) Modulation of SK channel trafficking by beta adrenoceptors enhances excitatory synaptic transmission and plasticity in the amygdala. J Neurosci 28:10803-10813.

Faber ES, Delaney AJ, Sah P (2005) SK channels regulate excitatory synaptic transmission and plasticity in the lateral amygdala. Nat Neurosci 8:635-641.

Fanselow MS, Dong HW (2010) Are the dorsal and ventral hippocampus functionally distinct structures? Neuron 65:7-19.

Fink AE, O'Dell TJ (2009) Short trains of theta frequency stimulation enhance CA1 pyramidal neuron excitability in the absence of synaptic potentiation. J Neurosci 29:11203-11214.

Fricker D, Miles R (2000) EPSP amplification and the precision of spike timing in hippocampal neurons. Neuron 28:559-569.

Giessel AJ, Sabatini BL (2010) M1 muscarinic receptors boost synaptic potentials and calcium influx in dendritic spines by inhibiting postsynaptic SK channels. Neuron 68:936-947.

Grienberger C, Chen X, Konnerth A (2014) NMDA receptor-dependent multidendrite Ca^{2+} spikes required for hippocampal burst firing in vivo. Neuron 81:1274-1281.

Gu N, Hu H, Vervaeke K, Storm JF (2008) SK ($KCa^{2+)}$ channels do not control somatic excitability in CA1 pyramidal neurons but can be activated by dendritic excitatory synapses and regulate their impact. J Neurophysiol 100:2589-2604.

Haring JH, Davis JN (1985) Differential distribution of locus coeruleus projections to the hippocampal formation: anatomical and biochemical evidence. Brain Res 325:366-369.

Hessler NA, Shirke AM, Malinow R (1993) The probability of transmitter release at a mammalian central synapse. Nature 366:569-572.

Hönigsperger C, Marosi M, Murphy R, Storm JF (2015) Dorsoventral differences in Kv7/M-current and its impact on resonance, temporal summation and excitability in rat hippocampal pyramidal cells. J Physiol (Lond) 593:1551-1580.

Huettner JE, Bean BP (1988) Block of N-methyl-D-aspartate-activated current by the anticonvulsant MK-801: selective binding to open channels. PNAS 85:1307-1311.

Jackman SL, Turecek J, Belinsky JE, Regehr WG (2016) The calcium sensor synaptotagmin 7 is required for synaptic facilitation. Nature 528:88-91.

Jensen MS, Azouz R, Yaari Y (1996) Spike after-depolarization and burst generation in adult rat hippocampal CA1 pyramidal cells. J Physiol (Lond) 492:199-210.

Kandel ER, Spencer WA (1961) Electrophysiology of hippocampal neurons. II. After potentials and repetitive firing. J Neurophysiol 25:243-259.

Kjelstrup KG, Tuvnes FA, Steffenach H-A, Murison R, Moser EI, Moser M-B (2002) Reduced fear expression after lesions of the ventral hippocampus. PNAS 99:10825-10830.

Leonardo ED, Richardson-Jones JW, Sibille E, Kottman A, Hen R (2006) Molecular heterogeneity along the dorsal-ventral axis of the murine hippocampal CA1 field: a microarray analysis of gene expression. Neuroscience 137:177-186.

Lin MT, Luján R, Watanabe M, Adelman JP, Maylie J (2008) SK2 channel plasticity contributes to LTP at Schaffer collateral-CA1 synapses. Nat Neurosci 11:170-177.

Lin MT, Luján R, Watanabe M, Frerking M, Maylie J, Adelman JP (2010) Coupled activity-dependent trafficking of synaptic SK2 channels and AMPA receptors. J Neurosci 30:11726-11734.

Maggio N, Segal M (2007) Unique regulation of long term potentiation in the rat ventral hippocampus. Hippocampus 17:10-25.

Maggio N, Shavit Stein E, Segal M (2015) Ischemic LTP: NMDA-dependency and dorso/ventral distribution within the hippocampus. Hippocampus 25:1465-1471.

Maingret F,Coste B, Hao J, Giamarchi A, Allen D, Crest M, Litchfield DW, Adelman JP, Delmas P (2008) Neurotransmitter modulation of small-conductance Ca^{2+}-activated K^{+} channels by regulation of Ca^{2+} gating. Neuron 59:439-449.

Malik R, Dougherty KA, Parikh K, Byrne C, Johnston D (2015) Mapping the electrophysiological and morphological properties of CA1 pyramidal neurons along the longitudinal hippocampal axis. Hippocampus 26:341-361.

Marcelin B, Lugo JN, Brewster AL, Liu Z, Lewis AS, McClelland S, Chetkovich DM, Baram TZ, Anderson AE, Becker A, Esclapez M, Bernard C (2012) Differential dorso-ventral distributions of Kv4.2 and HCN proteins confer distinct integrative properties to hippocampal CA1 pyramidal cell distal dendrites. J Biol Chem 287:17656-17661.

Moser MB, Moser EI (1998) Functional differentiation in the hippocampus. Hippocampus 8:608-619.

Mott DD, Lewis DV (1991) Facilitation of the induction of long-term potentiation by $GABA_B$ receptors. Science 252:1718-1720.

Ngo-Anh TJ, Bloodgood BL, Lin M, Sabatini BL, Maylie J, Adelman JP (2005) SK channels and NMDA receptors form a Ca^{2+}-mediated feedback loop in dendritic spines. Nat Neurosci 8:642-649.

Papatheodoropoulos C (2015) Striking differences in synaptic facilitation along the dorsoventral axis of the hippocampus. Neuroscience 301:454-470.

Papatheodoropoulos C, Kostopoulos G (2000) Decreased ability of rat temporal hippocampal CA1 region to produce long-term potentiation. Neurosci Lett 279:177-180.

Patel J, Fujisawa S, Berényi A, Royer S, Buzsáki G (2012) Traveling theta waves along the entire septotemporal axis of the hippocampus. Neuron 75:410-417.

Pentkowski NS, Blanchard DC, Lever C, Litvin Y, Blanchard RJ (2006) Effects of lesions to the dorsal and ventral hippocampus on defensive behaviors in rats. Eur J Neurosci 23:2185-2196.

Prange O, Murphy TH (1999) Correlation of miniature synaptic activity and evoked release probability in cultures of cortical neurons. J Neurosci 19:6427-6438.

Rauch A, La Camera G, Luscher HR, Senn W, Fusi S (2003) Neocortical pyramidal cells respond as integrate-and-fire neurons to in vivo-like input currents. J Neurophysiol 90:1598-1612.

Rank JB (1973) Studies of single neurons in dorsal hippocampal formation and septum in unrestrained rats, Part 1 Behavioral correlates and firing properties. Exp Neurol 41:461-531.

Rosenmund C, Clements JD, Westbrook GL (1993) Nonuniform probability of glutamate release at a hippocampal synapse. Science 262:754-757.

Sakai Y, Funahashi S, Shinomoto S (1999) Temporally correlated inputs to leaky integrate-and-fire models can reproduce spiking statistics of cortical neurons. Neural Netw 12:1181-1190.

Sara SJ Bouret S (2012) Orienting and reorienting: The locus coeruleus mediates cognition through arousal. Neuron 76:130-141.

Sekerli M, Del Negro CA, Lee RH, Butera RJ (2004) Estimating action potential thresholds from neuronal time-series: new metrics and evaluation of methodologies. IEEE Trans Biomed Eng 51:1665-1672.

Shadlen MN, Newsome WT (1994) Noise, neural codes and cortical organization. Curr Opin Neurobiol 4:569-579.

Stackman RW, Hammond RS, Linardatos E, Gerlach A, Maylie J, Adelman JP, Tzounopoulos T (2002) Small conductance Ca^{2+}-activated K^{+} channels modulate synaptic plasticity and memory encoding. J Neurosci 22:10163-10171.

Strange BA, Witter MP, Lein ES, Moser EI. 2014. Functional organization of the hippocampal longitudinal axis. Nat Rev Neurosci. 15:655-669.

Stuart G, Sakmann B (1995) Amplification of EPSPs by axo-somatic sodium channels in neocortical pyramidal neurons. Neuron 15:1065-1076.

Thomas MJ, Watabe AM, Moody TD, Makhinson M, O'Dell TJ (1998) Postsynaptic complex spike bursting enables the induction of LTP by theta frequency synaptic stimulation. J Neurosci 18:7118-7126.

Thompson CL, Pathak SD, Jeromin A, Ng LL, MacPherson CR, Mortrud MT, Cusick A, Riley ZL, Sunkin SM, Bernard A, Puchalski RB, Gage FH, Jones AR, Bajic VB, Hawrylycz MJ, Lein ES (2008) Genomic anatomy of the hippocampus. Neuron 60:1010-1021.

Tigaret CM, Olivo V, Sadowski JH, Ashby MC, Mellor JR (2016) Coordinated activation of distinct Ca^{2+} sources and metabotropic glutamate receptors encodes Hebbian synaptic plasticity. Nat Commun 7:10289 doi:10.1038/ncomms10289(2016).

Wang K, Lin MT, Adelman JP, Maylie J (2014) Distinct Ca^{2+} sources in dendritic spines of hippocampal CA1 neurons couple to SK and Kv4 channels. Neuron 81:379-387.

Wójtowicz T, Mozrzymas JW (2015) Diverse impact of neuronal activity at θ frequency on hippocampal long-term plasticity. J Neurosci Res 93:1330-1344.

4 CHAPTER IV Muscarinic Modulation of Pyramidal Cell Excitability and Long Term Potentiation Across Dorsal-Ventral Axis of Mouse Hippocampus.

4.1 Introduction

Behavioral, physiological, and anatomical evidence indicates that the dorsal and ventral zones of the hippocampus have distinct roles in cognition. How the unique functions of these zones might depend on differences in synaptic and neuronal function arising from the strikingly different gene expression profiles exhibited by dorsal and ventral CA1 pyramidal cells is unclear. To begin to address this question, I previously investigated the mechanisms underlying differences in synaptic transmission and plasticity at dorsal and ventral Schaffer collateral (SC) synapses and discovered that although basal synaptic transmission is similar, SC synapses in the dorsal and ventral hippocampus exhibit markedly different responses to theta-frequency patterns of stimulation. In contrast to dorsal hippocampus, theta-frequency stimulation fails to elicit postsynaptic complex-spike bursting and does not induce LTP at ventral SC synapses. Moreover, EPSP-spike coupling, a process that strongly influences information transfer at synapses, is weaker in ventral pyramidal cells. These results indicated that all these differences in postsynaptic function are due to an enhanced activation of SK-type K^+ channels that suppresses NMDA receptor (NMDAR)-dependent EPSP amplification at ventral SC synapses. Consistent with this, mRNA levels for the SK3 subunit of SK channels are significantly higher in ventral CA1 pyramidal cells (Cembrowski et al., 2016A).

Together, these findings indicated that a dorsal-ventral difference in SK channel regulation of NMDAR activation has a profound effect on the transmission, processing and storage of information at SC synapses and thus likely contributes to the distinct roles of the dorsal and ventral

hippocampus in different behaviors. Interestingly, SK channel activity at dendritic spines is strongly down-regulated by β-adrenergic (Carter et al. 2012) and muscarinic receptor activation (Buchanan et al. 2010; Giessel and Sabatini 2010). Thus, in addition to coincident pre- and postsynaptic activity, the induction of LTP at SC synapses in the ventral hippocampus may be highly state-dependent and require the release of modulatory neurotransmitters, such as norepinephrine or acetylcholine, to overcome the SK channel inhibition of NMDAR activation.

SK channels (small conductance calcium-activated potassium channels) are a subfamily of Ca^{2+}-activated K^{+} channels highly expressed throughout the CNS and hippocampus (Sailer et al., 2002). Previously reports indicate that SK channels are expressed and restricted to apical dendritic spines where they oppose depolarization and shunt amplitude of postsynaptic potentials and greatly regulate synaptic efficacy (Sah et al., 1996; Faber et al., 2005). Importantly SK channel activity in dendritic spines is down-regulated by muscarinic receptor activation (Buchanan et al., 2010; Giessel and Sabatini, 2010).

There are five muscarinic receptor subtypes (M1-M5) and all are expressed in the hippocampus (Hulme et al., 1999; Nathanson et al., 1987). The hippocampus receives rich cholinergic innervation from basal forebrain cholinergic neurons residing in the medial septum (Frotscher et al., 1985; Price et al., 1993) and effect of acetylcholine in the hippocampus is mediated primarily by muscarinic receptors (McKenney et al., 1984; Krnjevic 1993). Cholinergic projections from vertical and horizontal limb of diagonal band to the CA1 pyramidal cells are reported to be involved in the theta rhythm generation (Yoshida and Oka, 1994). Thus, muscarinic receptors are good candidates for neurotransmitter receptors that might modulate SK-

type K^+ channel activity, may serve as an essential trigger for plasticity in the ventral hippocampus during behaviors that contain greater emotional valence.

Two types of acetylcholine receptors, Muscarinic (mAchR) and Nicotinic (nAchR) receptors bind to acetylcholine are commonly found in the CNS. From here on, I will only focus on mAchRs, which are G-protein coupled, mediate a slow metabolic response via second messenger cascade, and are primary found in the CNS and more specifically in the hippocampus. There are five subtypes of mAchRs (M1-M5). M1, M3 and M5 cause activation of phospholipase C leading to increase in second messengers such as IP3, DAG, PKC and eventually lead to increase in intracellular Ca^{2+} while M2 and M4 inhibit adenylate cyclase thus leading to decrease in second messenger cAMP. M1 and M3 are widely expressed in pyramidal neurons while M2 and M4 are expressed in nonpyramidal neurons but M2 is expressed in discrete bands of fibers surrounding pyramidal neurons (Levey et al., 1995). Muscarinic acetylcholine receptor (mAchR) antagonists have been used to impair spatial memory (Falsafi et al., 2012), while mAchR agonists have been used to reverse learning and spatial memory impairment in animal models of Alzheimer's disease (Fisher et al., 2003). Behavior studies also indicate that increasing cholinergic levels in the ventral hippocampus but not dorsal hippocampus significantly reduces anxiety as measured in the plus-maze and shock-probe tests, indicating that only the ventral hippocampus cholinergic system in involved in the passive avoidance of painful stimuli and pointing towards a different modulatory roles of cholinergic response in the different hippocampal zones (Degroot et al., 2002). Thus, muscarinic cholinergic neurotransmission in the hippocampus plays a key role in a variety of higher brain functions, including learning and memory.

Here I investigated the mechanisms underlying dorsal-ventral differences in the LTP induction using theta pulse stimulation (TPS) patterns of SC fiber stimulation in control dorsal and ventral hippocampus slices as well as slices treated with various muscarinic neuromodulators. Our analysis of muscarinic neuromodulation of TPS-LTP provides important insights into how activation of mAchRs can modulate multiple aspects of synaptic function involved in the transfer, processing and storage of information in the hippocampus that could be targeted to attempt to reduce memory impairments in age related memory loss and Alzheimer's disease.

4.2 Material and Methods

Animals and slice preparation

Male C57Bl/6N mice (Charles River Laboratories, Cambridge, MA; 2-3 months old; housed in a 12/12 light/dark cycle) and *Syt7* knockout mice and wild type litter mates of both sexes (RRID: IMSR_JAX:004950, The Jackson Laboratory, Bar Harbor, ME; 2-3 months old; housed in a 12/12 light/dark cycle) were deeply anesthetized with isoflurane and following cervical dislocation the brain was rapidly removed and submerged in ice-cold, oxygenated (95% O_2/5% CO_2) ACSF containing (in mM) 124 NaCl, 4 KCl, 25 $NaHCO_3$, 1 NaH_2PO_4, 2 $CaCl_2$, 1.2 $MgSO_4$, and 10 glucose (Sigma-Aldrich, St. Louis, MO). On a cold plate, the brain hemispheres were separated, blocked, and the hippocampi removed. 400-µm-thick slices were then cut using a manual tissue chopper. Slices from the dorsal and ventral thirds of the hippocampus were used. Slices were maintained (at 30^{o}C) in interface-type chambers that were continuously perfused (2-3 ml/min) with ACSF and allowed to recover for at least 2 hours prior to recordings. All experimental techniques were approved by the Institutional Care and Use Committee at the University of California, Los Angeles.

Electrophysiological recordings

A bipolar, nichrome wire stimulating electrode was placed in *stratum radiatum* of the CA1 region and used to activate Schaffer collateral/commissural fiber synapses. For extracellular recordings, evoked fEPSPs (basal stimulation rate = 0.02 Hz) were recorded in *stratum radiatum* using a glass microelectrode (A-M Systems, Carlsborg, WA) filled with ACSF (resistance ranged from 5–10 MΩ). Interface-type recording chambers were used for extracellular recordings while whole-cell current-clamp recordings were done using slices maintained in submerged-slice type chambers. Whole-cell current-clamp recordings were used to examine intrinsic excitability, E-S coupling, and EPSP amplification. In these experiments recording electrodes (4–8 MΩ) were filled with a K^+-based electrode-filling solution containing (in mM) 122.5 K-gluconate, 17.5 KCl, 10 HEPES, 0.2 EGTA, 10 Na_2-phosphocreatine, 4 Mg-ATP, 0.3 Na-GTP (pH = 7.3, 290 mOsm). All cells were allowed to equilibrate for ≥ 3 minutes after break-in before starting experiments. Recordings where series resistance was ≥ 30 MΩ or unstable were discarded. Unless noted, reported membrane potentials are not adjusted for junction potentials.

LTP induction protocols

The induction of LTP by TPS was examined using a 30s long train of 5 Hz stimulation (150 pulses). At the start of each experiment the maximal fEPSP amplitude was determined and the intensity of presynaptic fiber stimulation was then adjusted to evoke fEPSPs with an amplitude ~50% of the maximal amplitude. Note that unlike more conventional theta-burst stimulation protocols, where bursts of presynaptic stimulation are delivered at 5 Hz, only single pulses of stimulation are delivered during TPS. The average slope of fEPSPs evoked between 40 and 45 min post-TPS (normalized to pre-TPS baseline) was used for statistical comparisons.

Basal properties of excitatory and inhibitory synaptic transmission

EPSP-spike (E-S) coupling was measured using whole-cell current-clamp techniques to record postsynaptic responses elicited by different intensities of SC fiber stimulation (membrane potential was set to -70 mV using current injection). Five responses were elicited at each stimulation intensity and the size of EPSPs was measured using the average EPSP slope. To examine EPSP amplification, current through the recording electrode was used to set V_m = -80 mV and the strength of SC fiber stimulation was adjusted to evoke ~5 mV EPSPs. Steady-state current injection was then used to examine the effect of membrane depolarization (up to -40 mV) on EPSP amplitude and duration. For each cell, the average of 5 EPSPs recorded at each membrane potential tested was used for analysis. D-APV was acquired from Alomone Labs. McN-A-343, Carbachol and Scopolamine were acquired from Sigma-Aldrich, St. Louis, MO, USA

Intrinsic excitability

Resting membrane potential was the steady-state membrane voltage with no current injection measured ≥ 3 min after break-in but before any kind of current injection to the neuron. All other intrinsic properties were measured with steady-state current injected to hold cells at -57 mV (~ -70 mV after correction for calculated junction potential), which was the approximate resting membrane potential for pyramidal cells. All protocols were repeated three times per cell and averaged. Firing frequency vs. injected current was measured as the number of spikes per 500 ms step in 25 pA increments from 0 pA to 150 pA.

Statistical significance was assessed using One-Way ANOVA followed by Neuman-Keuls multiple comparison test.

4.3 Results

Activation of AchRs facilitate LTP induction at SC fiber synapses in the Dorsal and Ventral hippocampus

In chapter III of this dissertation, I showed that TPS elicited complex, time-varying changes in both synaptic transmission and postsynaptic firing in dorsal slices (**Fig. 3-1**). At the SC synapse in dorsal hippocampus following an initial facilitation of synaptic transmission, EPSPs began to elicit bursts of multiple population spikes (**Fig. 3-1 A,B**). Although the facilitation gradually faded and synaptic transmission at later time points was depressed, EPSPs continued to elicit CS bursts for the remainder of the stimulation train (**Fig. 3-1B**). In stark contrast, the dynamics of synaptic transmission during TPS were less dramatic at SC synapses in the ventral hippocampus and, surprisingly, EPSPs failed to elicit postsynaptic CS bursts (**Fig. 3-1A,B**). Thus, this difference in EPSP-evoked CS bursting suggested that SC synapses in the dorsal and ventral hippocampus would exhibit an equally dramatic difference in their ability to undergo TPS-induced LTP. Indeed, TPS induced robust LTP in dorsal hippocampal slices but had no lasting effect on synaptic strength in ventral slices (**Fig. 3-1C**).

I have also previously shown that although apamin had little effect on bursting in dorsal cells, it strongly facilitated EPSP-evoked CS bursting and facilitated the induction of LTP in ventral pyramidal cells (**Fig. 3-6C**). Importantly, apamin alone did not facilitate EPSP-evoked CS bursting in ventral pyramidal cells where intracellular perfusion of MK-801 was used to block NMDARs, demonstrating both the crucial role for NMDAR activation in EPSP-evoked CS bursting and the direct role of SK channels in suppressing NMDAR activation. Giessel and Sabatini (2010) have previously shown that mAChR activation reduces the calcium sensitivity

of small conductance calcium-activated potassium (SK) channels that are found in dendritic spines, resulting in increased synaptic potentials and calcium transients.

To determine whether *AchRs* activation may differentially modulate synaptic plasticity in SC synapse in the CA1 region of both dorsal and ventral hippocampus, I next performed similar TPS-LTP experiments where I treated (present in bath solution before and after TPS-LTP induction) dorsal and ventral hippocampus slices with the cholinergic receptor agonist carbachol (CCh, 20 μM). Results (**Fig. 4-1**) indicate that AchR activation facilitates TPS-induced LTP in both dorsal ($P < 0.01$, dorsal control vs dorsal CCh), and ventral hippocampus ($P < 0.0001$, ventral control vs ventral CCh). The NMDAR antagonist APV (50 μM) blocked the induction of LTP induced by TPS in the presence of CCh in both dorsal and ventral hippocampal slices ($P < .0001$, dorsal CCh compared to dorsal CCh+APV and $P < 0.001$, ventral CCh compared to ventral CCh+APV), indicating that AchR activation facilitates the induction of NMDAR-dependent LTP. To determine if activation of muscarinic receptors underlie the ability of CCh to facilitate TPS-induced LTP I next examined whether the muscarinic receptor antagonist scopolamine (SCO, 10 μM) blocks the effects of CCh on TPS-induced LTP in the dorsal and ventral hippocampal slices.

Results from these experiments (**Fig. 4-2**), indicate that scopolamine alone does not block TPS-LTP in dorsal slices ($P > 0.05$, dorsal control compared to dorsal SCO). Scopolamine blocks the CCh induced LTP enhancement in both ventral slices ($P < 0.0001$, ventral CCh compared to ventral CCH+SCO) and CCh treated dorsal slices ($P < 0.0001$, dorsal CCh vs dorsal CCh+SCO). Surprisingly, although SCO alone had no effect on LTP in dorsal slices, it completely blocked TPS-induced LTP when co-applied with CCh. Importantly; CCh activates both muscarinic and nicotinic receptors agonist (French et al., 1999). Nicotinic acetylcholine receptors are found on

both GABAergic interneurons and presynaptic terminals (Ji et al., 2000; Alkondon et al., 2000). Therefore the decrease in TPS-LTP I see in CCh+SCO treated dorsal hippocampus slices could be due to nicotinic receptor activation on neighboring GABAergic interneurons, which are known to directly inhibit CA1 pyramidal neurons (Ji et al., 2000; Alkondon et al., 2000) and presynaptic terminals where it can block STP and LTP in the pyramidal cells (Ji et al., 2001). This suggests that cholinergic modulation of plasticity in the hippocampus exhibits a striking degree of regional specificity with excitatory synapses in the ventral hippocampus being especially sensitive to the effects of mAchR activation.

Carbachol (CCh) and Scopolamine (SCO) are very general cholinergic ligands. CCh is agonist for both muscarinic M1/M2 receptors and SCO is a general cholinergic antagonist. In particular, CCh is also a mix muscarinic and nicotinic receptor (nAChR) agonist (French et al., 1999). In the hippocampus, M1 receptors are widely distributed subtype in hippocampus and are enriched in the soma of CA1 pyramidal neurons and their proximal apical and basal dendrites (Levey et al., 1995). M2 receptors are located on axon terminals of GABAergic interneurons that provide strong inhibitory input to pyramidal cells (Freund et al., 1997; Hajos et al 1998; Ji et al., 2000; Alkondon et al., 2000). Previous studies have also shown that nAChRs (α7) are also located on pyramidal neurons as well as interneurons (Ji et al., 2001). Thus applying carbachol not only can activate M1 receptors postsynaptically but they can also activate M2 receptors presynaptically and nicotinic receptors on GABAergic interneurons and perhaps nicotinic receptors postsynaptically.

Therefore, to more directly identify the particular subtype of mAchR involved in TPS-LTP in dorsal and ventral regions of hippocampus I used more specific M1 receptor agonist, McN-A-

343 (4-(m-chlorophenyl-carbamoyloxy)-2-butynyltrimethylammonium chloride). McN-A-343 is M1 receptor agonists known to specifically bind and activate M1 receptor in the hippocampus (Ohno et al., 1994; Gisabella et al., 2005). Selectivity for M1 receptor in the hippocampus over other muscarinic receptor types also expresses in the hippocampus although at a much lower level appears to arise from the high efficacy at the M1 receptors (Michelletti et al., 1990). TPS-LTP experiments results (**Fig. 4-3**) in ventral hippocampal slices in the presence of muscarinic agonist McN-A-343 (50 µM) did not enable CS bursting (**Fig. 4-3C**) but muscarinic receptor activation (**Fig. 4-3B**) did facilitate TPS-LTP in ventral hippocampal slices compared to control conditions (post-TPS fEPSPs were 134 ± 5% in ventral slices in presense of McN-A-343 compared to 103 ± 3% in untreated ventral slices) and comparable to TPS-LTP in presence of CCH. However, once again similar to CCH, McN-A-343 had minimal effect on LTP induction (**Fig. 4-3A**) and CS bursting (**Fig. 4-3C**) in dorsal hippocampal slices (post-TPS fEPSPs were 143 ± 3% in dorsal control slices and 151 ± 8% in dorsal slices treated with McN-A-343). This indicates that muscarinic receptor activation has more critical role in cholinergic response in the ventral hippocampus compared to dorsal hippocampus. To further elucidate the mechanism by which muscarinic receptor activation enhances TPS-LTP in ventral hippocampus CA1 region I next looked at the EPSP-Spike coupling in dorsal and ventral CA1 region in presence of muscarinic receptor activator McN-A-343.

Activation of muscarinic receptors enhance EPSP-Spike Coupling at SC synapses in ventral hippocampus

Muscarinic M1 activation depolarize hippocampal CA1 pyramidal neurons and increases EPSP-Spike (E-S) coupling (Dennis et al., 2016) strongly implicates role of muscarinic modulation

of hippocampal pyramidal cells of dorsal hippocampus. We were left to wonder if there is differential muscarinic modulation of the ventral hippocampus compared to dorsal hippocampus. To determine if there is enhanced EPSP-Spike coupling of ventral hippocampus in presence of muscarinic neuromodulators, intrinsic excitability and EPSP-spike coupling was measured using whole-cell current-clamp techniques in presence of muscarinic M1 agonist McN-A343.

Similar to what I reported earlier (**Fig. 3-6A,B**) there was no significant difference between dorsal and ventral CA1 pyramidal cells in the number of APs elicited by somatic injection of pulses of depolarizing current (**Fig. 4-4**). Muscarinic agonist McN-A-343 also had no effect on number of APs elicited by somatic injection of pulses of depolarizing current (**Fig. 4-4**). In presence of muscarinic against McN-A-343, although McN-A-343 did not enhance CS bursts in dorsal CA1 pyramidal cells (**Figure 4-4A**, **top panel**) EPSPs reliably elicit robust CS bursts in CA1 pyramidal cells in ventral hippocampus slices at slopes ≈ 12 mV/ms (Fig. 5A, bottom panel). Indicating that the ability of EPSPs to elicit APs is significantly enhanced in ventral pyramidal cells in presence of muscarinic M1 receptor agonist McN-A-343.

Activation of muscarinic receptors enhance EPSP amplification at SC synapses in ventral hippocampus

To gain further insight into the mechanisms responsible for the dorsal-ventral difference in E-S coupling enhanced by muscarinic M1 receptor activation, I next examine the voltage-dependent amplification of EPSPs that occurs with membrane depolarization in pyramidal cells in presence of muscarinic M1 receptor agonist McN-A-343. I previously showed that under control conditions, although robust EPSP amplification was observed in dorsal pyramidal cells, there was little, if any, depolarization-induced amplification of EPSPs in ventral pyramidal cells (**Fig. 3-**

3A,B). Blocking SK channels with apamin (100 nM) significantly enhanced EPSP amplification in ventral pyramidal cells, abolishing the dorsal-ventral difference in EPSP amplification observed previously under control conditions (**Fig. 3-5B,C**). Next, I performed similar experiments to determine if muscarinic M1 receptor activation enhances EPSP amplification at the SC synapse in ventral hippocampus.

In presence of muscarinic agonist McN-A-343, CA1 pyramidal cells in ventral hippocampus exhibited enhanced EPSP amplification at various membrane potentials (-60 mV $^{**}P < 0.01$, -50mV and -40 mV $^{***}P < 0.001$, two-way ANOVA) compared to control untreated slices and similar to amplification seen in dorsal CA1 pyramidal cells (**Fig. 4-6A,B**). Muscarinic agonist McN-A-343 did not enhance or had very little effect on EPSP amplification in dorsal CA1 pyramidal cells as determined by looking at the ratio of EPSP integral at -40 and -80 mV.

Discussion

Previously our results indicated that differences in long-term plasticity can also support the segregation of hippocampal function along its dorsal-ventral axis. Specifically, we found that although theta-frequency patterns of synaptic stimulation induce robust LTP at SC synapses in the dorsal CA1 region, activation of SK-type K^+ channels potently suppresses NMDAR activation and prevents TPS-induced LTP at SC synapses in the ventral hippocampus. Although the optimal activity patterns for inducing LTP at ventral SC synapses remain unclear, SK channels have been shown to be inhibited by adrenergic receptor activation (Maingret et al., 2008) and SK channel activity in dendritic spines is down-regulated by metabotropic glutamate receptor activation (Tigaret et al., 2016) as well as β-adrenergic (Faber et al., 2008) and muscarinic receptor activation (Buchanan et al. 2010; Giessel and Sabatini 2010). Thus, in addition to coincident pre- and postsynaptic activity, the induction of LTP at SC synapses in the ventral hippocampus may be highly state-dependent and require the release of modulatory neurotransmitters, such as acetylcholine or norepinephrine, to overcome the SK channel inhibition of NMDAR activation.

Interestingly, a variety of neuromodulatory projections, including cholinergic inputs from the septohippocampal projections, are topographically organized with the ventral hippocampal formation receiving inputs both from the DBB and the intermediolateral septum (McKinney et al., 1983). These cholinergic septohippocampal projections from the medial sepal area to the hippocampus are proposed to have an important role in "arousal", attention, recall, memory formation (Blockland et al., 1992; Green et al., 2005) and cognition by modulating the properties of the hippocampal network by altering spike activity during rhythmic network oscillations and consequently modulate the induction and expression of both short- and long-term synaptic

plasticity (Shimoshige et al., 1997, Shinoe et al., 2005, Hasselmo et al., 2006). There is also behavior evidence indicating that mAChR antagonists impair encoding of new memories and increase cognitive impairments (Aigner et al, 1991; Erskine et al, 2004) while Ache inhibitors enhance cognitive performance (Aigner et al., 1987). Other behavior studies indicate that increase cholinergic levels in the dorsal and ventral hippocampus significantly reduces anxiety but only the ventral hippocampus cholinergic system in involved in the passive avoidance of painful stimuli (Degroot et al., 2002).

Reports also indicate that SK channels are expressed and restricted to apical dendritic spines where they oppose depolarization and shunt amplitude of postsynaptic potentials and greatly regulate synaptic efficacy (Sah et al., 1996; Faber et al., 2005). Importantly SK channel activity in dendritic spines are also down-regulated by muscarinic receptor activation (Buchanan et al., 2010; Giessel and Sabatini, 2010). This suggests that muscarinic receptor activation in the hippocampus alters neuronal excitability and synaptic plasticity, suggesting a key role for acetylcholine in learning and memory. Thus, acetylcholine and muscarinic receptors, as well as other modulatory neurotransmitters that regulate SK channel activity, may serve as an essential trigger for plasticity in the ventral hippocampus during behaviors that contain greater emotional valence.

Here I used electrophysiological approaches to examine the postsynaptic effects of muscarinic reporter activation in CA1 pyramidal neurons in dorsal and ventral hippocampus in presence of different Sub-type selective, mAchR agonists and antagonists. Consistent with our previous results at least within the CA1 component of this circuit, the distinct functional roles of the dorsal and ventral hippocampus are supported by pronounced differences in both pre- and

postsynaptic function that can fundamentally influence the processing and storage of information. We find that although theta-frequency patterns of synaptic stimulation induce robust LTP at SC synapses in the dorsal CA1 region but not in ventral CA1 region, activation of Acetylcholine receptors by non-selective cholinergic agonist Carbachol (CCh) and more selective muscarinic M1 agonist McN-A-343 facilitates TPS-induced LTP at SC synapses in the ventral hippocampus. Surprisingly although muscarinic agonists had little effect on bursts of multiple population spikes, which are due to CS bursts of postsynaptic APs, in dorsal cells, it failed to facilitated or elicit bursts of multiple population spikes in ventral pyramidal cells.

Moreover, inhibiting muscarinic M1 receptors with the selective M1 antagonist scopolamine (SCO) blocks muscarinic facilitated TPS induced LTP in both dorsal and ventral CA1 regions. Surprisingly, although SCO alone had no effect on LTP in dorsal slices, it completely blocks TPS-induced LTP when co-applied with CCh in both dorsal and ventral hippocampus slices. One possible explanation for this might be that CCh is nonselective AchR agonist. CCh can activate both muscarinic and nicotinic receptors and GABAergic interneurons; known to directly inhibit CA1 pyramidal cells (Ji et al., 2000). APV blocked the induction of LTP induced by TPS in presence of muscarinic receptor agonist in both dorsal and ventral hippocampal slices indicating that cholinergic receptor activation facilitate NMDAR-dependent LTP. This evidence suggests that cholinergic modulation of plasticity in the hippocampus exhibits a striking degree of regional specificity with excitatory synapses in the ventral hippocampus being especially sensitive to the effects of mAchR activation.

To further elucidate the mechanism by which muscarinic receptor activation enhances TPS-LTP in ventral hippocampus CA1 region I next looked at the EPSP-Spike coupling in dorsal

and ventral CA1 region in presence of selective muscarinic M1 receptor agonist, McN-A-343. I previously showed that EPSP-spike coupling, a process that strongly influences information transfer at synapses, is weaker in ventral pyramidal cells. Results indicated that all these differences in postsynaptic function were due to an enhanced activation of SK-type K^+ channels that suppresses NMDA receptor (NMDAR)-dependent EPSP amplification at ventral SC synapses. Next, I looked at whether muscarinic receptor activation enhances EPSP E-S coupling in ventral hippocampus via SK channel inhibition.

Consistent with previous report (Dennis et al., 2016) muscarinic agonist McN-A-343 depolarize hippocampal CA1 pyramidal neurons and increases EPSP-Spike (E-S) coupling strongly implicates role of muscarinic modulation of hippocampal pyramidal cells of ventral hippocampus. Muscarinic M1 activation had no effect on number of APs elicited by somatic injection of pulses of depolarizing current. In presence of muscarinic against McN-A-343, although McN-A-343 did not enhance E-S coupling in dorsal CA1 pyramidal cells EPSPs reliably enhanced E-S coupling in CA1 pyramidal cells in ventral hippocampus slices at slopes ≈ 12 mV/ms. Indicating that the ability of EPSPs to elicit APs is significantly enhanced in ventral pyramidal cells in presence of muscarinic M1 receptor agonist McN-A-343. This is in contrast to our TPS-induced LTP at SC synapses in the ventral hippocampus results where muscarinic agonist failed to enhance bursts of multiple population spikes. One possible explanation for this inconsistency might that muscarinic receptor activation suppress KCNQ/M (Kv7) potassium channel activity. Reports indicate that KCNQ/M (Kv7) potassium channel family play a key role in regulating membrane excitability during repetitive action potential discharges (Delmas et Al., 2005; Peters et al., 2005). Thus, muscarinic acetylcholine receptor mediated suppression of M-current generated by the family of KCNQ/M (Kv7) potassium channels could be responsible for

the enhanced excitability without the enhanced bursts of multiple population spikes that we observed with SK channel inhibition. Another possible explanation for the lack of TPS induced CS busting in presence of muscarinic receptor agonist McN-A-343 is that bursting requires voltage-dependent Na^+ channel currents that promote repetitive neuronal firing and modulate synaptic input (Hoehn et al., 1993). These Na^+ channels are not only responsible for initiation and propagation of action potential in hippocampal neurons but are also important regulators of neuronal excitability in the hippocampus. Research indicates that muscarinic receptor activation produces reduction in tetrodotoxin-sensitive voltage-dependent peak Na^+ currents (Cantrell et al., 1996) leading to reduction in duration burst of neuronal activity.

Another possible mechanism for this enhanced E-S coupling seen in ventral pyramidal cells in presence of muscarinic receptor agonist could be explained by examining the NMDA receptor (NMDAR)-dependent EPSP amplification at ventral SC synapses that occurs with membrane depolarization. In presence of muscarinic agonist McN-A-343, CA1 pyramidal cells in ventral hippocampus exhibited significantly enhanced EPSP amplification at various membrane potentials compared to control untreated slices and similar to amplification seen in dorsal CA1 pyramidal cells. Muscarinic agonist McN-A-343 did not enhance EPSP amplification in dorsal CA1 pyramidal cells as determined by looking at the ratio of EPSP integral at -40 and -80 mV. These results indicated that all these differences in postsynaptic function are due to an enhanced muscarinic receptor activation in the ventral SC synapse.

These data indicate that muscarinic receptor activation has more critical role in cholinergic response in the ventral hippocampus compared to dorsal hippocampus. Suggesting that activation of cholinergic receptors differentially regulate postsynaptic excitability and synaptic plasticity in

the CA1 region of dorsal and ventral hippocampus. Our findings confirm and extend these earlier observations by demonstrating that regional differences in muscarinic receptor activity provide a mechanism for generating functionally distinct types of synapses where theta-frequency patterns of synaptic activity can have profoundly different effects on both synaptic transmission and long-term synaptic plasticity.

4.4 Figures

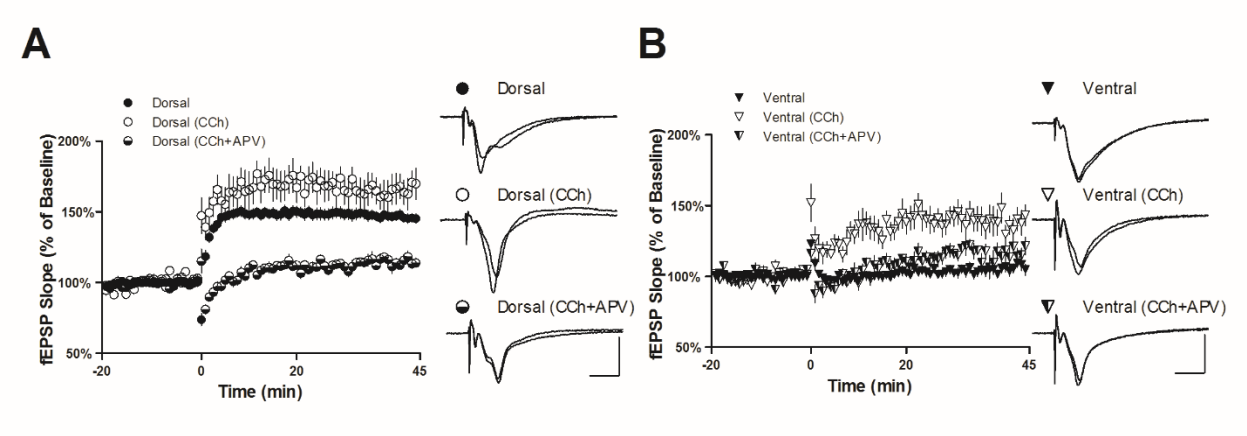

Figure 4-1 TPS induce LTP at SC fiber synapses in dorsal and ventral hippocampus in presence of non-selective muscarinic receptor agonist Carbachol (CCh).

A, TPS was delivered at time = 0 45 minutes post-TPS fEPSPs were potentiated to 146 ± 3% (mean ± SEM) of pre-TPS baseline in Control dorsal slices (n = 22, $P = 3.2 \times 10^{-12}$, Student's t-test). ***B***, In ventral slices 45 minutes post-TPS fEPSPs were potentiated to 106 ± 3% of pre-TPS baseline (n = 13, $P = .075$, Student's t-test). ***A** and **B***, In presence of CCh (20µM) 45 minutes post-TPS fEPSPs were potentiated to 167 ± 9% (mean ± SEM) of pre-TPS baseline in dorsal slices (n = 8, $P = 9.4 \times 10^{-5}$, Student's t-test) and were 138 ± 7% of baseline in ventral slices (n = 7, $P = 1.3 \times 10^{-3}$, Student's t-test). ***A** and **B***, APV (50 µM) attenuates CCh induced enhancement in dorsal and ventral slices. In presence of CCh (20 µM) and APV (50 µM) 45 minutes post-TPS fEPSPs were potentiated to 115 ± 2% (mean ± SEM) of pre-TPS baseline in dorsal slices (n = 7, $P = 4.0 \times 10^{-5}$, Student's t-test) and were 117 ± 4% of pre-TPS baseline in ventral slices (n = 5, $P = 9.0 \times 10^{-3}$, Student's t-test). Traces show superimposed EPSPs recorded during baseline and 45 minutes post-LTP induction. Calibration bars are 2 mV and 5 ms.

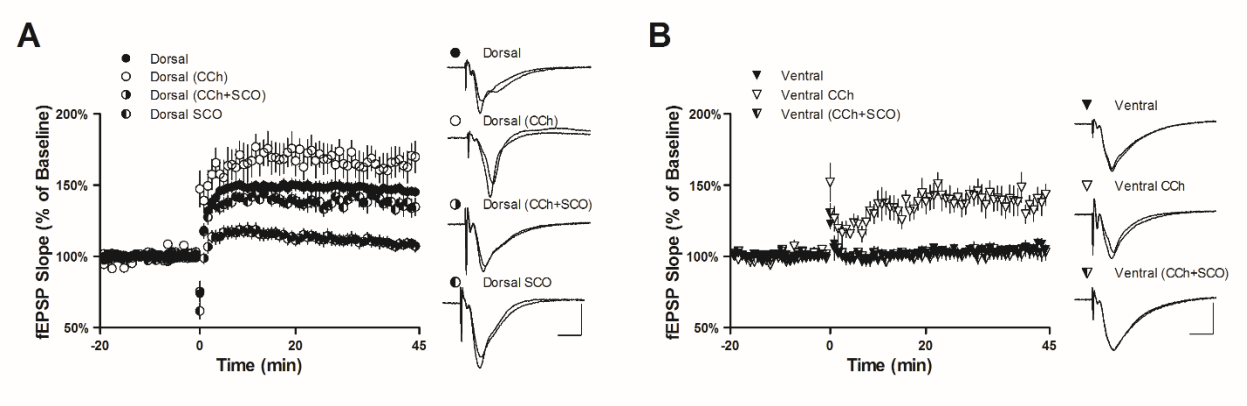

Figure 4-2 TPS induce LTP at SC fiber synapses in dorsal and ventral hippocampus in presence of non-selective muscaranic receptor agonist CCh and antagonist Scopolomin (SCO).

A, TPS was delivered at time = 0. 45 minutes post-TPS fEPSPs were potentiated to 146 ± 3% (mean ± SEM) of pre-TPS baseline in Control dorsal slices (n = 22 , $P = 3.2 \times 10^{-12}$, Student's t-test). ***B****,* In ventral slices 45 minutes post-TPS fEPSPs were potentiated to 106 ± 3% of pre-TPS baseline in ventral slices (n = 13, $P = .075$, Student's t-test). ***A*** *and* ***B****,* In presence of CCh (20 µM) 45 minutes post-TPS fEPSPs were potentiated to 167 ± 9% (mean ± SEM) of pre-TPS baseline in dorsal slices (n = 8, $P = 9.4 \times 10^{-5}$, Student's t-test) and were 138 ± 7% of pre-TPS baseline in ventral slices (n = 7, $P = 1.4 \times 10^{-3}$, Student's t-test). ***A*** *and* ***B****,* In presence of SCO (10 µM) 45 minutes post-TPS (delivered at time = 0) fEPSPs were potentiated to 136 ± 6% (mean ± SEM) of pre-TPS baseline in dorsal slices (n = 7, $P = 4.5 \times 10^{-5}$, Student's t-test). SCO (10 µM) blocks CCh induced enhancement in dorsal and ventral slices. In presence of CCH and SCO 45 minutes post-TPS fEPSPs were potentiated to 108 ± 4% (mean ± SEM) of pre-TPS baseline in dorsal slices (n = 11, $P = 1.9 \times 10^{-2}$, Student's t-test) and were 103 ± 5% of pre-TPS baseline in ventral slices (n = 8, $P = .054$, Student's t-test). Traces show superimposed EPSPs recorded during baseline and 45 minutes post-LTP induction. Calibration bars are 2 mV and 5 ms.

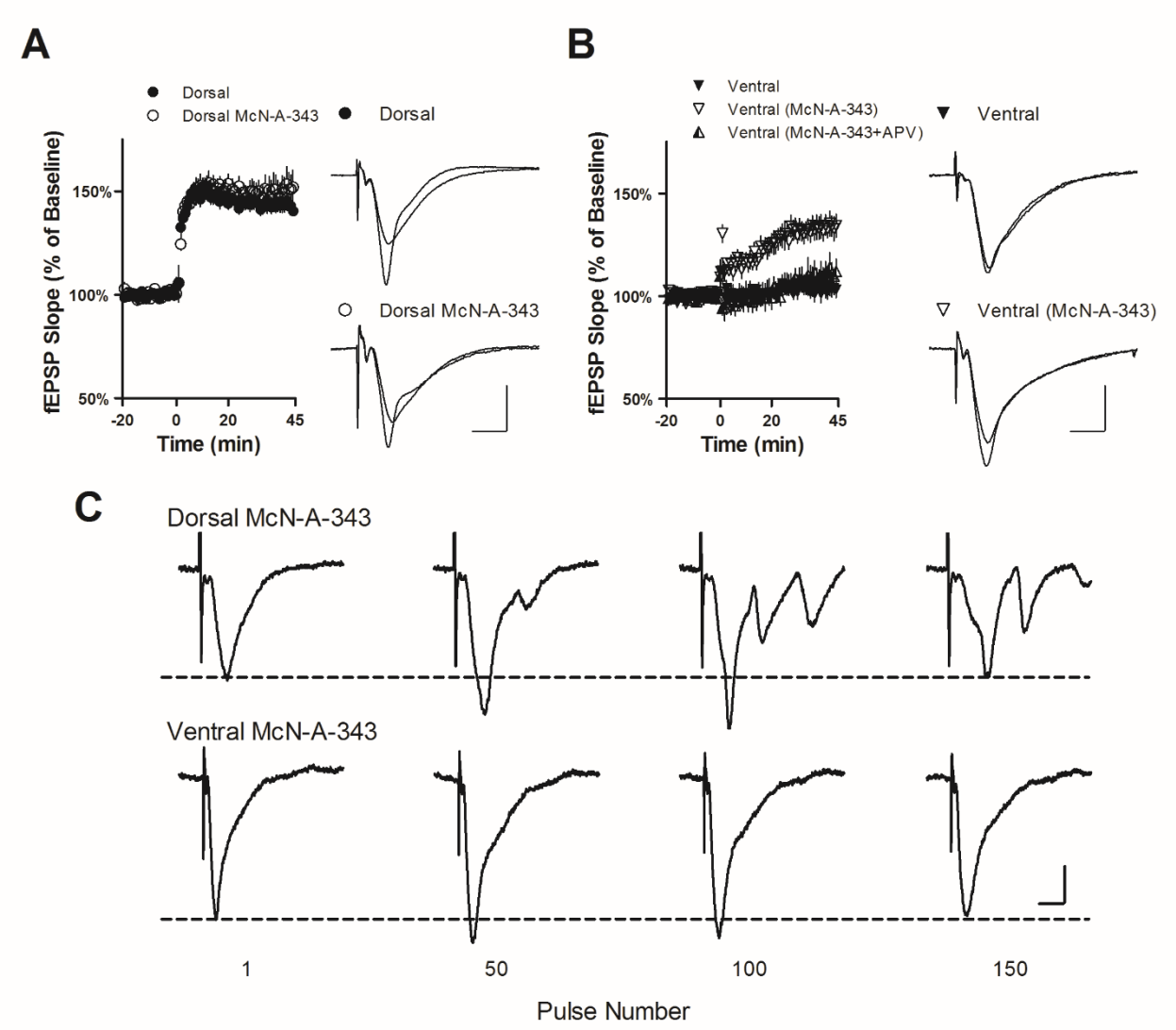

Figure 4-3 TPS induce LTP at SC fiber synapses in dorsal and ventral hippocampus in presence of selective muscarinic M1 receptor agonist McN-A-343.

TPS was delivered at time = 0 45 minutes post-TPS fEPSPs were potentiated to 143 ± 3% (mean ± SEM) of pre-TPS baseline in Control dorsal slices ***(A)*** (n = 12, $P = 4.23 \times 10^{-13}$, Student's t-test) and were 103 ± 3% of pre-TPS baseline in ventral slices ***(B)*** (n = 9, $P = .431$, Student's t-test). ***A and B***, In presence of McN-A-343 (50 µM) 45 minutes post-TPS fEPSPs were potentiated to 151 ± 8% (mean ± SEM) of pre-TPS baseline in dorsal slices (n = 10, $P = 4.1 \times 10^{-6}$, Student's t-test) and were 134 ± 5% of baseline in ventral slices (n = 9, $P = 1.1 \times 10^{-5}$, Student's t-test). ***B***, APV (50 µM) blocked McN-A-343 induced enhancement in ventral slices. In presence of McN-A-343 (50

μM) and APV (50 μM) 45 minutes post-TPS fEPSPs were potentiated to 111 ± 5% of pre-TPS baseline in ventral slices (n = 5, *P* = .135, Student's t-test). Traces show superimposed EPSPs recorded during baseline and 45 minutes post-LTP induction. Calibration bars are 2 mV and 5 ms. ***C,*** Examples of fEPSPs evoked by TPS in dorsal (top) and ventral hippocampal slices (bottom) in presense of muscarinic agonist McN-A-343. Note the prominent, multiple population spikes elicited during TPS in dorsal hippocampal slices but not in ventral hippocampus slices in presense of McN-A-343. Calibration bars are 2 mV and 5 ms.

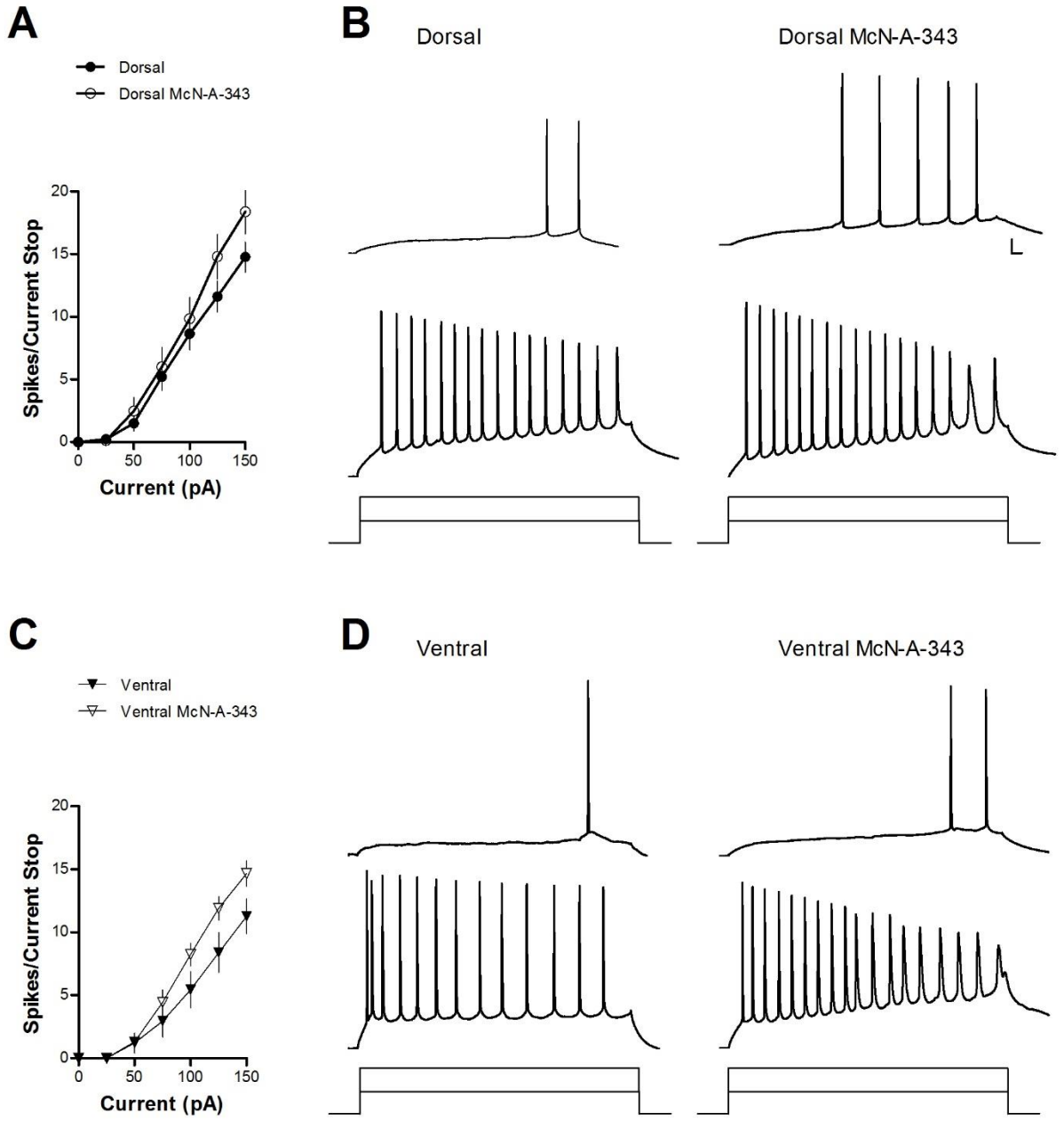

Figure 4-4 Similar intrinsic excitability in dorsal and ventral CA1 pyramidal cells.

A, Depolarization induced by somatic current injection elicits similar numbers of APs in dorsal and ventral pyramidal cells (n = 15 dorsal and 13 ventral cells, $P > 0.05$, two-way ANOVA). McN-A-343 had no effect on intrinisc excitabiluty in dorsal or ventral CA1 pyramidal cells (n = 11 dorsal McN-A-343 and 15 ventral McN-A-343, $P > 0.05$, two-way ANOVA***) B***, Traces show

examples of APs elicited by 50 and 100 pA current injections in dorsal and ventral cells with and without McN-A-343. Calibration bars correspond to 20 mV and 20 ms.

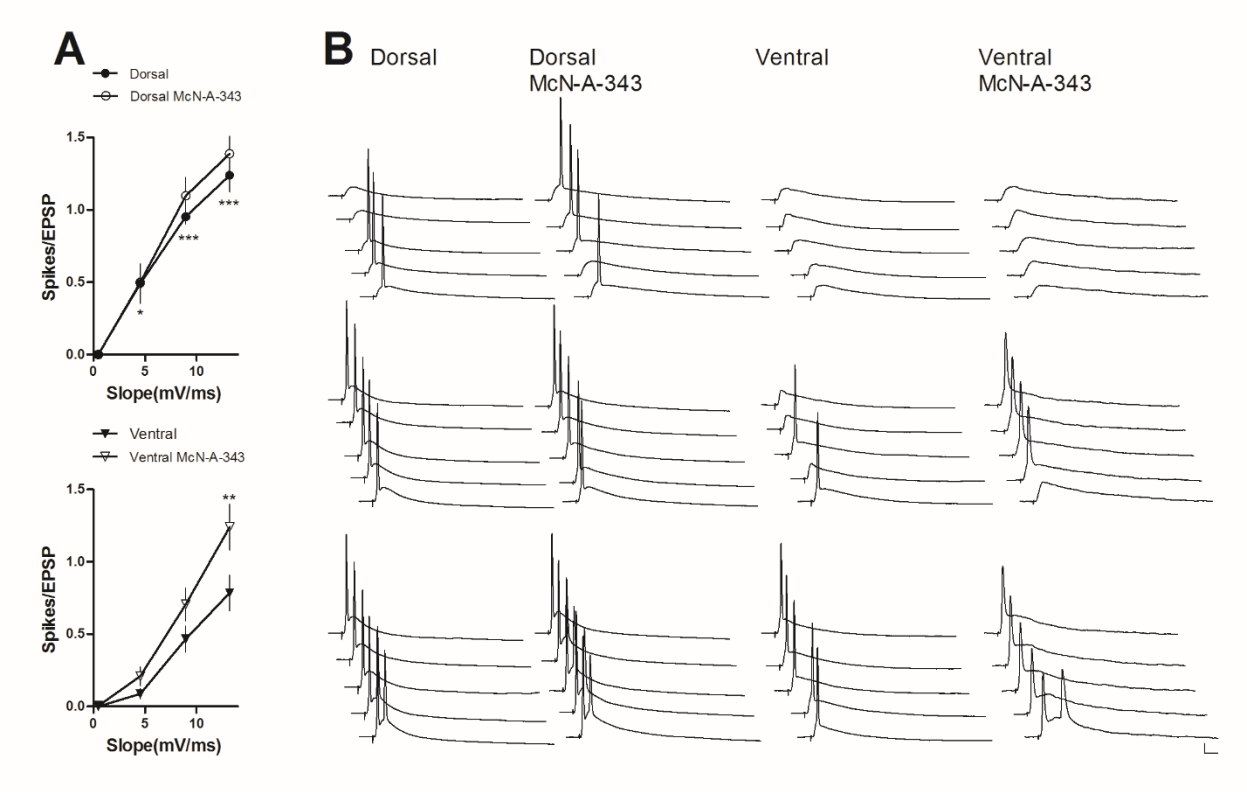

Figure 4-5 Muscarinic agonist McN-A-343 enhances the ability of EPSPs to elicit postsynaptic APs at SC synapses in ventral hippocampusin.

A, The ability of EPSPs to elicit postsynaptic APs is significantly reduced in ventral pyramidal cells (EPSP slope ≈ 5 mV/ms (**P* < 0.01), EPSP slope ≈ 8 mV/ms and 12 mV/ms (****P* < 0.001), two-way ANOVA, n = 10 dorsal and 10 ventral cells). In Presense of McN-A-343 the ability of EPSPs to elicit postsynaptic APs is significantly enhanced in ventral pyramidal cells (***P* < 0.01, two-way ANOVA, n = 10 ventral control and 11 ventral (McN-A-343)). There was no significant difference between dorsal pyramidal cells and dorsal pyramidal cells in presense of McN-A-343 (*P* > 0.05). ***B***, Traces show examples of postsynaptic responses evoked by small (top, EPSP slope ≈ 5 mV/ms), medium (middle, EPSP slope ≈ 8 mV/ms) and larger EPSPs (bottom, EPSP slope ≈ 12 mV/ms). Calibration bars correspond to 10 mV and 20 ms.

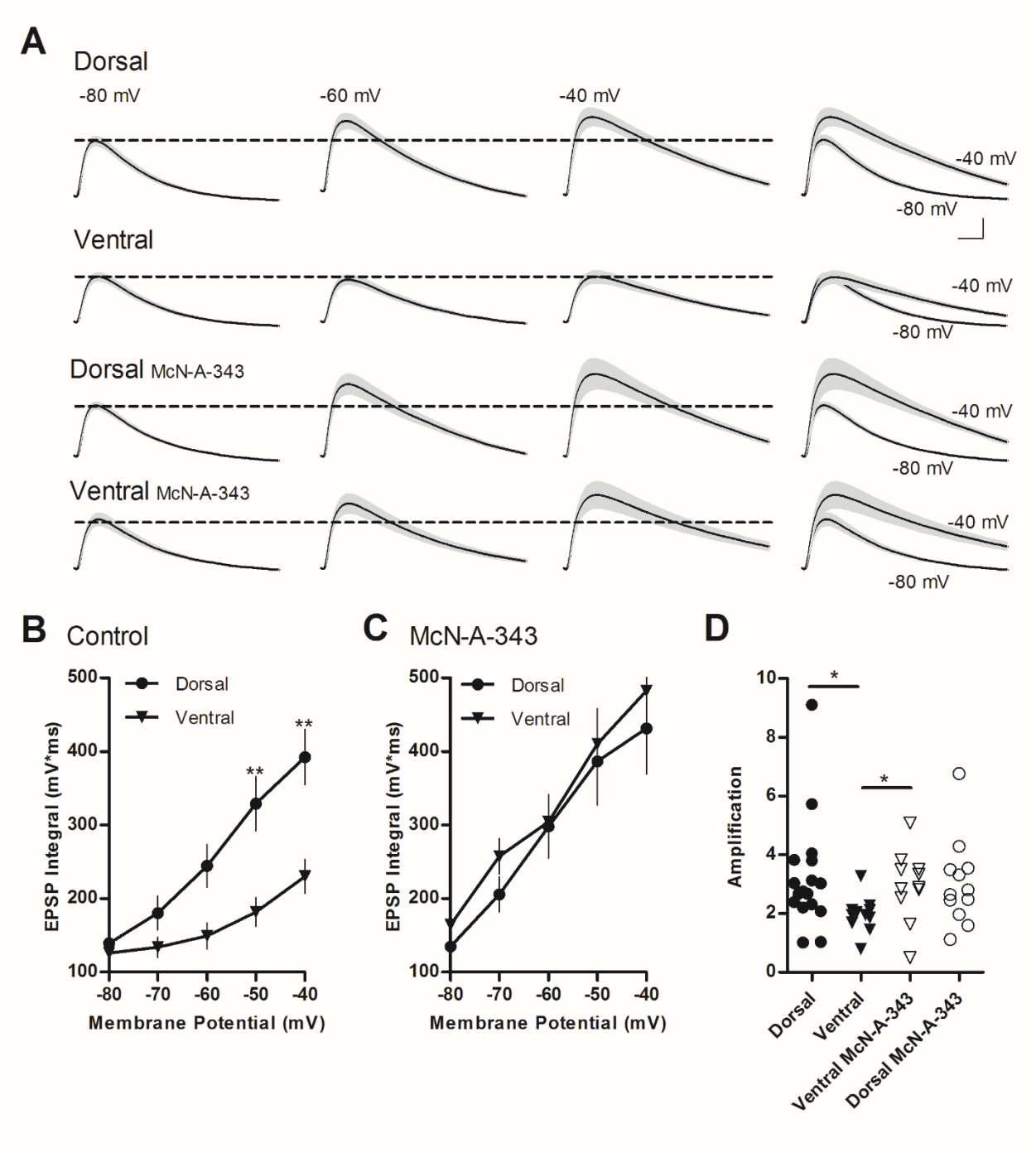

Figure 4-6 Muscarinic agonist McN-A-343 enhances EPSP amplification at SC synapses in ventral hippocampus.

A, Average EPSPs recorded from 17 dorsal cells, 13 ventral control cells and 11 dorsal McN-A-343 (50 μM) and 11 ventral McN-A-343 (50 μM) (treated cells at the indicated membrane

potentials (shading indicates SEM). Traces at right show superimposed EPSPs recorded at -80 and -40 mV. Scale bars are 2 mV and 20 ms. ***B***, Increase in EPSP integrals with depolarization (EPSP amplification) is significantly smaller in ventral pyramidal cells (***P* < 0.001, two-way ANOVA). ***C***, EPSP amplification is significantly smaller in ventral pyramidal cells compared to ventral pyramidal cells in presense of McN-A-343 (-60 mV ***P* < 0.01, -50mV and -40 mV ****P* < 0.001, two-way ANOVA). ***C***, Amplification determined from the ratio of EPSP integrals at -40 and -80 mV for all cells for results shown in (B and C). In ventral control recordings the amplification in ventral cells (1.9 ± 0.18) was significantly lower (**P* < 0.05, unpaired Student's t-test) than that seen in both dorsal control (3.2 ± 0.45) and ventral pyramidal cells in presense of McN-A-343 (2.9 ± 0.35). There was no significant difference (**P* > 0.05, unpaired Student's t-test) in amplification between dorsal pyramidal cells and dorsal pyramidal cells in presence of McN-A-343 (3.0 ± 0.42).

4.5 References:

Alkondon, Manickavasagom, et al. "Nicotine at concentrations found in cigarette smokers activates and desensitizes nicotinic acetylcholine receptors in CA1 interneurons of rat hippocampus." Neuropharmacology 39.13 (2000): 2726-2739.

Andreasen M Lambert JC (1998) Somatic amplification of distally generated subthreshold EPSPs in rat hippocampal pyramidal neurones. J Physiol (Lond) 519:85-100.

Ballesteros-Merino, Carmen, et al. "Differential subcellular localization of SK3-containing channels in the hippocampus." European Journal of Neuroscience 39.6 (2014): 883-892.

Bannerman, D. M., et al. "Ventral hippocampal lesions affect anxiety but not spatial learning." Behavioural brain research 139.1 (2003): 197-213.

Bartus, Raymond T., et al. "The cholinergic hypothesis of geriatric memory dysfunction." Science 217.4558 (1982): 408-414.

Behnisch, Thomas, and Klaus G. Reymann. "Inhibition of apamin-sensitive calcium dependent potassium channels facilitate the induction of long-term potentiation in the CA1 region of rat hippocampus in vitro." Neuroscience letters 253.2 (1998): 91-94.

Blank, Thomas, et al. "Small-conductance, Ca^{2+}-activated K+ channel SK3 generates age-related memory and LTP deficits." Nature neuroscience 6.9 (2003): 911-912.

Bloodgood, Brenda L., and Bernardo L. Sabatini. "Nonlinear regulation of unitary synaptic signals by CaV 2.3 voltage-sensitive calcium channels located in dendritic spines." Neuron 53.2 (2007): 249-260.

Bolger, John P., Brian D. Carpenter, and Milton E. Strauss. "Behavior and affect in Alzheimer's disease." Clinics in geriatric medicine 10.2 (1994): 315-337.

Buchanan, Katherine A., et al. "Facilitation of long-term potentiation by muscarinic M 1 receptors is mediated by inhibition of SK channels." Neuron68.5 (2010): 948-963.

Calabresi, Paolo, et al. "Endogenous ACh enhances striatal NMDA-responses via M1-like muscarinic receptors and PKC activation." European Journal of Neuroscience 10.9 (1998): 2887-2895.

Cantrell, Angela R., et al. "Muscarinic modulation of sodium current by activation of protein kinase C in rat hippocampal neurons." Neuron 16.5 (1996): 1019-1026.

Carter, Brett C., et al. "Transient sodium current at subthreshold voltages: activation by EPSP waveforms." Neuron 75.6 (2012): 1081-1093.

Cembrowski, Mark S., et al. "Spatial gene-expression gradients underlie prominent heterogeneity of CA1 pyramidal neurons." Neuron 89.2 (2016A): 351-368.

Cembrowski, Mark S., et al. "Hipposeq: a comprehensive RNA-seq database of gene expression in hippocampal principal neurons." eLife 5 (2016B): e14997.

Davies, Peter, and A. J. F. Maloney. "Selective loss of central cholinergic neurons in Alzheimer's disease." The Lancet 308.8000 (1976): 1403.

Deacon, Robert MJ, David M. Bannerman, and J. Nicholas P. Rawlins. "Anxiolytic effects of cytotoxic hippocampal lesions in rats." Behavioral neuroscience 116.3 (2002): 494.

Degroot, Aldemar, and Dallas Treit. "Dorsal and ventral hippocampal cholinergic systems modulate anxiety in the plus-maze and shock-probe tests." Brain research 949.1 (2002): 60-70.

Delmas, Patrick, and David A. Brown. "Pathways modulating neural KCNQ/M (Kv7) potassium channels." Nature Reviews Neuroscience 6.11 (2005): 850-862.

Dennis, Siobhan H., et al. "Activation of muscarinic M1 acetylcholine receptors induces long-term potentiation in the hippocampus." Cerebral Cortex 26.1 (2016): 414-426.

Dong, Hong-Wei, et al. "Genomic–anatomic evidence for distinct functional domains in hippocampal field CA1." Proceedings of the National Academy of Sciences 106.28 (2009): 11794-11799.

Dougherty KA, Islam T, Johnston D (2012) Intrinsic excitability of CA1 pyramidal neurones from the rat dorsal and ventral hippocampus. J Physiol. 590:5707-5722.

Dougherty, Kelly A., et al. "Differential expression of HCN subunits alters voltage-dependent gating of h-channels in CA1 pyramidal neurons from dorsal and ventral hippocampus." Journal of neurophysiology 109.7 (2013): 1940-1953.

Faber ES, Delaney AJ, Power JM, Sedlak PL, Crane JW, Sah P (2008) Modulation of SK channel trafficking by beta adrenoceptors enhances excitatory synaptic transmission and plasticity in the amygdala. J Neurosci 28:10803-10813.

Faber ES, Delaney AJ, Sah P (2005) SK channels regulate excitatory synaptic transmission and plasticity in the lateral amygdala. Nat Neurosci 8:635-641.

Falsafi, Soheil Keihan, et al. "Scopolamine administration modulates muscarinic, nicotinic and NMDA receptor systems." PloS one 7.2 (2012): e32082.

Fanselow, Michael S., and Hong-Wei Dong. "Are the dorsal and ventral hippocampus functionally distinct structures?." Neuron 65.1 (2010): 7-19.

Fernández, Manuel, Ana L. Gobartt, and Montse Balañá. "Behavioural symptoms in patients with Alzheimer's disease and their association with cognitive impairment." BMC neurology 10.1 (2010): 87.

Fisher, Abraham, et al. "M 1 muscarinic agonists can modulate some of the hallmarks in Alzheimer's disease." Journal of Molecular Neuroscience 20.3 (2003): 349-356.

Francis, Paul T., et al. "The cholinergic hypothesis of Alzheimer's disease: a review of progress." Journal of Neurology, Neurosurgery & Psychiatry 66.2 (1999): 137-147.

French, Sarah J., et al. "Hippocampal neurotrophin and trk receptor mRNA levels are altered by local administration of nicotine, carbachol and pilocarpine." Molecular brain research 67.1 (1999): 124-136.

Freund, Tamás F., and Attila I. Gulyás. "Inhibitory control of GABAergic interneurons in the hippocampus." Canadian journal of physiology and pharmacology 75.5 (1997): 479-487.

Fricker D, Miles R (2000) EPSP amplification and the precision of spike timing in hippocampal neurons. Neuron 28:559-569.

Frotscher, Michael, and Csaba Léránth. "Cholinergic innervation of the rat hippocampus as revealed by choline acetyltransferase immunocytochemistry: a combined light and electron microscopic study." Journal of Comparative Neurology 239.2 (1985): 237-246.

Gisabella, Barbara, Vadim Y. Bolshakov, and Francine M. Benes. "Regulation of synaptic plasticity in a schizophrenia model." Proceedings of the National Academy of Sciences of the United States of America 102.37 (2005): 13301-13306.

Giessel, Andrew J., and Bernardo L. Sabatini. "M1 muscarinic receptors boost synaptic potentials and calcium influx in dendritic spines by inhibiting postsynaptic SK channels." Neuron 68.5 (2010): 936-947.

Grienberger C, Chen X, Konnerth A (2014) NMDA receptor-dependent multidendrite Ca^{2+} spikes required for hippocampal burst firing in vivo. Neuron 81:1274-1281.

Gu N, Hu H, Vervaeke K, Storm JF (2008) SK (KCa2) channels do not control somatic excitability in CA1 pyramidal neurons but can be activated by dendritic excitatory synapses and regulate their impact. J Neurophysiol 100:2589-2604.

Hajos, N., et al. "Distinct interneuron types express m2 muscarinic receptor immunoreactivity on their dendrites or axon terminals in the hippocampus." Neuroscience 82.2 (1997): 355-376.

Halliwell, James V., and Paul R. Adams. "Voltage-clamp analysis of muscarinic excitation in hippocampal neurons." Brain research 250.1 (1982): 71-92.

Hoehn, Katja, et al. "A novel tetrodotoxin-insensitive, slow sodium current in striatal and hippocampal beurons." Neuron10.3 (1993): 543-552.

Hönigsperger, Christoph, et al. "Dorsoventral differences in Kv7/M-current and its impact on resonance, temporal summation and excitability in rat hippocampal pyramidal cells." The Journal of physiology 593.7 (2015): 1551-1580.

Hu, Hua, Koen Vervaeke, and Johan F. Storm. "M-channels (Kv7/KCNQ channels) that regulate synaptic integration, excitability, and spike pattern of CA1 pyramidal cells are located in the perisomatic region." Journal of Neuroscience 27.8 (2007): 1853-1867.

Hughes, Charles P., et al. "A new clinical scale for the staging of dementia." The British journal of psychiatry 140.6 (1982): 566-572.

Hulme, E. C., N. J. M. Birdsall, and N. J. Buckley. "Muscarinic receptor subtypes." Annual review of pharmacology and toxicology 30.1 (1990): 633-673.

Ishibashi, Masaru, et al. "Nicotinic and muscarinic agonists and acetylcholinesterase inhibitors stimulate a common pathway to enhance GluN2B-NMDAR responses." Proceedings of the National Academy of Sciences 111.34 (2014): 12538-12543.

Ji D, Dani JA. Inhibition and disinhibition of pyramidal neurons by activation of nicotinic receptors on hippocampal interneurons. J Neurophysiol 2000; 83: 2682–90

Ji, Daoyun, Remigijus Lape, and John A. Dani. "Timing and location of nicotinic activity enhances or depresses hippocampal synaptic plasticity." Neuron 31.1 (2001): 131-141.

Kjelstrup, Kirsten G., et al. "Reduced fear expression after lesions of the ventral hippocampus." Proceedings of the National Academy of Sciences99.16 (2002): 10825-10830.

Lancaster, B., and P. R. Adams. "Calcium-dependent current generating the afterhyperpolarization of hippocampal neurons." Journal of Neurophysiology55.6 (1986): 1268-1282.

Krnjević, K. "Central cholinergic mechanisms and function." Progress in brain research 98 (1993): 285-292.

Leonardo, E. D., et al. "Molecular heterogeneity along the dorsal–ventral axis of the murine hippocampal CA1 field: a microarray analysis of gene expression." Neuroscience 137.1 (2006): 177-186.

Levey, A. I., et al. "Expression of m1-m4 muscarinic acetylcholine receptor proteins in rat hippocampus and regulation by cholinergic innervation." Journal of Neuroscience 15.5 (1995): 4077-4092.

Lin, Mike T., et al. "SK2 channel plasticity contributes to LTP at Schaffer collateral–CA1 synapses." Nature neuroscience 11.2 (2008): 170-177.

Madison, D. V., B. Lancaster, and R. A. Nicoll. "Voltage clamp analysis of cholinergic action in the hippocampus." Journal of Neuroscience 7.3 (1987): 733-741.

Maggio, Nicola, and Menahem Segal. "Unique regulation of long term potentiation in the rat ventral hippocampus." HIPPOCAMPUS-NEW YORK-CHURCHILL LIVINGSTONE- 17.1 (2007): 10.

Malik R, Dougherty KA, Parikh K, Byrne C, Johnston D (2015) Mapping the electrophysiological and morphological properties of CA1 pyramidal neurons along the longitudinal hippocampal axis. Hippocampus 26:341-361.

Marcelin, Béatrice, et al. "Differential dorso-ventral distributions of Kv4. 2 and HCN proteins confer distinct integrative properties to hippocampal CA1 pyramidal cell distal dendrites." Journal of Biological Chemistry 287.21 (2012): 17656-17661.

McKinney, M., and Elliott Richelson. "The coupling of the neuronal muscarinic receptor to responses." Annual review of pharmacology and toxicology 24.1 (1984): 121-146.

Micheletti, R., and A. Schiavone. "Functional determination of McN-A-343 affinity for M1 muscarinic receptors." Journal of Pharmacology and Experimental Therapeutics 253.1 (1990): 310-314.

Moser MB, Moser EI (1998) Functional differentiation in the hippocampus. Hippocampus 8:608-619.

Nathanson, Neil M. "Molecular properties of the muscarinic acetylcholine receptor." Annual review of neuroscience 10.1 (1987): 195-236.

Ngo-Anh TJ, Bloodgood BL, Lin M, Sabatini BL, Maylie J, Adelman JP (2005) SK channels and NMDA receptors form a Ca^{2+}-mediated feedback loop in dendritic spines. Nat Neurosci 8:642-649.

Nilsson, Lena, et al. "Physostigmine restores 3 H-acetylcholine efflux from Alzheimer brain slices to normal level." Journal of neural transmission 67.3 (1986): 275-285.

Ohno, Masuo, Tsuneyuki Yamamoto, and Shigenori Watanabe. "Blockade of hippocampal M 1 muscarinic receptors impairs working memory performance of rats." Brain research 650.2 (1994): 260-266.

Papatheodoropoulos, C. "Striking differences in synaptic facilitation along the dorsoventral axis of the hippocampus." Neuroscience 301 (2015): 454-470.

Papatheodoropoulos, Costas, and George Kostopoulos. "Decreased ability of rat temporal hippocampal CA1 region to produce long-term potentiation." Neuroscience letters 279.3 (2000): 177-180.

Pentkowski, Nathan S., et al. "Effects of lesions to the dorsal and ventral hippocampus on defensive behaviors in rats." European Journal of Neuroscience 23.8 (2006): 2185-2196.

Peters, H. Christian, et al. "Conditional transgenic suppression of M channels in mouse brain reveals functions in neuronal excitability, resonance and behavior." Nature neuroscience 8.1 (2005): 51-60.

Power, A. E., et al. "Cholinergic modulation of memory in the basolateral amygdala involves activation of both m1 and m2 receptors." Behavioural pharmacology 14.3 (2003): 207-213.

Sah, Pankaj, and John M. Bekkers. "Apical dendritic location of slow afterhyperpolarization current in hippocampal pyramidal neurons: implications for the integration of long-term potentiation." Journal of Neuroscience 16.15 (1996): 4537-4542.

Sailer, Claudia A., et al. "Regional differences in distribution and functional expression of small-conductance Ca^{2+}-activated K+ channels in rat brain." Journal of Neuroscience 22.22 (2002): 9698-9707.

Price, Donald L., Vassilis E. Koliatsos, and Richard C. Clatterbuck. "Cholinergic systems: human diseases, animal models, and prospects for therapy." Progress in brain research 98 (1993): 51-60.

Sheffler, Douglas J., et al. "A novel selective muscarinic acetylcholine receptor subtype 1 antagonist reduces seizures without impairing hippocampus-dependent learning." Molecular pharmacology 76.2 (2009): 356-368.

Shimoshige, Yukinori, et al. "Involvement of M 2 receptor in an enhancement of long-term potentiation by carbachol in Schaffer collateral-CA1 synapses of hippocampal slices." Neuroscience research 27.2 (1997): 175-180.

Shinoe, Toru, et al. "Modulation of synaptic plasticity by physiological activation of M1 muscarinic acetylcholine receptors in the mouse hippocampus." Journal of Neuroscience 25.48 (2005): 11194-11200.

Stackman, Robert W., et al. "Small conductance Ca^{2+}-activated K+ channels modulate synaptic plasticity and memory encoding." Journal of Neuroscience22.23 (2002): 10163-10171.

Strange, Bryan A., et al. "Functional organization of the hippocampal longitudinal axis." Nature Reviews Neuroscience 15.10 (2014): 655-669.

Stuart G, Sakmann B (1995) Amplification of EPSPs by axo-somatic sodium channels in neocortical pyramidal neurons. Neuron 15:1065-1076.

Tian, Meng, et al. "STEP activation by Gαq coupled GPCRs opposes Src regulation of NMDA receptors containing the GluN2A subunit." Scientific Reports 6 (2016).

Thomas, Mark J., et al. "Postsynaptic complex spike bursting enables the induction of LTP by theta frequency synaptic stimulation." Journal of Neuroscience 18.18 (1998): 7118-7126.

Thompson, Carol L., et al. "Genomic anatomy of the hippocampus." Neuron60.6 (2008): 1010-1021.

Wang K, Lin MT, Adelman JP, Maylie J (2014) Distinct Ca^{2+} sources in dendritic spines of hippocampal CA1 neurons couple to SK and Kv4 channels. Neuron 81:379-387.

Yoshida, Kazunori, and Hiroshi Oka. "Topographical projections from the medial septum-diagonal band complex to the hippocampus: a retrograde tracing study with multiple fluorescent dyes in rats." Neuroscience research 21.3 (1995): 199-209.

Yue, Cuiyong, and Yoel Yaari. "KCNQ/M channels control spike afterdepolarization and burst generation in hippocampal neurons." Journal of Neuroscience 24.19 (2004): 4614-4624.

5 Conclusion

Hippocampus not only plays an important role in learning and memory but also is also involved in spatial navigation, emotion, and anxiety. The hippocampus is one of the most extensively studied regions of the nervous system since the discovery that lesions of hippocampus leads to severe loss of short term and long term memory as well as the discovery of long term potentiation, long lasting activity dependent enhancement of synaptic transmission, in the hippocampus excitatory circuitry. Long term potentiation is considered the most prominent candidate for mechanism of learning and memory and there are detailed hypotheses about how signals that drive learning are encoded and how they might be stored. Because of its simple architecture, organization of the trisynaptic excitatory circuitry it is perfectly suited for examining how neuromodulatory projections can affect synaptic plasticity and cell excitability and how this modulatory signal can drive learning at the circuit level.

In chapter 1, I examined whether calcium-independent, metabotropic forms of NMDAR signaling might have an important role in synaptic plasticity. The results from these experiments indicate that there is a crucial role for NMDAR-mediated Ca^{2+} signaling in NMDAR-dependent LTD at excitatory synapses on hippocampal CA1 pyramidal neurons. This is consistent with a large body of previous results, all of which support a crucial role for NMDAR-mediated Ca^{2+} signaling in LTD, an activity-dependent depression of EPSP due to low rate (1 Hz) stimulation over long periods (10-15 minutes).

In Chapter II, we examined whether mis-timed feeding impact learning and memory in mice. The results from these experiments indicated that time-restricted feeding had dramatic negative effects on commonly used learned behaviours such as hippocampal-dependent contextual

fear conditioning and novel object recognition. In addition, we found that LTP was significantly impaired in the misaligned group, indicating significant deficits in synaptic plasticity in the misaligned hippocampus. This is the first demonstration that the time of eating can impact the physiological underpinning of learned behaviour.

In Chapter III, I examined the mechanisms underlying differences in synaptic transmission and plasticity at dorsal and ventral Schaffer collateral (SC) synapses in the mouse hippocampus. The results from these experiments indicated that dorsal and ventral SC synapses exhibit markedly distinct responses to TPS and, in contrast to dorsal hippocampus, TPS fails to induce LTP at ventral synapses. Excitatory postsynaptic potential (EPSP) amplification is also strongly reduced at ventral synapses and, as a result, both EPSP-spike (E-S) coupling and EPSP-evoked complex spike (CS) bursting are significantly weaker in ventral pyramidal cells. These results also indicate that all of these differences in postsynaptic function arise from a common mechanism: an enhanced activation of Ca^{2+}-activated SK-type K^+ channels that strongly inhibits NMDA receptor (NMDAR) activation at ventral SC synapses. These results suggest that modulatory neurotransmitter receptors that that regulate SK channel function may have an especially important role in regulating synaptic plasticity in the CA1 region of the ventral hippocampus.

In chapter IV, I examined the potential role of cholinergic muscarinic neuromodulation in regulating TPS-LTP in dorsal and ventral Schaffer collateral (SC) synapses in the mouse hippocampus. The results from these experiments provide a detailed characterization of cholinergic modulation of NMDAR-dependent EPSP amplification and EPSP-Spike coupling in dorsal and ventral CA1 pyramidal cells and that cholinergic inhibition of SK-type K^+ channels via mAchR activation might provide a mechanism to gate LTP induction in the ventral CA1 region.

These results show that muscarinic receptor activation plays more critical role in the cholinergic response in the ventral hippocampus compare to dorsal hippocampus suggesting that muscarinic receptors differentially regulate pyramidal cell excitability and synaptic plastic in the CA1 regions of dorsal and ventral hippocampus. Further research needs to be done to elucidate the mechanism by which mAchR activation inhibit SK-Type K^+ and to determine the role of KCNQ/M (Kv7) potassium channels in TPS induced LTP without the bursts of multiple population spikes in ventral pyramidal cells.

One important implication for this work is that manipulations in the hippocampus like these described here open the door to future experiments focused on age- or disease-initiated changes in these circuits such as in Alzheimer's disease (AD). Alzheimer's disease is the most common form of dementia that affects memory, thinking, and behavior. Alzheimer's disease symptoms include memory impairments, language deficits, visuospatial impairments, executive dysfunction and most importantly impairment of activities of daily living (Hughes et al., 1982; Francis et al., 1999; Teri et al., 1992; Bolger et al., 1994; Fernández et al., 2010).

In Alzheimers disease patients it been reported that there is substantial decrease in enzymes responsible for synthesis of acetylcholine (Ach), Choline acetyltransferase (ChAT) (Davies and Maloney, 1976), loss of presynaptic cholinergic neurosome (Whitehouse et al., 1982) and subsequently loss of Ach release (Nilsson et al., 1986). Given these data, it was proposed that degeneration of cholinergic neurons in the basal forebrain and the associated loss of cholinergic neurotransmission in the cerebral cortex and other areas contributed significantly to the deterioration in cognitive function seen in patients with Alzheimer's disease (Bartus et al., 1982). Previously studies have also found that there is increase in SK3 type channel in hippocampus of

aged mice contributing to impaired hippocampus dependent learning and LTP (Blank et al., 2003). Therefore these data help provide some insight into role of hippocampus in learning and memory and the key role modulatory signal such as cholinergic system play in modulating synaptic plasticity in the hippocampus.

5.1 References

Bartus, Raymond T., et al. "The cholinergic hypothesis of geriatric memory dysfunction." Science 217.4558 (1982): 408-414.

Blank, Thomas, et al. "Small-conductance, Ca^{2+}-activated K^{+} channel SK3 generates age-related memory and LTP deficits." Nature Neuroscience 6.9 (2003): 911-912.

Bolger J, Carpenter B, Strauss M: Behavior and affect in Alzheimer's disease. Clinics in Geriatric Medicine. 1994; 10: 315-337.

Davies, Peter, and A. J. F. Maloney. "Selective loss of central cholinergic neurons in Alzheimer's disease." The Lancet 308.8000 (1976): 1403.

Fernández et al. Behavioural symptoms in patients with Alzheimer's disease and their association with cognitive impairment, BMC Neurology 2010, 10:87

Francis, Paul T., et al. "The cholinergic hypothesis of Alzheimer's disease: a review of progress." Journal of Neurology, Neurosurgery & Psychiatry 66.2 (1999): 137-147.

Hughes C, Berg L, Danziger W, et al: A new clinical scale for the staging of dementia. British Journal of Psychiatry. 1982; 140: 566-572.

Teri L, Wagner A: Alzheimer's disease and depression. Journal of Consulting and Clinical Psychology. 1992; 60: 379 -391.

Whitehouse, Peter J., et al. "Alzheimer's disease and senile dementia: loss of neurons in the basal forebrain." *Science* 215.4537 (1982): 1237-1239.